Jannick Duchet-Rumeau, Jean-François Gérard, Giancarlo Galli (Eds.)

Polymers and Ionic Liquids

WILEY-VCH

Polymers and Ionic Liquids

Selected Contributions from:
EUPOC 2013 Polymers & Ionic Liquid
Gargnano, Italy
September 1 – 5, 2013

Symposium Editors:
Jannick Duchet-Rumeau, Jean-François Gérard,
(Institut National des Sciences Appliquées
de Lyon, France)

Giancarlo Galli
(Università di Pisa, Italy)

Macromolecular Symposia: Vol. 342

Articles published on the web will appear through:

wileyonlinelibrary.com

Cover: This EUPOC CONFERENCE on September 2013 in Gargnano, Italy, provided the opportunity for merging the expertises from ionic liquids and polymers scientific communities. The conference focussed on the progress and prospect for applications of ionic liquids in the preparation of functional polymers.

Polymers and Ionic Liquids

Gargnano, Italy

Table of Contents

Preface

In the last decade, ionic liquids have moved from relative obscurity to something that most chemists are now very aware of. At present, the interest in ionic liquids shows a continuous increase. On the opposite, ionic liquids are being examined as new components within polymer-based materials for a wide range of applications of advanced materials. For those who are not familiar with ionic liquids and who wish to begin exploring the combination of polymers and ionic liquids as well as the related materials for a given application, it can be a daunting task to become familiar with their properties. The unique set of physico-chemical properties of ionic liquids finely tuned from their chemical structure makes them suitable in numerous applications in polymer science. Ionic liquids represent new media for macromolecular synthesis and modification of polymers and used as solvents for poorly soluble polymers such biopolymers. A special interest to ionic liquids is related to their 'green solvent' character. The ionic liquids are also investigated as additives for designing polymer materials as novel electrolytes in batteries, templates for porous polymers, plasticizers, surfactants in the preparation of functional polymers, etc. Their quite rapid emergence as alternative solvents has involved a fast growing number of examples of application but the understanding and study of their physical properties has lagged behind. A better knowledge for polymer scientists on specific properties of ionic liquids must be required so that the true potential of ionic liquids in polymer science can be highlighted.

This EUPOC CONFERENCE on September 1–5, 2013 in Gargnano (Italy) was a unique opportunity for merging the expertises from ionic liquids and polymers scientific communities and to provide a forum for discussion of state of the art approaches both in the field of ionic liquids and polymers combined with ILs. The conference has focused on future progress and prospect for applications of ionic liquids in the preparation of functional polymers. The synthesis, the physico-chemical properties and the physical aspects associated with ionic liquids and their combination with polymers as solvents, processing aids, and polymerization media for advanced materials have been covered. The exciting topics (perhaps together with the beauty of the Garde Lake) attracted 92 participants from 22 countries who gave 11 main lectures as well as 38 oral and 34 poster communications. The participants have created not only a fruitful discussion but also in an exciting and enjoyable environment. We wish to express our gratitude to all participants for supporting the meeting, to the organizing committee for their very good job and to the contributors for their carefully prepared papers.

J. Duchet-Rumeau
J.-F. Gérard

PEG-Bis Phosphonic Acid Based Ionic Supramolecular Structures

Lidia González, Anne Ladegaard Skov, Søren Hvilsted*

Summary: A number of supramolecular structures are prepared by mixing stoichiometric amounts of a phosphonic acid terminated poly(ethylene glycol) with propargyl amine, hexamethylene diamine, tris(2-aminoethyl)amine, and the first generation of a poly(propylene imine) dendrimer in turn at room temperature. The resulting ionic assemblies are very comprehensively characterized by ATR-FTIR, proton, and carbon-13 NMR spectroscopy that unequivocally demonstrate the ionic network formation through ammonium phophonates. The resulting salt and ionic networks are additionally analyzed by differential scanning calorimetry and thermogravimetric analysis. The conclusion is that mixing the virgin components at room temperature spontaneously form either a salt or ionic supramolecular networks.

Keywords: differential scanning calorimetry; ionic networks; IR spectroscopy; NMR spectroscopy; supramolecular chemistry; thermogravimetric analysis

Introduction

The supramolecular chemistry have exploited the non-covalent interactions such as hydrogen bonds, electrostatic ionic bonds, $\pi - \pi$ stacking, metal-ligand bonds, or hydrophobic interactions for decades.[1] Often low molar mass building blocks or monomers are exploited to create supra-molecular polymers which additionally display a reversible feature that can improve processing, induce self-healing behavior or provide stimuli responsiveness. The ionic interactions in particular offer a great potential in this respect due to the immense arsenal of available starting materials. In this respect the emergence of building blocks from renewable sources is important. Also the introduction of the new cations and anions emerging from the ionic liquid (IL) chemistry community has revitalized classical applications of poly-electrolytes,[2] to related fields like energy conversions,[3] gas separation membranes[4] or stimuli-responsive materials.[5] More-over many of the self-assembling properties of ILs have been utilized in the classical polymer fields. Of particular interest is the pioneering work by Wathier and Grinstaff[6] reporting on preparation of supramolecular ionic networks based on multicationic and multianionic building blocks, however, employing somehow com-plex ILs. More recently Mecerreyes and coworkers presented supramolecular ionic polymers based on small di- or trifunctional carboxylic acids that were allowed to form ammonium carboxylates by reaction with di- or trialkyl amines.[7] These materials combine the unique rheological properties related to supramolecular polymers where a sharp transition between a viscoelastic gel and a viscous liquid provides an unique relationship between the ionic conductivity and the temperature. It was furthermore argued that the chemistry sets the scene for preparation of polymer materials with self-healing properties. Additionally the same group[8] synthesized supramolecular ionic networks based on citric acid and aliphatic diamines. Here it was demonstrated that the dynamic viscoelastic behavior of the

Danish Polymer Centre, Department of Chemical and Biochemical Engineering, Technical University of Denmark, Building 227, DK-2800 Kgs. Lyngby, Denmark
E-mail: sh@kt.dtu.dk

supramolecular networks were the same in both solid and liquid states. We recently introduced the preparation of supramolecular polymeric networks by simple room temperature mixing of neat carboxylic acid terminated poly(ethylene glycol) PEG of various lengths and first or second generation of multifunctional dendritic amines of poly(propylene imine).[9] The resulting supramolecular ionic networks displayed a significantly higher thermal stability than the constituting precursors.

Here we introduce a new family of polymeric ionic networks where the core molecule is phosphonic acid terminated PEG (of molecular weight $\sim$840) that is reacted with various amines with primary amine functionality from 2–4. This generic type of ionic networks where the cross-linking units are various ammonium ions are of particular interest for potential applications in interpenetrating networks to be used as dielectric electroactive polymers in actuator applications. The ionic networks are expected to attain high dielectric permittivity especially at the desired low frequencies employed in wave energy harvesting.

Experimental Part

Materials
Bis Propylphosphonic acid-PEG 840 (DiPO(OH)$_2$-PEG 840) (Specific Polymers, Clapiers, France), first generation poly(propylene imine) dendrimer based on a diaminobutane core (PPI G1) (SyMO-Chem BV, Eindhoven, The Netherlands), hexamethylene diamine (HMDA) (Aldrich), tris(2-aminoethyl)amine (TAEA) (Aldrich), and propargyl amine (PPGA) (Aldrich) were used as received.

Sample Preparation
The supramolecular structures were all prepared by brief stirring of the stoichiometric amounts of the components at room temperature. Five minutes stirring in all instances transformed the liquid starting materials into solids.

Characterization
The attenuated total reflectance (ATR) FTIR analysis was performed on Perkin-Elmer Spectrum One. The spectra were recorded in the range of 4000–600 cm^{-1} with 4 cm^{-1} resolution. NMR spectra were recorded on a Bruker 300 MHz instrument employing D$_2$O as solvent at 25 °C. The thermal transitions (glass transition temperatures (T_g) and melting points (T_m)) were determined with a DSC Q1000 calorimeter from TA instruments with heating and cooling rates of 20 °C min^{-1} on 9–12 mg samples. T_g was determined from the second heating trace as the midpoint of the transition. Thermal stability was assessed by thermogravimetric analysis (TGA) by use of a TGA Q500 TA instrument ranging from 20 to 600 °C at a heating rate of 20 °C min^{-1} under nitrogen.

Results and Discussion

The supramolecular structures were generated by mixing Bis Propylphosphonic acid-PEG 840 (DiPO(OH)$_2$-PEG) with various amines of increasing primary amine functionality (f_a): hexamethylenediamine (HMDA) (2), tris(2-aminoethyl)amine (TAEA) (3), and the first generation dendrimer PPI G1 (4) at room temperature. Since the DiPO-(OH)$_2$-PEG has difunctional end groups the functionality of the proton donor (f_d) is 4. The network is expected to be linked by ammonium phosphonate pairs. Thus 3-dimensional structures are expected even when the primary amine functionality matches the proton donor functionality. In order to verify the network formation and the claimed structural components a thorough spectroscopic analysis was undertaken by application of ATR-FTIR as well as ^{1}H and ^{13}C NMR. In fact, also a mono functional amine, propargyl amine (PPGA), was protonated by the proton donor that results in the most simple protonated structure.

Spectroscopic characterization
The chemical structure of the components used and formed in the simple salt formation when DiPO(OH)$_2$-PEG 840 protonates
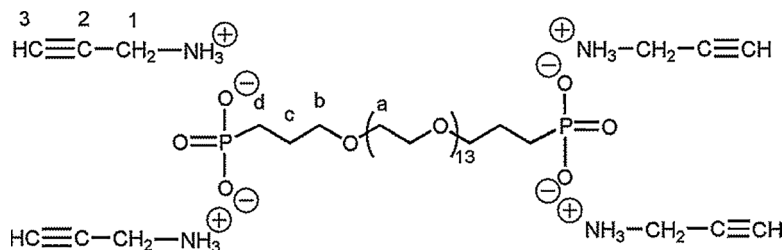
Figure 1.
Structure of DiPO(OH)₂-PEG 840: PPGA salt (1).

propargyl amine (PPGA) in a 1:4 molar ratio is shown in Figure 1 (the numbers and small letters are employed in Tables 1 and 2).

Figure 2 depicts the FTIR spectra of all components involved in this salt formation. Inspection of the spectrum of the pure DiPO(OH)₂-PEG reveals the wide absorption band at 3600–3200 cm^{-1}, with a maximum at about 3403 cm^{-1} that can be assigned to the O-H stretching mode of hydroxyl groups and adsorbed water. The band at 1662 cm^{-1} could be attributed to H-O-H deformation of adsorbed water[10] and the absorption peak at 1246 cm^{-1} can be ascribed to P=O deformation vibration.[11] Durmus et al.[12] assigned a band at 1143 cm^{-1} to the stretching mode (P=O)

for a poly(vinyl phosphonic acid) sample. Additionally, absorbances at 2340, 985, and 936 cm^{-1} belong to (=O)PO-H vibration.[13–18] Indeed, all these peaks are not present in the spectrum of the DiPO(OH)₂-PEG/PPGA salt. These bands have been replaced by several new bands at 1624, 1557, 1217, 1023, and 913 cm^{-1}. Furthermore, in the salt spectrum, the band at 3365 cm^{-1} related to the N-H stretching vibrations of the PPGA amino group is suppressed. New bands at 3242, 2867, 2663 and 2125 cm^{-1} have appeared. The sharp peak at 2867 cm^{-1} is attributed to both the C-H stretching vibrations from the alkyne group and the CH₂ stretching vibrations of the alkane moiety. The latter have shifted from 2923 and 2853 cm^{-1} in the pure

Table 1.
Proton chemical shifts (ppm in D₂O (multiplicity)) of DiPO(OH)₂-PEG 840, multifunctional amines, and the supramolecular ionic structures derived.

Chemical structure	Protons								
	1	2	3	4	5	a	b	c	d
a b c d -(CH₂CH₂O)ₙCH₂CH₂CH₂-PO₂H₂* 3 1						3.55(s)	3.45(t)	1.68(s)	1.71(s)
HC≡CCH₂NH₂(PPGA)	4.71(s)		3.30(s)						
Ionic salt (1)	4.67(s)		3.62(s)			3.55(s)	3.42(t)	1.34(m)	1.61(m)
3 2 1 -(CH₂CH₂CH₂NH₂)₂ (HMDA)	2.54(t)	1.36(t)	1.26(m)						
Ionic network (2)	2.83(t)	1.53(m)	1.27(m)			3.55(s)	3.41(t)	1.27(m)	1.53(m)
2 1 N(CH₂CH₂NH₂)₃ (TAEA)	2.67(t)	2.50(t)							
Ionic network (3)	2.97(t)	2.66(t)				3.55(s)	3.40(t)	1.24(m)	1.57(m)
1 2 3 4 5 -(CH₂CH₂N(CH₂CH₂CH₂NH₂)₂)₂ (PPI G1)	1.34(m)	2.37(m)	2.37m)	1.50(m)	2.50(t)				
Ionic network (4)	1.60(m)	2.53(m)	2.53(m)	1.74(m)	2.85(t)	3.55(s)	3.40(t)	1.25(m)	1.37(m)

* phosphonic acid protons resonate at 4.73 ppm.

Table 2.
Carbon-13 chemical shifts (ppm in D_2O) of DiPO(OH)$_2$-PEG 840, multifunctional amines, and the supramolecular ionic structures derived.

Chemical structure	Carbons								
	1	2	3	4	5	a	b	c	d
a b c d -(CH$_2$CH$_2$O)nCH$_2$CH$_2$CH$_2$-PO$_3$H$_2$						69.6	69.1	22.1	23.8
3 2 1 HC≡CCH$_2$NH$_2$(PPGA)	29.7	84.2	71.6						
Ionic salt (1)	29.0	75.5	71.7			69.6	69.0	23.5	24.0
3 2 1 -(CH$_2$CH$_2$CH$_2$NH$_2$)$_2$(HMDA)	40.6	31.9	26.1						
Ionic network (2)	39.2	26.5	25.1			69.5	69.0	23.9	24.4
2 1 N(CH$_2$CH$_2$NH$_2$)$_3$ (TAEA)	37.9	56.4							
Ionic network (3)	36.9	50.9				69.5	69.1	24.1	24.6
1 2 3 4 5 -(CH$_2$CH$_2$N(CH$_2$CH$_2$CH$_2$NH$_2$)$_2$)$_2$ (PPI G1)	23.5	53.0	50.8	28.4	39.2				
Ionic network (4)	22.9	52.7	50.0	23.3	37.7	69.5	69.0	24.1	24.6

PPGA. Additionally, the characteristic shoulder at ∼2663 cm^{-1} associated with the -NH$_3^+$ absorption band is identified. The band at ∼2125 cm^{-1} is ascribed to the C≡C stretching absorption of the alkyne groups. All these observations strongly support complete protonation of all amino groups originally present in the mixture.

The salt formation was additionally analyzed by NMR spectroscopy in D_2O. Figure 3 shows the proton NMR spectra of the starting components and the salt (**1**). The chemical shifts and the resonance multiplicity are listed in Table 1. The proton spectrum of PPGA (Figure 3.2) is verysimple consisting of only 2 singlets where the area of **1** is twice
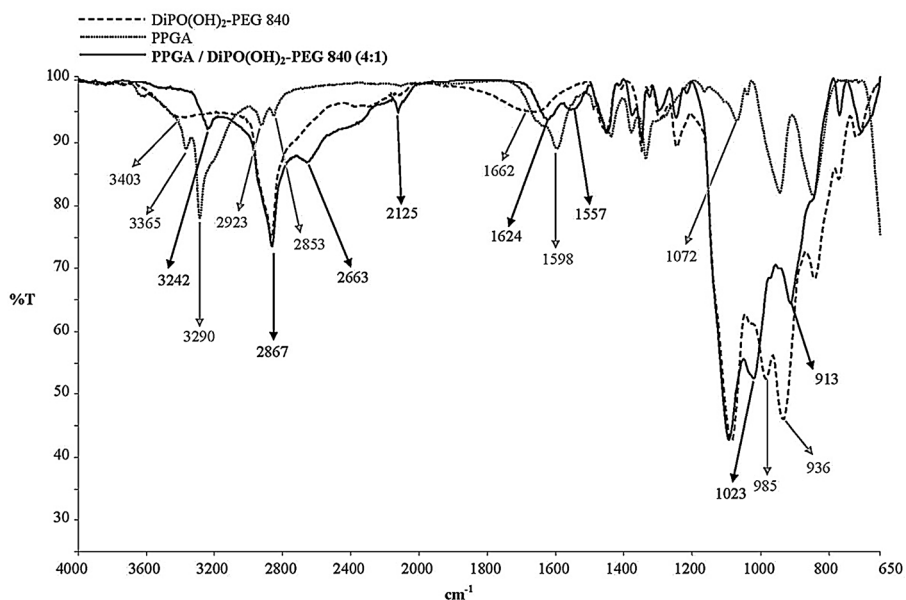
Figure 2.
ATR-FTIR spectra of DiPO(OH)$_2$-PEG 840, PPGA, and the salt (1) formed from a PPGA/DIPO(OH)$_2$-PEG 840 (4:1) mixture.
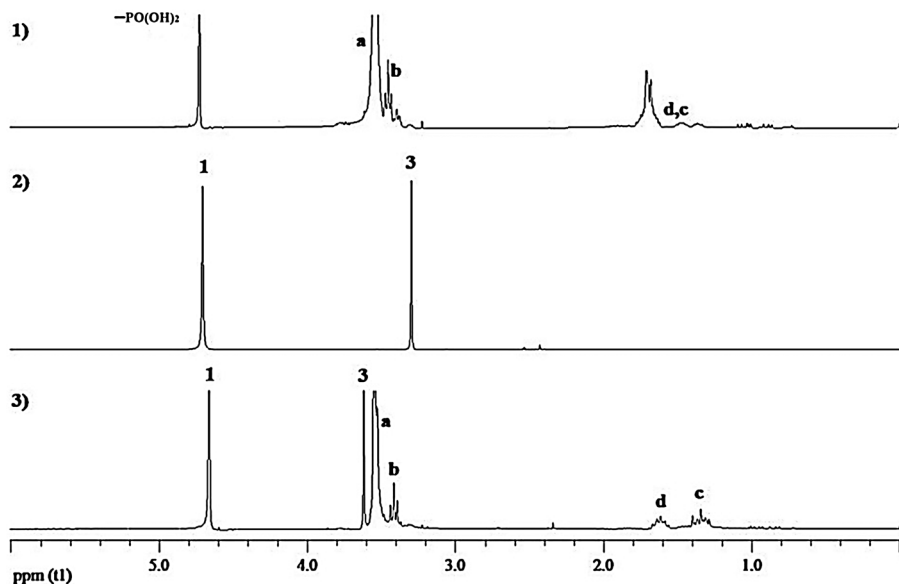
Figure 3.
Proton NMR of DiPO(OH)$_2$-PEG 840 (1), PPGA (2) and the salt 1 (3).

that of **3**. The singlets are clearly visible in the salt spectrum (Figure 3.3) where the methylenes (1) next to the ammonium ion have experienced a 0.32 ppm deshielding. Most importantly is the complete lack of any PPGA in the salt spectrum strongly supporting the total salt formation between the stoichiometric reactants. Also the complete disappearance of the phosponic acid protons at 4.73 ppm is noticed. In the centre part of the DiPO(OH)$_2$-PEG 840 salt the largest effect is noticed for the c methylenes that are shielded almost 0.34 ppm. Similar pronounced effects are observed in the carbon-13 NMR spectra of the salt components shown in Figure 4 with the carbon-13
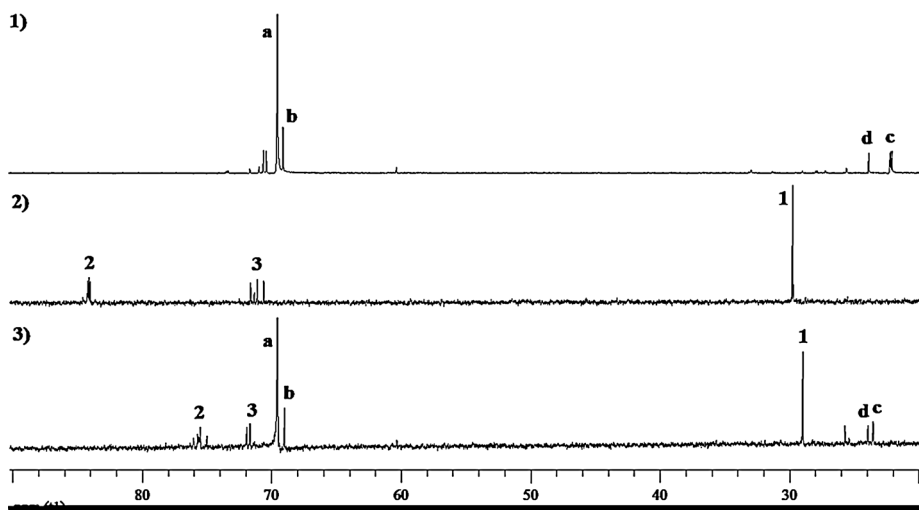
Figure 4.
Carbon-13 NMR spectra of DiPO(OH)$_2$-PEG 840 (1), PPGA (2), and salt 1 (3).

chemical shifts listed in Table 2. A large 8.7 ppm shielding is experienced for the quaternary 2 carbon, whereas methylene carbon 1 feels a ~1 ppm deshielding in the salt. The rather large differences in the shielding observed is due to the inherent nature of the neighbour effects caused by ammonium ions as compared to the amines.

In summary, the three spectroscopic techniques all unequivocally point to the supramolecular salt formation.

Figure 5 illustrates the ammonium phosphonates that link the components of the ionic network 2 formed from the 2 hexamethylenediamine (HMDA):1 DiPO-$(OH)_2$-PEG 840 mixture.

The ionic supramolecular structure of this ionic network was also analyzed by infrared spectroscopy where especially in the network **2** spectrum the stretching vibrations of -NH_2 asymmetric and symmetric bands of HMDA ranging from 3329 to 3170 cm^{-1} are suppressed as compared to the situation in the HMDA spectrum. Additionally, the protonation of the -NH_2 groups of HMDA is strongly suggested by the disappearance of the band at 1606 cm^{-1} attributed to the strong in-plane -NH_2 scissoring bending vibration of the non-protonated HMDA. Furthermore, the characteristic shoulders at ~2653, 2572 and ~2245 cm^{-1} corresponding to the -NH_3^+ absorption bands are clearly visible in the spectrum of the ionic network **2**.

The proton chemical shifts of the ionic network **2** are listed in Table 1. In the network both methylene protons in α-position (1) and in β-position (2) to the ammonium ions are deshielded as com-

pared to the resonances in the HMDA. Thus the 1 methylenes are deshielded by 0.3 ppm and the 2 methylenes a little less by 0.17 ppm. Similarly the carbon-13 resonances listed in Table 2 clearly show significant differences between the HMDA and the ionic network **2**. The resonances of carbons 1, 2, and 3 in the network are all shielded although to different degrees with 2 experiencing a large (5.4 ppm) difference as also observed previously in the similar salt spectrum. In summary the spectroscopies conclusively corroborate the ionic network formation.

Figure 6 illustrates the cross-linking units of the ionic network **3** based on TAEA and $DiPO(OH)_2$-PEG 840 in a 1: 0.75 molar ratio.

In the ionic network FTIR spectrum the asymmetric and symmetric stretching vibration bands of -NH_2 of TAEA at 3357 and 3276 cm^{-1} are completely suppressed. Also the strong in-plane -NH_2 scissoring bending vibration of the non-protonated TAEA at 1590 cm^{-1} is absent in the spectrum of the ionic network **3**. Additionally, the characteristic shoulders at about 2628, 2532 and 2238 cm^{-1} associated with the -NH_3^+ absorption bands are identified in the spectrum of **3** substantiating the protonation of the primary amino groups of TAEA. Moreover, another strong indication of the protonation of the primary amino groups of TAEA, is the disappearance of the broad band around 861 cm^{-1} associated with the out-of-plane wagging (bending vibrations) of -NH_2, which is characteristic
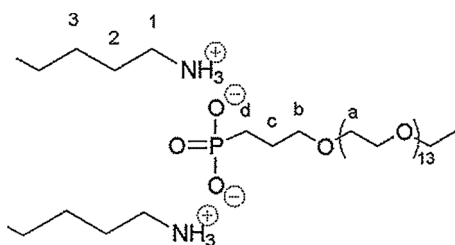
Figure 5.
Ionic components in ionic network 2.
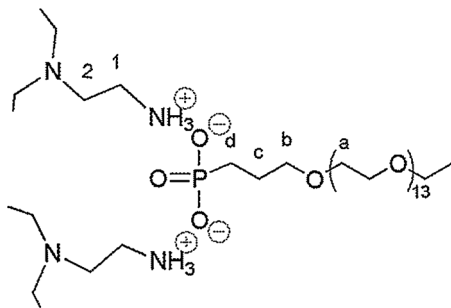
Figure 6.
Basic ionic components in ionic network 3.

of primary amines. Similar results were observed in a previous work when TAEA was employed in a similar fashion to create ionic networks with two short biscarboxy-methyl ether terminated poly(ethylene glycols) (DiCOOH-PEGs).[9] In addition the new bands at 1628, 1556, 1213, 974 and $767 \, cm^{-1}$ confirm the protonation of the amino groups of TAEA. The bands at 985 and $936 \, cm^{-1}$ ascribed to $(O=)PO\text{-}H$ vibration in the $DiPO(OH)_2$-PEG 840 spectrum, are not present in the spectrum of the ionic network **3**.

The proton NMR spectrum of TAEA is also very simple with only two coupled triplets with the shifts listed in Table 1. In the ionic network **3** both triplets are significantly deshielded with the largest effect (0.3 ppm) on methylene protons 1. In case of the methylenes 2 the difference is 0.16 ppm. Neither of the original resonances from the TAEA spectrum are visible in the ionic network spectrum. However, the short ethylene chains between the primary amines and the tertiary amine in TAEA prevent NMR to provide information on possible protonation of the tertiary amine in the ionic network. Similar observations are made in the carbon-13 spectra with the chemical shifts listed in Table 2. Here the carbon 2 in the network **3** spectrum is

shielded 5.5 ppm compared to the TAEA spectrum, whereas a smaller difference (1 ppm) is observed for carbon 1. Again the results of the NMR analyses very strongly support the findings from FTIR that all primary amines of TAEA take part in the ionic network **3** formation.

The mixing of stoichiometric amounts of $DiPO(OH)_2$-PEG 840 and PPI G1 created the ionic network **4**. The cross-linking unit of the ionic network **4** involving 4 ammonium phosphates from one PPI G1 is shown in Figure 7.

The structure of the ionic network 4 was elucidated by use of the overlaid FTIR spectra displayed in Figure 8. Most of the features already discussed for the salt (1) and the other ionic networks (2 and 3) can be identified in the spectrum of this ionic network as well. An important observation is the lack of the NH_2 asymmetric and symmetric bands from PPI G1 dendrimer at 3355 and $3277 \, cm^{-1}$ in the network spectrum implying complete protonation of the external primary amino groups of the dendrimer. Also the bending NH_2 band of the non-protonated starting dendrimer at $1596 \, cm^{-1}$ is not present in the network spectrum. Another interesting observation is the symmetric stretching band of the CH_2 groups attached to the tertiary nitrogen
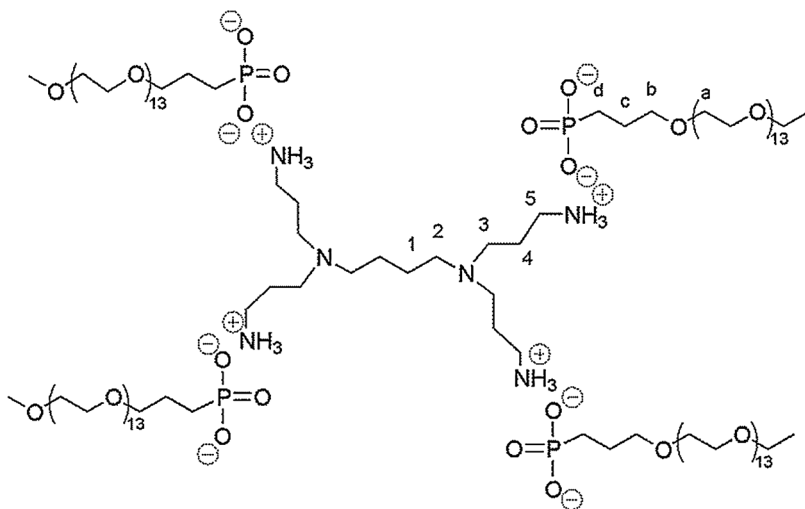
Figure 7.
Ionic components in ionic network 4.
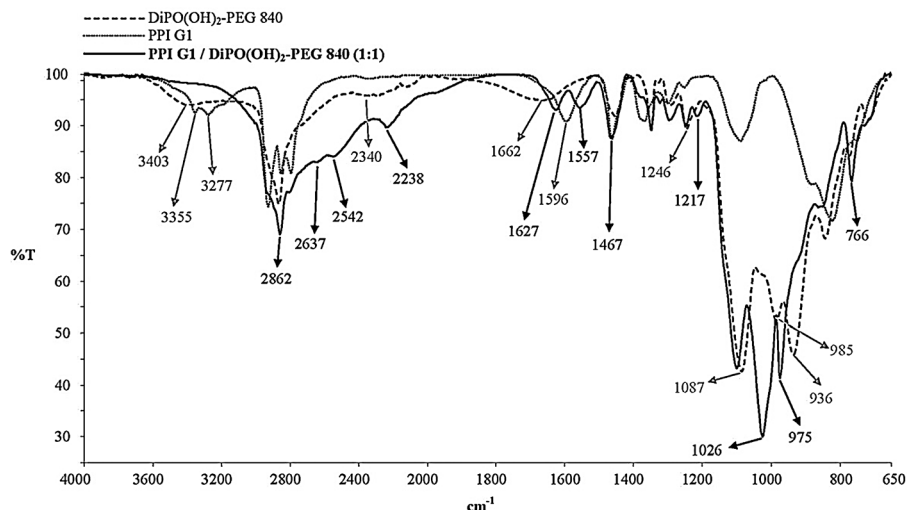
Figure 8.
ATR-FTIR spectra of DiPO(OH)₂-PEG 840, PPI G1, and the ionic network (4) formed from a PPI G1/DiPO(OH)₂-PEG 840 (1:1) mixture.

located at 2862 cm⁻¹, which is seen in both the dendrimer and (unaltered) in the ionic network spectra, and thus implying no protonation of the tertiary amines. This band should normally be detected at 2850 cm⁻¹ and it would be related to the interactions between the lone pair of the nitrogen and the C-H bond, which lies in a *trans* position to it.[19,20] This effect does not occur when the lone pair is delocalized or donated into a vacant orbital. The ionic network spectrum similarly lacks the two strong absorptions at 985 and 936 cm⁻¹ associated with the (O=)PO-H absorption identified in the DiPO(OH)₂-PEG 840 spectrum. Taken together all these obser-

vations seem to confirm the protonation of the external primary amino groups only and the ionic network 4 cross-linked by the unit displayed in Figure 7.

The structural elucidation of the ionic network 4 was supplemented by analyses of the proton NMR spectra displayed in Figure 9 and the carbon-13 spectra shown in Figure 10 with the corresponding chemical shifts collected in Tables 1 and 2. In the proton spectrum of PPI G1 in D₂O (Figure 9.1) the resonances of methylenes 1, 4 and 5 are well separated, where as methylenes 2 and 3 surrounding the tertiary N are overlapped. In the ionic network spectrum (Figure 9.2) the 5 methylene α to
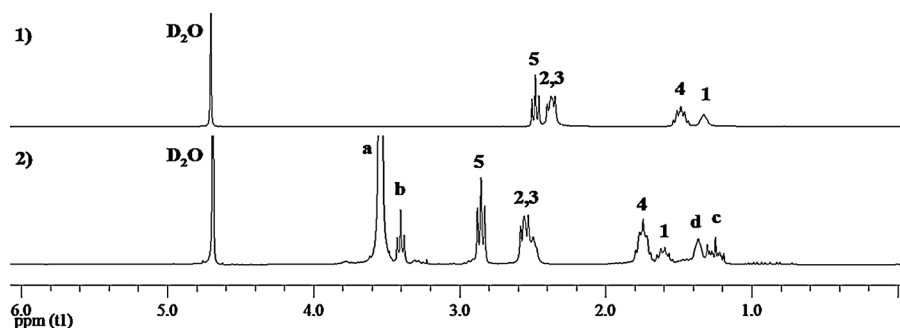
Figure 9.
Proton NMR spectra PPI G1 (1), and network 4 (2).

1)

2)
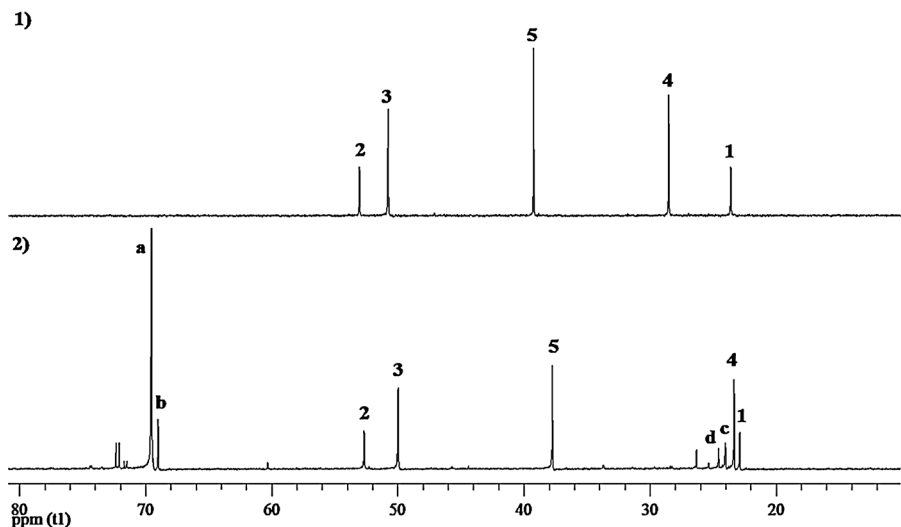
Figure 10.
Carbon-13 NMR spectra of PPI G1 (1), and network 4 (2).

the ammonium ions is deshielded by 0.35 ppm to a position at 2.85 ppm. Also the methylenes 4 in β position to the ammonium ions are deshielded from 1.50 to 1.74 ppm. On the other hand, the d protons next to the phosphonic acid groups are shielded in ionic network to 1.37 ppm from originally 1.71 ppm in the unreacted phosphonic acid.

The carbon-13 spectrum of unreacted PPI G1 (Figure 10.1) shows the resonances of the 5 different methylene carbons. These resonances are also clearly identified in the ionic network spectrum (Figure 10.2) where the most noticeable effects are the shieldings of the 2 methylene carbons closest to the ammonium ions where 5 has moved from 39.2 ppm to 37.7 ppm and 4 from 28.4 ppm to 23.3 ppm. The remaining carbons (1,2,3) in the core of PPI G1 or closest to the tertiary N are almost unaffected in the ionic network spectrum. In addition some deshielding effects are noticed on the d and c methylenes of the phosphonate part of the ionic network.

In summary, the performed NMR analyses support the conclusions of the FTIR analysis that only the primary amines are involved in the formation of the ionic network and thus strongly corroborate the cross-linking unit of ionic network 4

displayed in Figure 7. It is noted that both ^{31}P and ^{15}N NMR spectroscopy although not performed could further strengthen the spectroscopical conclusions where the former would monitor the behaviour of the PEG chain ends, and the latter additionally probe the amine behaviour within the networks.

Thermal Investigations
The thermal transitions of the phosphonic acid based supramolecular ionic structures were analyzed by DSC. The results are listed in Table 3 and, for the sake of comparison, results of similar investigations on ionic structures based on a biscarboxylic acid terminated PEG were also included. The phosphonic acid based ionic networks clearly reveal a more complex behaviour with two T_gs, of which the lowest one is quite close to the T_g of the precursor DiPO(OH)$_2$-PEG 840. This T_g is thus tentatively assigned to the longer PEG chains of these networks. The fact that two T_g's appear in each network suggests some kind of phase separation within the network. The longer PEG chain in DiPO-(OH)$_2$-PEG 840 is apparently a decisive factor. The higher T_g is hypothesized to be due to ion clusters that are formed at each end of the phosphonic acid precursors or

Table 3.
Transition temperatures of supramolecular ionic networks based on PEGs terminated with carboxylic acids and phosphonic acids and of the precursors.

Entry	Chemical structure	(molar ratio)	T_{g1} (°C)	T_{g2} (°C)	T_m (°C)	Ref.
1	PPI G1		−107			9
2	DiCOOH-PEG 600		−60			9
3	DiPO(OH)$_2$-PEG 840		−46			this work
4	HMDA:DiCOOH-PEG 600	1:1	−30			9
5	HMDA:DiPO(OH)$_2$-PEG 840	2:1	−49	−3	138	this work
6	TAEA:DiCOOH-PEG 600	1:1.5	−24			9
7	TAEA:DiPO(OH)$_2$-PEG 840	2:1.5	−40	5		this work
8	PPI G1:DiCOOH-PEG 600	1:2	−25			9
9	PPI G1:DiPO(OH)$_2$-PEG 840	1:1	−45	26		this work

around the multifunctional amines. These clusters apparently has less local mobility than the PEG segments. In fact the largest cluster that is anticipated formed with the PPI G1 dendrimer is expected to have the lowest mobility. The highest T_g (26 °C) is also observed here. In the case of the HMDA/DiPO(OH)$_2$-PEG 840 (entry 5) even a melting point is additionally identified. A hypothetical explanation is that a poly(phosphonamide) is formed during the heating in the DSC instrument during the analysis. Support for this hypothesis is that polyamides have previously been produced by heating a stoichiometric mixture of HMDA and DiCOOH-PEG 600 at 275 °C. Here there covered polyamide was clearly identified by two new bands at 1660 cm^{-1} (the amide I band) and at 1537 cm^{-1} (the amide II band), associated with the amide linkage. A brief account of this can be found in ref.[9]

The thermal stability of the supramolecular ionic networks and the precursors were
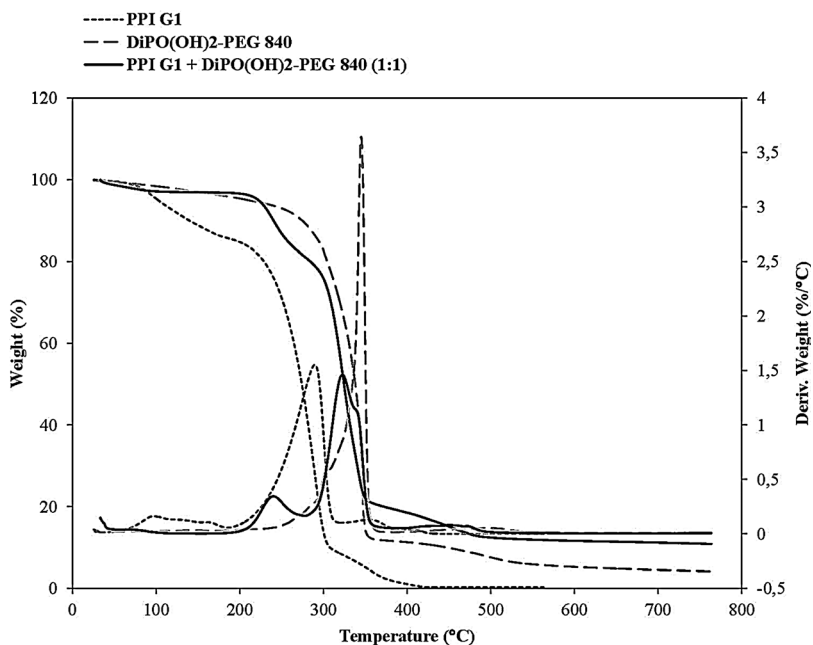
Figure 11.
TGA traces of PPI G1, DiPO(OH)$_2$-PEG 840, and PPI G1:DiPO(OH)$_2$-PEG 840 (1:1) ionic network during heating at 20 °C/min under N$_2$. Both the weight loss (←) and the first derivative weight loss (→) are shown.

Table 4.
Thermal stability of precursors and supramolecular ionic networks based on PEGs terminated with carboxylic acids and phosphonic acids.

Entry	Formulation/chemical	$T_{d2\%}$[a] ($^\circ$C)	$T_{d10\%}$[a] ($^\circ$C)	T_{max}[b] ($^\circ$C)	Char Yield[c] (%)	Ref
1	HMDA	39	84	127	0.2	this work
2	TAEA	74	116	182	0.3	this work
3	PPI G1	81	139	290	0.3	this work
4	DiCOOH-PEG 600	239	362	414	1.7	9
5	DiPO(OH)$_2$-PEG 840	116	274	345	5.2	this work
6	HMDA:DiCOOH-PEG 600 (1:1)	64	195	420	3.3	9
7	HMDA:DiPO(OH)$_2$-PEG 840 (2:1)	106	247	329	13.1	this work
8	TAEA:DiCOOH-PEG 600 (1:1.5)	140	363	413	4.6	9
9	TAEA:DiPO(OH)$_2$-PEG 840 (2:1.5)	147	264	336	14.4	this work
10	PPI G1:DiCOOH-PEG 600 (1:2)	194	337	411	3.1	9
11	PPI G1:DiPO(OH)$_2$-PEG 840 (1:1)	68	240	322	11.6	this work

[a] Temperature of 2 and 10 wt% loss determined by TGA. [b] Temperature for maximum degradation rate. [c] Char yield at 600 $^\circ$C.

likewise studied by TGA under nitrogen. Figure 11 shows the analyses of the ionic network PPI G1:DiPO(OH)$_2$-PEG 840 system as a representative example. In order to qualitatively compare the behaviour of the different ionic networks some key numbers are extracted and listed in Table 4 that furthermore contains similar information from the carboxylic acid based PEG networks. A striking feature is the much lower thermal stability of phosphonic acid containing PEG (Table 4 entry 5) compared to the carboxylic acid based analogue (entry 4) where the difference for the 10% weight loss ($T_{d10\%}$) is 88 $^\circ$C. This cannot be due to the PEG chains since these are quite comparable in length. Thus the phosphonic acid end groups play a
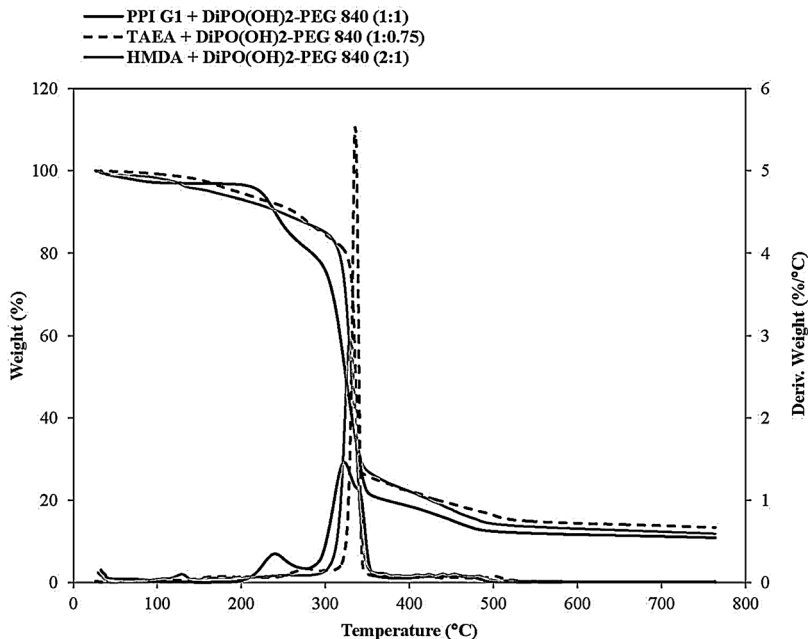
Figure 12.
TGA traces of ionic networks based on DiPO(OH)$_2$-PEG 840, and PPI G1, TAEA, or HMDA during heating at 20 $^\circ$C/min under N$_2$. Both the weight loss ($\leftarrow$) and the first derivative weight loss ($\rightarrow$) are shown.

deciding role in the degradation process. In general this effect is carried over to the phosphonic acid containing PEG ionic networks since they are all less thermally stable ($T_{d10\%}$ ∼50–100 °C lower) than the corresponding carboxylic acid based networks. It is clearly illustrated by Figure 12 that the thermal stability of the phosphonic acid containing networks (entries 7,9,11) is strongly coupled to the stability of the phosphonic acid terminated PEG precursor (entry 5). It is also noted that all the phosphonic acid containing networks have a relatively high char (residue) content (12–14 wt%) at 600 °C, whereas the carboxylic acid based ionic networks only have a 3–5 wt% residue. This may tentatively be attributed to the cleavage of the C-P bond leaving a $PO(OH)_2$ radical that by hydrogen abstraction leads to the formation of phosphorous acid (H_3PO_3). Then this can dehydrate to the oxide, P_2O_3, and water,[21] which can account for the observed residue. In fact, the observed char residue is highest for the TAEA:DiPO(OH)$_2$-PEG 840 network with the highest initial content of phosphonic acid terminated PEG precursor, and lowest for the PPI G1:DiPO(OH)$_2$-PEG 840 network with the lowest PEG precursor content.

Conclusion

The simple mixing of a phosphonic acid terminated PEG with hexamethylene (HMDA), tris-(2-aminoethyl)amine (TAEA), or the first generation PPI dendrimer (PPI G1) has created a new family of supramolecular ionic networks. The spontaneous protonation of the constituting primary amines forming the linking ammonium phosphonates is corroborated by FTIR, proton, and carbon-13 NMR spectroscopy. The ionic networks based on phosphonic acid terminated PEG have higher T_gs than the PEG precursor.In terms of thermal stability, the corresponding carboxylic acid based networks have better stability than the phosphonic acid terminated PEG. The elucidated ionic network strategy suggests the development of novel polymer materials with self-healing properties. Moreover, in combination with orthogonal cross-linking chemistry the design of interpenetrating networks[22] seems an attractive feasible approach.

[1] J. M. Lehn, "*Supramolecular Chemistry: Concepts and Perspectives*", Wiley, Weinheim, Germany **1995**.

[2] a) D. Mecerreyes, *Prog. Polym. Sci.* **2011**, *36*, 1629; b) J. Yuan, D. Mecerreyes, M. Antonietti, *Prog. Polym Sci.*, **2013**, *38*, 1009.

[3] A. S. Shaplov, E. I. Lozinskaya, Y. S. Vygodskii, *in Electrochemica Properties and Applications of Ionic Liquids*, A. A. J. Torriero, M. J. A. Shiddiky, Eds., Nova Science Publishers Inc., New York **2011**, Ch. 9.

[4] a) J. E. Bara, D. E. Camper, D. L. Gin, R. Noble, *Acc. Chem. Res.* **2010**, *43*, 152; b) L. Tome, D. Mecerreyes, C. Freire, I. Marrucho, L. P. Rebelo, *J. Membr. Sci.* **2013**, *428*, 260; c) J. F. Stanzione, III, R. E. Jensen, P. J. Costanzo, G. R. Palmese, *ACS Appl. Mater. Interfaces* **2012**, *4*, 6142.

[5] a) K. Vijayakrishna, S. K. Jewrajka, A. Ruiz, R. Marcilla, J. A. Pomposo, D. Mecerreyes, D. Taton, Y. Gnanou, *Macromolecules* **2008**, *41*, 6299; b) A. Ozwald, J. S. Parent, R. A. Whitney, *J. Polym. Sci. Part A: Polym. Chem.* **2013**, *51*, 2438.

[6] a) M. Wathier, M. W. Grinstaff, *J. Am. Chem. Soc.* **2008**, *130*, 9648. b) M. Wathier, M. W. Grinstaff, *Macromolecules* **2010**, *43*, 9529.

[7] M. A. Aboudzadeh, M. E. Muñoz, A. Santamaria, R. Marcilla, D. Mecerreyes, *Macromol. Rapid Commun.* **2012**, *33*, 314.

[8] M. A. Aboudzadeh, M. E. Muñoz, A. Santamaría, M. J. Fernández-Berridi, L. Irusta, D. Mecerreyes, *Macromolecules* **2012**, *45*, 7599.

[9] L. González, A. L. Skov, S. Hvilsted, *J. Polym. Sci. Part A: Polym. Chem.* **2013**, *51*, 1359.

[10] M. J. D. Low, P. Ramamurthy, *J. Phys. Chem.* **1968**, *72*, 3161.

[11] N. Cinausero, N. Azema, M. Cochez, M. Ferriol, M. Essahli, F. Ganachaud, J. M. L. Cuesta, *Polym. Adv. Technol.* **2008**, *19*, 701.

[12] Z. Durmus, H. Kavas, H. Sozeri, M. S. Toprak, A. Aslan, A. Baykal, *J. Supercon. Nov. Magn.* **2012**, *25*, 1185.

[13] E. Pretsch, P. Bühlmann, M. Badertscher, *Structure Determination of Organic Compounds*, Springer, Berlin **2009**, p. 329.

[14] P. Kim, S. C. Jones, P. J. Hotchkiss, N. Haddock, B. Kippelen, S. R. Marder, J. W. Perry, *Adv. Mater.* **2007**, *19*, 1001.

[15] P. H. Mutin, G. Guerrero, A. Vioux, *J. Mater. Chem.* **2005**, *15*, 3761.

[16] C. Yee, G. Kataby, A. Ulman, T. Prozorov, H. White, A. King, M. Rafailovich, J. Sokolov, A. Gedanken, *Langmuir* **1999**, *15*, 7111.

[17] S. Pawsey, K. Yach, L. Reven, *Langmuir* **2002**, *18*, 5205.

[18] W. Gao, L. Dickinson, C. Grozinger, F. G. Morin, L. Reven, *Langmuir* **1996**, *12*, 6429.

[19] L. J. Bellamy, *The Infrared Spectra of Complex Molecules* 3rd Ed., Chapman and Hall, London **1975**, p. 16.

[20] F. Bohlmann, *Chem. Ber.* **1957**, *91*, 2157.

[21] D. D. Jiang, Q. Yao, M. A. McKinney, C. A. Wilkie, *Polym. Degrad. Stab.* **1999**, *63*, 423.

[22] a) F. B. Madsen, I. Dimitrov, A. E. Daugaaard, S. Hvilsted, A. L. Skov, *Polym. Chem.* **2013**, *4*, 1700. b) L. Yu, L. Gonzalez, S. Hvilsted, A. L. Skov, *Proceedings of SPIE* **2014**, *9056*, 90560C.

Cholinium Lactate Methacrylate: Ionic Liquid Monomer for Cellulose Composites and Biocompatible Ion Gels

Mehmet Isik,[1] *Raquel Gracia,*[1] *Lessie C. Kollnus,*[1] *Liliana C. Tome,*[2] *Isabel M. Marrucho,*[2] *David Mecerreyes*[*1]

Summary: Cholinium, a quaternary ammonium cation, trimethylethanol ammonium, is an essential micronutrient which supports several biological functions. In this work, a new cholinium based ionic liquid methacrylate monomer was used to process cellulose and produce optically transparent coatings through a simple photopolymerization procedure. The same monomer was also employed to manufacture biocompatible ion gels. Simply, the methacrylic monomer was photopolymerized within the ionic liquid matrix to form a gel type material.

Keywords: cellulose composites; ion-gel; ionic liquid

Introduction

Incorporation of renewable sources either as a reactive component or as a filler into polymeric systems gathered attention due to environmental concerns.[1–3] For this reason, a general trend is to develop new types of ionic liquids from renewable sources, which are also known as, bioionic liquids. It is well known that cellulose is one of the most important raw materials on earth being the structural component of plant cell walls.[1] Therefore, it is necessary to take advantage of this material by using it for different applications other than just using as a raw material for paper industry. It is well known from literature that some ionic liquids can efficiently dissolve cellulose.[4,5] Among these ionic liquids, imidazolium based ionic liquids are commonly employed due to their ability to dissolve cellulose efficiently.[4] The major drawback for these ionic liquids is their low biocompatibility and biodegradability.[6,7] There-fore, In this study, we focused on the preparation of cellulose-poly(ionic liquid) composites by using a new bioionic liquid monomer to process cellulose and subsequent photopolymerization.[8] The monomer of choice was 2-cholinium lactate methacrylate since cholinium moiety is known to have low toxicity and to be biocompatible.[9] Another potential application of this monomer consists in producing biocompatible ion gels. There are many examples in literature for the fabrication of ion gels containing different ionic liquids.[10] The ionic liquid of choice is determined by taking into account the application and the miscibility of the ionic liquid with the matrix material to have a homogeneous material in the end. Ion gels can simply be categorized into three major classes; organic gels containing polymers and gelators,[11] inorganic gels made of ceramics, carbon nanotubes or sol-gel chemistry[12] and hybrid organic-inorganic ion gels containing both organic and inorganic parts to have materials with hybrid properties.[13] The common feature of these materials is that they have an ionic liquid which is immobilized in a solid matrix. By this way, dimensional stability is given to the ionic liquid.

[1] Polymat, University of the Basque Country, Avda. Tolosa 72, 20018, San Sebastian, Spain
E-mail: david.mecerreyes@ehu.es
[2] Instituto de Tecnologia Química e Biológica, Universidade Nova de Lisboa, Av. República, 2780-157 Oeiras, Portugal

Experimental Part

Ionic liquid monomer was synthesized through quaternization of commercially available 2-dimethylaminoethylmethacrylate monomer. Stoichiometrically excess 2-bromoethanol was reacted with the monomer at room temperature for 24 hours in bulk. The resulting crude product was washed with ethylacetate. The yield of quaternization was over 90%. Anion exchange reaction was performed with silver lactate to obtain the final 2-cholinium lactate methacrylate monomer. Silver bromide byproduct was removed by filtration. The desired monomer was clear viscous liquid at room temperature. The yield of the anion exchange reaction was calculated as 86%. ^{1}HNMR was used to confirm the formation of the monomers (Figure 1). Photopolymerization was conducted on a Dymax UV conveyor belt system having an iron halide lamp with a power of 900 mW/cm^2. ATR-FTIR spectra were recorded on a Nicolet iS10 FTIR Spectrometer using photopolymerized films on diamond crystal with an incident angle of 42°. 32 scans with a resolution of 4 cm^{-1} were averaged for each spectrum. The ^{1}HNMR measurement was carried out on a Bruker AC-500 instrument in deuterium oxide as the solvent.

Polymerized Ionic Liquid (PIL)-Cellulose Composites

In order to prepare the cellulose composites, different amounts (1–10 wt %) of cellulose were mixed with 2-cholinium lactate methacrylate monomer at room temperature. The resulting viscous cellulose/ionic liquid monomer solutions were formulated with a small amount of 2,2-dimethoxy-2-phenylacetophenone photoinitiator and applied onto a glass substrate by using doctor blade method. Photopolymerization was performed on the conveyor belt system. The monomer photopolymerized and led to a thin solid polymeric coating on the substrate. The
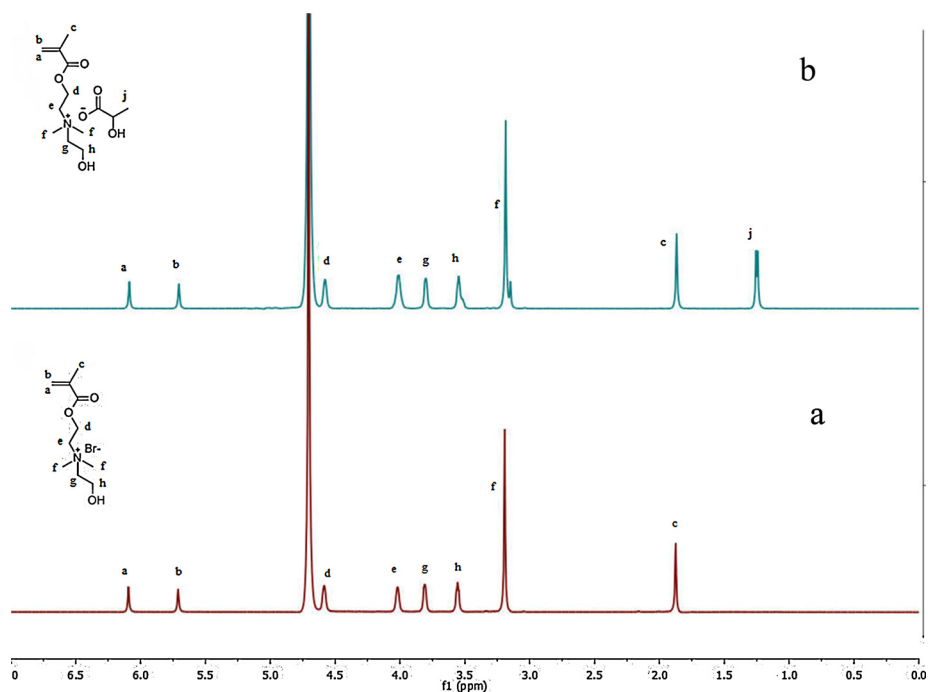
Figure 1.
^{1}HNMR spectra of ionic liquid monomers (a) before and (b) after anion exchange reactions.
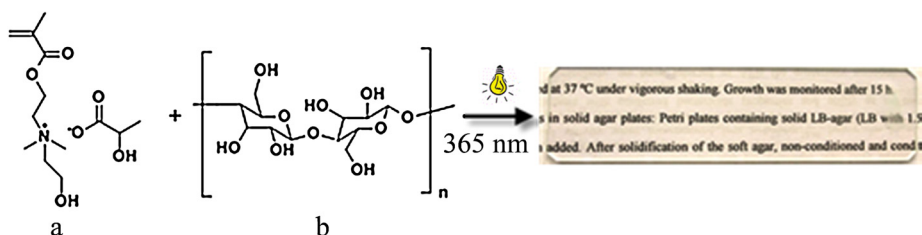
Figure 2.
2-cholinium lactate methacrylate ionic liquid monomer (a) – 5 wt% cellulose (b) and picture of the resulting composite coating produced through photopolymerization.

resulting coating with 5 wt% of cellulose is displayed in Figure 2. As it can be seen from the image, a transparent coating was obtained as a result of facile and straightforward photopolymerization process. The transparency of the coating decreased as the amount of cellulose exceeded 5 wt%.

Cholinium Based Ion Gels

In order to produce the ion gels, cholinium lactate ionic liquid was blended with the ionic liquid monomer which afterwards photopolymerized in the presence of the photoinitiator. The ion gels were designed to contain 60 wt% free ionic liquid and
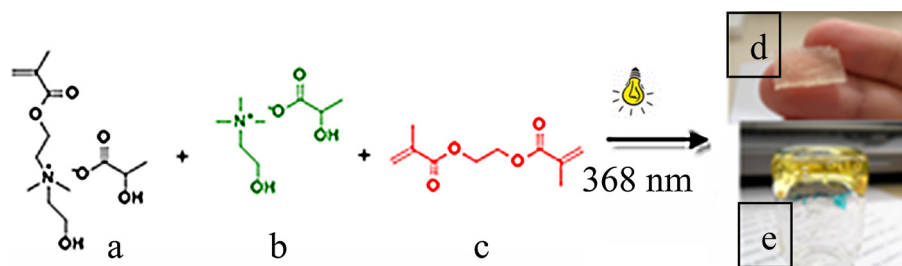
Figure 3.
Schematic representation of ion gels produced (d-with crosslinker, e-without crosslinker) with ionic liquid monomer (a), cholinium lactate ionic liquid (b) and difunctional crosslinker (c) through photopolymerization.
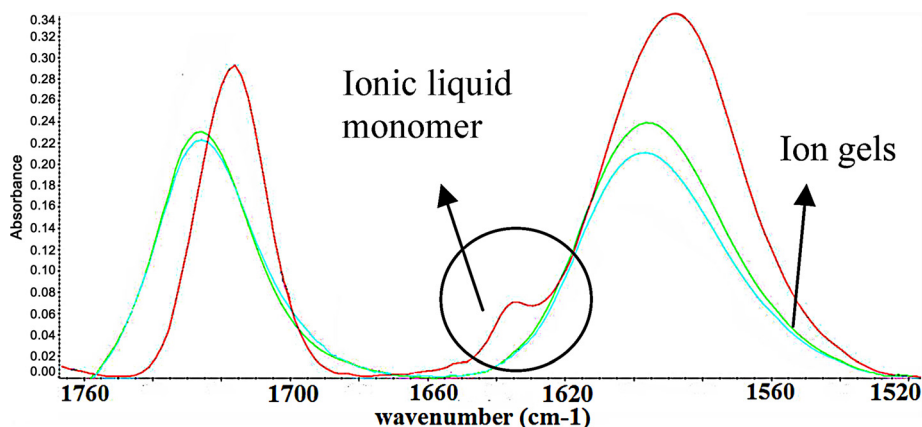
Figure 4.
ATR-FTIR spectra of the ion gels and the ionic liquid monomer (red line) in 1520–1760 cm^{-1} region.

40 wt% monomer. 4 wt% difunctional crosslinker monomer was introduced (Figure 3) to increase the integrity of the final material. The mixture of ionic liquid and monomer was adjusted as 1 gr and casted into a mold to give a film having a thickness around 0.5 mm. ATR-FTIR was used to determine the extent of photopolymerization by following the dissappearance of C=C stretching band which should be present in the monomer but not in the polymeric form. The dissappearance of C=C stretching band around $1640\,cm^{-1}$ confirmed the conversion of the monomer to polymeric form (Figure 4).

All the ion gels produced were homogeneous, meaning that there was no phase separation between the polymer matrix and the ionic liquid after photopolymerization. While the ion-gel that is produced without the crosslinker was soft and jelly-like, the ion gel with 4 wt% difunctional crosslinker displayed better integrity as it can be seen from the Figure 4d. Ion-gels are important materials for emerging technologies and this work presents ion gels based in low toxicity cholinium ionic liquids[9] which may open their application in fields like bioelectronics.

Conclusion

A new cholinium based ionic liquid monomer was designed and used for the preparation of cellulose composites and biocompatible ion gels through fast and simple photopolymerization method. The coatings that were obtained were transparent indicating good processability of cellulose in the ionic liquid monomer. Cholinium based homogeneous ion gels were produced with the combination of cholinium lactate ionic liquid and 2-cholinium lactate methacrylate ionic liquid monomer.

[1] M. N. Belgacem, A. Gandini, In *Monomers, Polymers and Composites from Renewable Sources*; Elsevier, Amsterdam **2008**, p. 1.

[2] M. Moreno, M. A. Aboudzadeh, M. J. Barandiaran, D. Mecerreyes, *J. Polym. Sci., Part A: Polym. Chem.* **2012**, 50, 1049.

[3] M. A. Aboudzadeh, M. E. Munoz, A. Santamaria, M. J. Fernandez-Berridi, L. Irusta, D. Mecerreyes, *Macromolecules* **2012**, 45, 7599.

[4] R. P. Swatloski, S. K. Spear, J. D. Holbrey, R. D. Rogers, *J. Am. Chem. Soc.* **2002**, 124, 4974.

[5] M. Murakami, Y. Kaneko, J. Kadokawa, *Carbohydr. Polym.* **2007**, 69, 378.

[6] J. Ranke, M. Cox, A. Muller, C. Schmidt, D. Beyersmann, *Toxicol. Environ. Chem.* **2006**, 88, 273.

[7] S. Stolte, S. Abdulkarim, J. Arning, A.-K. Blomeyer-Nienstedt, U. Bottin-Weber, M. Matzke, J. Ranke, B. Jastorff, J. Thoming, *Green Chem.* **2008**, 10, 214.

[8] M. Isik, R. Gracia, L. C. Kollnus, L. C. Tome, I. M. Marrucho, D. Mecerreyes, *ACS Macro Lett.* **2013**, 2, 975.

[9] Y. Fukaya, Y. Lizuka, K. Sekikawa, H. Ohno, *Green Chem.* **2007**, 9, 1155.

[10] J. L. Bideau, L. Viau, A. Voux, *Chem. Soc. Rev.* **2011**, 40, 907.

[11] K. Lunstroot, K. Driesen, P. Nockeemann, L. Viau, P. H. Mutin, A. Vioux, K. Binnemans, *Phys. Chem. Chem. Phys.* **2010**, 12, 1879.

[12] M. A. Neouze, J. L. Bideau, F. Leroux, A. Vioux, *Chem. Comm.* **2005**, 1082.

[13] F. Gayet, L. Viau, F. Leroux, F. Mabille, S. Monge, J.-J. Robin, A. Vioux, *Chem. Mater.* **2009**, 21, 5575.

Study on Weather Aging of Nitrile Rubber Composites Containing Imidazolium Ionic Liquids

Anna Marzec,[2] *Anna Laskowska,*[1] *Gisele Boiteux,*[2] *Marian Zaborski,*[2] *Olivier Gain,*[2] *Anatoli Serghei*[2]

Summary: Weather aging of nitrile rubber composites containing hydrophilic 1-ethyl-3-methylimidazolium thiocyanate (EMIM SCN) and hydrophobic 1-ethyl-3-methylimidazolium bis(trifluoromethylsulfonyl)imide (EMIM TFSI), and 1-allyl-3-methylimidazolium bis(trifluoromethylsulfonyl)imide (AMIM TFSI) ionic liquids was investigated. The mechanical properties at small (dynamic mechanical analysis) and high deformation (tensile test), the hardness and the electrical properties were measured before and after the aging process. It was found that the presence of hydrophobic ionic liquids in the nitrile rubber enhanced the retention of their mechanical properties (tensile strength, stiffness) and slightly reduced surface defects (as determined by scanning electron microscopy), thereby retarding the aging of rubber composites. However, the presence of hydrophilic EMIM SCN in the composite accelerated the degradation of the studied materials because of its high crosslinking activity during the aging process. The electrical studies showed also lower stability of hydrophilic ionic liquid (EMIM SCN) in the studied nitrile matrix (leaking effects) compared to the hydrophobic one (EMIM TFSI, AMIM TFSI).

Keywords: acrylonitrile-butadiene rubber; elastomer composites; ionic conductivity; ionic liquids; mechanical properties; weather aging

Introduction

Nitrile rubber is a type of synthetic rubber that is obtained by the low-temperature polymerization of butadiene and acrylonitrile. Nitrile rubber is mainly used for manufacturing oil-resistant rubber products, which are widely used in the automotive and aerospace industries, oil exploration, petrochemicals, textiles, wire and cable, printing and food packaging.[1] Elastomeric materials are especially sensitive to oxidative degradation. During a long period of service most polymers and their products gradually lose their useful proper-ties as a result of polymer chain degradation. During their outdoor exposure, elastomers containing diene units (C=C) are subjected to different environmental factors.[2–5] Oxygen, high temperature and UV radiation are among the most significant factors degrading polymeric materials by chemical modification at the molecular scale because of their sensitivity towards oxidation.[6–11] After a certain period of time, an oxidized skin is formed on the surface of polymer composites; these oxidative coatings act as stress concentrators. The formation of oxidized groups involves chain scissions and the formation of new covalent bonds between chains (crosslinking), resulting in the deterioration of the physical and mechanical properties of rubber materials.[12–15] The competition between these two opposing phenomena (chain scissions and crosslinking) depends on several factors including the conditions of the aging and the chemical structure of

[1] Technical University of Lodz, Institute of Polymer and Dye Technology, Stefanowskiego 12/16, 90924 Lodz, Poland
Fax: +48(42) 636 25 43;
E-mail: marzec.anna@hotmail.com
[2] University of Lyon, Université Claude Bernard Lyon1, Ingénierie des Matériaux Polymères, UMR CNRS 5223, 43 Bd du 11 Novembre 1918, 69622 Villeurbanne, France

the polymer.[16] Some indicators of polymer oxidation are changes in the mechanical properties (tensile strength, hardness), changes in the weight and color and a change in the glass temperature T_g.[17] Not only the chemical structure of the rubber materials is important with respect to its stability but also additives such as fillers, curatives (peroxides or sulfur-based systems), accelerators, dyes, pigments, modifiers, etc. Few articles have dealt with the influence of reinforcing fillers such as carbon black[18,19] and nano-clay[20] on the thermal aging of elastomer composites. In many cases, dyes and pigments can also have a marked influence on the thermal and photochemical stability of the polymer material.[21,22] Ionic liquids have found use in polymers as plasticizers,[23] antistatic additives[24] and have been used to enhance the ionic conductivity and the mechanical and thermal properties of the polymer composites, as well as to improve the filler dispersion (e.g., carbon nanotubes,[25–27] carbon black,[28,29] or silica[30,31]) in hydrophobic matrices. Some reports have described the thermal degradation of polychloroprene rubber (CR) composites based on unmodified and ionic liquid 1-butyl-3-methylimidazolium bis(trifluoromethylsulfonyl)imide (BMIM TFSI) modified multi-walled carbon nanotubes (MWCNTs).[32,33] The authors concluded that the composites with modified MWCNTs exhibited higher mechanical properties (tensile modulus, hardness) and thermal stability than the composites with unmodified MWCNTs. ILs were also found to have multifunctional roles (as antioxidants, as coupling agents) in the composites. However, a lack of scientific information exists about weather aging the rubber composites with ionic liquids, which is an important issue to predict the polymer lifetime because this aging is induced by light, oxygen, ozone, moisture and any combination of these individual agents. The current work is aimed at studying rubber/ionic liquids composites as a continuation of our previous results.[34] The aim of the present paper was to characterize the changes that occur during weather aging of acrylonitrile-butadiene rubber (NBR) composites filled with hydrophilic 1-ethyl-3-methylimidazolium thiocyanate (EMIM SCN) and hydrophobic 1-ethyl-3-methylimidazolium bis(trifluoromethylsulfonyl)imide (EMIM TFSI), and 1-allyl-3-methylimidazolium bis(trifluoromethylsulfonyl)imide (AMIM TFSI) ionic liquids.

Materials and Methods

Acrylonitrile-butadiene rubber NBR (Perbunan 28-45F) containing 28 wt% of acrylonitrile (Lanxess, GmbH). The Mooney viscosity was (ML1 + 4(100 °C):45). NBR rubber was cured using a conventional sulfur (Siarkpol, Poland)-based crosslinking system in the presence of mercaptobenzothiazole as an accelerator (MBT Lanxess, GmbH). Zinc oxide (Lanxess, GmbH) and stearic acid (Sigma Aldrich, GmbH) were used as activators in the sulfur vulcanization. Hydrophilic fumed silica Aerosil 380 (Evonik Degussa, GmbH) was used as a reinforcing filler. The ionic liquids: 1-ethyl-3-methylimidazolium bis(trifluoromethylsulfonyl)imide (EMIM TFSI), 1-allyl-3-methylimidazolium bis(trifluoromethylsulfonyl)imide (AMIM TFSI), and 1-ethyl-3-methylimidazolium thiocyanate (EMIM SCN) were provided by Sigma Aldrich. The rubber mixture consisted of the following: NBR (100 phr), sulfur (2 phr), mercaptobenzothiazole (2 phr), zinc oxide (5 phr), stearic acid (1 phr), Aerosil 380 (30 phr) and ionic liquid (5 phr). The preparation of the rubber mixtures was performed by following a two-step procedure. Homogenization of the rubber and SiO_2 filler mixed with the ionic liquid was performed in an internal mixer (Brabender Measuring Mixer N50). The rubber compounds were processed at a rotor speed of 50 rpm and an initial temperature of 50 °C. Subsequently, the compounded rubbers were then milled with sulfur, mercaptobenzothiazole, zinc oxide and stearic acid in a laboratory rolling mill (roll dimensions: D = 200 mm, L = 450 mm).

The stress-strain tests before and after aging were performed with a universal material testing machine (Zwick model 1435) with a crosshead speed of 500 mm/min, according to the standard PN-ISO 37-2005. To measure the mechanical properties, five different dumbbell-shaped specimens were punched from each rubber sample (mean ± std). The tensile strength and elongation at break were measured at room temperature. The crosslinking density in the vulcanized network was determined using the method of equilibrium swelling. The vulcanizates were subjected to equilibrium swelling in toluene for 48 h at room temperature. The swollen samples were then weighed on a torsion balance, dried in a dryer at a temperature of $60\,^{\circ}C$ to a constant weight and reweighed after 48 h. The crosslinking density was determined on the basis of the Flory–Rehner equation.[35] The surface morphologies of the composite before and after aging were characterized using scanning electron microscopy with a Zeiss SEM microscope. Prior to the measurements, the samples were coated with carbon. Dynamic mechanical analysis of the composites was performed in a Dynamic Mechanical Analyzer (TA Instrument Q 800 DMA, USA). The storage modulus (E′) and loss tangent (tan δ) were measured in tension mode in the temperature range of -90 to $100\,^{\circ}C$ at a frequency of 10 Hz and a heating rate of $2\,^{\circ}C/min$. Dielectric measurements were conducted with broadband dielectric spectroscopy (Novocontrol alpha analyzer, Hundsagen, Germany) in the frequency range from 10^{-1} to 10^{7} Hz at room temperature. The samples were placed between two copper electrodes with diameters of 20 mm. Weather aging was carried out using a Weather-Ometer (Atlas; Ci4000). The measurement lasted for 216 h and consisted of two alternately repeating segments with the following parameters: daily segment (radiation intensity $0.4\,W/m^2$, temperature $60\,^{\circ}C$, humidity 60%, duration 4 h), night segment (no UV radiation, temperature $50\,^{\circ}C$, humidity 50% duration 3 h). The samples were controlled every 24 hours. The aging coefficient S was calculated according to the following relationship: $S = [TS_A \times Eb_A]/[TS_B \times Eb_B]$, where TS corresponds to the tensile strength, Eb to the elongation at break, and TS_A and Eb_A correspond to the values of the TS and Eb after aging, respectively. The color of the obtained vulcanizates was measured by means of a CM-3600d spectrophotometer. The instrument provided the color in the terms of the CIE $L^*a^*b^*$ color space system. In this color space, L represented the lightness (or brightness), a and b were color coordinates, where $+a^*$ was the red direction, $-a^*$ was the green direction, $+b^*$ was the yellow direction, and $–b^*$ was the blue direction. Moreover, changes in individual components allowed to estimate the total change of color E. The spectral range of the apparatus was 360–740 nm, where the change of color ΔE was calculated by the equation below.

$$\Delta E = \sqrt[2]{(\Delta L)^2 + (\Delta a)^2 + (\Delta b)^2}$$

ΔL corresponds to the difference in the brightness intensity between light and dark, Δa corresponds to the difference of intensity between green and red, Δb corresponds to the difference of intensity between blue and yellow, and the Δ symbol implies the difference in the colors of the samples before and after aging. The spectra of the vulcanizates were recorded with a Nicolet 700 IR spectrophotometer.

Results and Discussion

Tensile properties are commonly used to measure the degradation (damage) of elastomers. The NBR/SiO$_2$/AMIM TFSI and NBR/SiO$_2$/EMIM TFSI samples before aging exhibited higher strain and elasticity compared to the NBR/SiO$_2$/EMIM SCN and neat NBR/SiO$_2$ composites, as previously described.[34] For samples containing EMIM TFSI and AMIM TFSI, the strain at break was found to be approximately 699% and 695% before aging. The mechanical behavior of these materials was different after 24 h of aging, with a lower elongation

at break of approximately 25% and 26% for EMIM TFSI and AMIM TFSI, respectively. The decrease in the elongation at break for the neat NBR/SiO$_2$ was the most pronounced and reached around 35%. The reason for the low elasticity values in the NBR/SiO$_2$ and NBR/SiO$_2$/IL composites was most likely due to the large increase in the composite crosslink density during the aging process (Figure 2 b).

From the results in Figure 1 (a, b, c) a better retention of the mechanical properties was observed in composites using EMIM TFSI and AMIM TFSI (higher S coefficient) as opposed to NBR/SiO$_2$ and NBR/SiO$_2$/EMIM SCN. Figure 1 (a, b) shows the change in the tensile strength and elongation at break of the composites during the aging process. The tensile strength decreases very rapidly for to
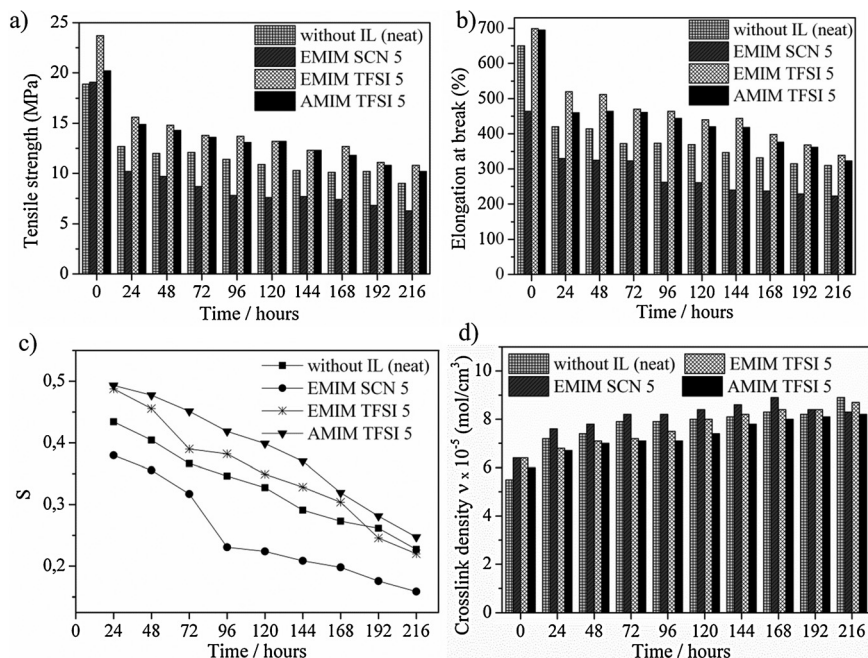
Figure 1.
Tensile strength (a), elongation at break (b), aging coefficient S (c) and crosslink density v (d) as a function of the aging time of the NBR composites.
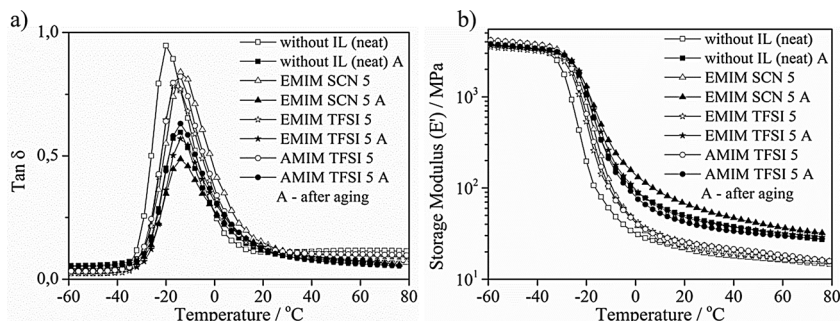
Figure 2.
Temperature dependence of the loss tangent tan δ (a) and the storage modulus E' (b) values at 10 Hz for the NBR/SiO$_2$ and NBR/SiO$_2$/IL composites before and after aging for 216 h.

NBR/SiO$_2$ and NBR/SiO$_2$/EMIM SCN with an increase in the exposure time. However, the decrease in the strain at break of samples with EMIM TFSI and AMIM TFSI was not as rapid as it was observed for NBR/SiO$_2$ and NBR/SiO$_2$/EMIM SCN composites. This is most likely due to the lower tendency to the crosslinks formation in the presence of the hydrophobic ILs in nitrile composites, during outdoor exposure. The EMIM SCN showed a high crosslinking activity during the aging pro-

cess what increased brittleness of the samples and a faster degradation of the polymer. The effect of the weather aging time on the tensile modulus (stress at 100%, 200% and 300% elongation) of the NBR/SiO$_2$ and NBR/SiO$_2$/IL composites is shown in Table 1. The modulus are related to the stiffness and cross-linking density (Figure 2 d) of the rubber compounds. It can be observed that the stress modulus of the compounds increased with the increasing aging time; this increase was especially

Table 1.
The results of the tensile properties as a function of the aging time.

NBR composites	Time [a] hours	SE$_{100}$ [b] MPa	SE$_{200}$ [c] MPa	SE$_{300}$ [d] MPa	TS [e] MPa	Eb [f] %	Hardness Shora A
neat	–	2.2 ± 0.1	3.3 ± 0.1	4.0 ± 0.3	18.9 ± 1.6	650 ± 12	76
neat	24	2.6 ± 0.2	5.1 ± 0.2	6.5 ± 0.3	12.0 ± 2.0	420 ± 10	79
neat	48	3.4 ± 0.2	5.3 ± 0.1	7.8 ± 0.3	11.2 ± 1.1	414 ± 8	81
neat	72	3.1 ± 0.1	5.4 ± 0.2	8.8 ± 0.4	12.1 ± 1.4	372 ± 11	82
neat	96	3.4 ± 0.2	5.5 ± 0.3	8.7 ± 0.3	11.4 ± 1.2	373 ± 12	81
neat	120	3.4 ± 0.3	5.9 ± 0.3	9.8 ± 0.4	10.9 ± 1.2	369 ± 7	82
neat	144	4.1 ± 0.2	7.2 ± 0.3	11.3 ± 0.3	10.3 ± 1.0	347 ± 9	82
neat	168	4.3 ± 0.2	7.3 ± 0.3	11.0 ± 0.4	10.1 ± 0.9	332 ± 10	82
neat	192	4.4 ± 0.3	7.1 ± 0.3	10.8 ± 0.3	10.2 ± 2.0	315 ± 11	83
neat	216	4.5 ± 0.3	7.2 ± 0.3	10.7 ± 0.2	9.0 ± 1.2	310 ± 9	83
EMIM SCN	–	3.0 ± 0.1	5.4 ± 0.2	7.2 ± 0.2	19.1 ± 1.7	464 ± 13	77
EMIM SCN	24	3.3 ± 0.2	5.1 ± 0.2	7.5 ± 0.3	10.2 ± 2.0	330 ± 5	78
EMIM SCN	48	3.5 ± 0.2	4.7 ± 0.3	7.3 ± 0.2	9.7 ± 1.1	325 ± 7	80
EMIM SCN	72	3.5 ± 0.2	5.4 ± 0.1	8.1 ± 0.3	8.7 ± 0.9	323 ± 14	82
EMIM SCN	96	3.7 ± 0.1	5.6 ± 0.2	–	7.8 ± 0.8	262 ± 9	82
EMIM SCN	120	3.8 ± 0.1	5.9 ± 0.4	–	7.6 ± 0.7	261 ± 8	83
EMIM SCN	144	4.4 ± 0.2	6.5 ± 0.2	–	7.7 ± 1.0	240 ± 7	83
EMIM SCN	168	4.7 ± 0.2	7.4 ± 0.3	–	7.4 ± 1.2	237 ± 6	82
EMIM SCN	192	4.6 ± 0.3	7.5 ± 0.4	–	6.8 ± 2.0	229 ± 6	80
EMIM SCN	216	4.6 ± 0.2	7.4 ± 0.3	–	6.3 ± 1.1	223 ± 5	79
EMIM TFSI	–	2.3 ± 2.0	3.1 ± 0.1	4.3 ± 0.3	23.7 ± 2.0	698 ± 15	73
EMIM TFSI	24	3.1 ± 2.0	4.2 ± 0.3	6.0 ± 0.3	15.6 ± 2.2	520 ± 12	75
EMIM TFSI	48	3.4 ± 0.3	4.3 ± 0.2	7.4 ± 0.2	14.8 ± 2.1	512 ± 13	77
EMIM TFSI	72	3.5 ± 0.1	4.1 ± 0.1	5.5 ± 0.1	13.8 ± 2.0	470 ± 14	80
EMIM TFSI	96	3.7 ± 0.2	5.3 ± 0.3	7.4 ± 0.2	13.7 ± 1.3	464 ± 11	80
EMIM TFSI	120	3.6 ± 0.2	5.3 ± 0.1	7.6 ± 0.1	13.9 ± 1.0	440 ± 12	80
EMIM TFSI	144	4.2 ± 0.1	5.6 ± 0.2	8.9 ± 0.3	12.3 ± 1.3	444 ± 13	81
EMIM TFSI	168	4.1 ± 0.2	6.1 ± 0.3	8.4 ± 0.3	12.7 ± 0.9	398 ± 10	83
EMIM TFSI	192	4.3 ± 2.0	6.5 ± 0.3	9.2 ± 0.2	11.1 ± 1.1	368 ± 11	82
EMIM TFSI	216	4.3 ± 0.3	6.8 ± 0.3	9.8 ± 0.4	10.8 ± 0.8	339 ± 7	83
AMIM TFSI	–	1.9 ± 0.1	2.5 ± 0.2	4.0 ± 0.2	20.2 ± 1.4	695 ± 14	73
AMIM TFSI	24	3.3 ± 0.2	4.4 ± 0.3	5.4 ± 0.3	15.1 ± 1.6	460 ± 9	75
AMIM TFSI	48	3.1 ± 0.3	4.1 ± 0.2	5.7 ± 0.3	14.3 ± 1.3	464 ± 13	78
AMIM TFSI	72	3.4 ± 0.1	4.9 ± 0.3	6.8 ± 0.2	13.6 ± 1.1	461 ± 10	80
AMIM TFSI	96	3.4 ± 0.1	5.1 ± 0.3	7.6 ± 0.3	13.1 ± 1.2	444 ± 9	81
AMIM TFSI	120	3.5 ± 0.2	4.9 ± 0.1	7.0 ± 0.2	13.2 ± 1.0	420 ± 8	80
AMIM TFSI	144	3.5 ± 0.3	5.7 ± 0.3	7.8 ± 0.3	12.3 ± 1.3	418 ± 10	80
AMIM TFSI	168	3.7 ± 0.2	5.6 ± 0.2	8.3 ± 0.3	11.8 ± 1.1	376 ± 13	81
AMIM TFSI	192	4.0 ± 0.2	5.8.9 ± 0.1	9.2 ± 0.1	10.8 ± 0.8	362 ± 13	82
AMIM TFSI	216	4.1 ± 0.3	6.0 ± 0.3	9.0 ± 0.3	10.2 ± 1.2	323 ± 9	81

[a] Time – weathering time. [b] SE$_{100}$–modulus at 100% elongation. [c] SE$_{200}$–modulus at 200% elongation. [d] SE$_{300}$–modulus at 300% elongation. [e] TS – tensile strength. [f] Eb – elongation at break.

pronounced for the NBR/SiO$_2$ and NBR/SiO$_2$/EMIM SCN composites. Furthermore, decrement in the stress at 300% elongation of NBR/SiO$_2$/EMIM SCN was observed when the irradiation was longer than 96 h. These changes were directly associated with changes in the original crosslinked structure, i.e., main chain scission and crosslinking.[36] The formation of photo-products and a crosslinked network in the studied materials during aging led to an increase in the stiffness of the composites. As a consequence, the materials become more brittle, lose flexibility and their surface get cracked what results in a decrease in mechanical strength of the samples. The crosslink densities increased for all the samples in the studied aging time. The crosslink density was found to be the highest for NBR/SiO$_2$/EMIM SCN composite. It seems that this IL most likely acts as an accelerator for the formation of crosslinks in NBR sulfur-based systems upon aging. The hardness (Shore A) values of the unaged and aged composites are reported in Table 1. With the increasing aging time, an increment in the hardness was found for all studied composites, which is correlated with an increase brittleness of the samples due to an increase crosslink density.[33,37,38] The lowest values of hardness during weathering were obtained for NBR/SiO$_2$/AMIM TFSI, which is in good agreement with its the lowest crosslink density, as determined from the swelling measurements. For all composites, the difference between the mechanical

responses of the unaged and aged materials is most likely due to the formation of an oxidative layer during the thermal- and photo-aging. In fact, the hardening at the surface during irradiation is linked to the formation of a crosslinked network, and the oxidized products hinder the mobility of the macromolecules.[39,40]

These constraints at the surface of the material imply the formation of cracks during elongation, which leads to a lower strain at break compared to the unaged material. It is well-known that the change in the mechanical properties of materials during aging is due to the changes in the conformation of the macromolecular chains. During the outdoor exposure of rubber, the formation of three-dimensional networks by means of crosslinks leads to a decrease in the chain mobility and a decrease in the loss factor maximum (tan δ).[41] A change in T_g of the composites, as observed from the DMA, is also a sign of crosslinking/scission. An up-shift in T_g indicates crosslinking, and a down-shift in T_g indicates chain scission.[17] Figure 2 and Table 2 show the change of tan δ and the ratio E' of the studied materials before and after 216 h of irradiation.

After 216 hours of the weather aging test, the tan δ of all composites decreased and T_g was shifted to higher temperatures. Only for the EMIM SCN composite was a slight reduction in T_g observed, which was most likely due to the intensification of the chain scission process. Moreover, for NBR/SiO$_2$ and NBR/SiO$_2$/IL, a decrease in tan δ

Table 2.
DMA properties of the NBR composite after aging for 216 h.

NBR composites	Time [a] hours	E' [b] MPa 25 °C	E' MPa 40 °C	tan δ [c]	Value T °C
neat	–	21.3	18.6	0.95	−16.2
neat	216	45.6	37.6	0.60	−15.1
EMIM SCN	–	20.1	17.9	0.85	−13.1
EMIM SCN	216	60.3	46.9	0.57	−14.2
EMIM TFSI	–	24.3	21.1	0.80	−15.6
EMIM TFSI	216	43.8	37.0	0.48	−14.0
AMIM TFSI	–	24.1	21.2	0.85	−15.4
AMIM TFSI	216	39.1	33.7	0.63	−14.3

[a] Time – weathering time. [b] E' – storage modulus. [c] tan δ – loss tangent.

was observed, which suggests variations in the change of the visco-elastic properties during outdoor aging of the NBR-based materials. The lowest changes after the 216 h exposure were found for the NBR/SiO$_2$/AMIM TFSI composite; tan δ values changed from 0.85 to 0.63, which is in good agreement with previously described results. Considering the unaged samples, IL-filled composites demonstrate a lower tan δ than neat NBR/SiO$_2$ due to the higher number of crosslinks. After a 216 h irradiation, we observed increases in the E′ and decreases in the tan δ of all the aged samples compared to their unaged counterparts, which is mainly due to the increase in the crosslinking density.[42] A significant increase in the storage modulus was observed for NBR/SiO$_2$/EMIM SCN (60.3 MPa at room temperatutre), whereas that for NBR/SiO$_2$, the E′ reached 45.6 MPa under the same temperature conditions. However, the increase in the E′ value of composites containing AMIM TFSI (38%, at room temperature) and EMIM TFSI (45%, at room temperature) was lower in the comparison to the NBR/SiO$_2$ sample (54%, at room temperature).

Table 3 illustrates the AC conductivity of the studied samples before and after the aging process. The ionic conductivities of unaged NBR/SiO$_2$ and NBR/SiO$_2$/EMIM SCN were found to be 3.6×10^{-10} S · cm^{-1} and 1.8×10^{-9} S · cm^{-1}, respectively, whereas for the composites containing TFSI anion, NBR/SiO$_2$/EMIM TFSI and NBR/

SiO$_2$/AMIM TFSI, the ionic conductivities were both 1.3×10^{-8} S · cm^{-1}. However after an exposure time of 216 h, the conductivities of the neat NBR/SiO$_2$ and compounds with TFSI anion decreased. This can be explained through the increased crosslink density of aged rubber compounds, that affects T$_g$ of the composites. The increase in T$_g$ value results from lowered mobility of the polymer chains and may decrease the ionic conductivity of the composites. Contrary to the samples discussed up to this point, the conductivity of NBR/SiO$_2$/EMIM SCN shows a slight increase, up to 1.1×10^{-8} S · cm^{-1}. This is most likely because of the hydrophilic nature of the liquid. Due to the action of factors such as temperature and light, the ionic liquid was probably leaked onto the surface of the composite, increasing its conductivity after aging test. This phenomenon was not observed for the composites filled with hydrophobic ionic liquids containing TFSI anion. Better stability in nitrile rubber may be provided by the compatibility of hydrophobic ILs with a hydrophobic polymer matrix and the interaction of the ILs with the functional groups of the polymer. Marwanta[43] reported a Raman study of NBR/EMIM TFSI composites that detected the existence of an interaction between the TFSI anion and the –CN group, which may be responsible for the improved compatibility of this type of ionic liquid with a polar matrix. Das[26] studied the coupling activity of 1-allyl-3-methylimidazolium chloride between diene elastomers and multi-walled carbon nanotubes. He concluded that the double bond present in the of 1-allyl-3-methylimidazolium chloride molecules was chemically linked with the double bond of the diene rubber molecules by sulfur bridges, thus providing superior mechanical and electrical properties. In our investigation 1-allyl-3-methylimidazolium bis(trifluoromethanesulfonyl) imide (AMIM TFSI) has a double bond attached to the imidazolium cation ring, which can exhibit similar behavior in nitrile rubber and improve the ionic liquid stability in the polymer matrix.

Table 3.
Ionic conductivity σ$_{AC}$ after 216 h weathering for the NBR composites.

NBR composites	Time [a] hours	σ$_{AC}$[b] S · cm^{-1}, 1 kHz, 25 °C
neat	–	3.6×10^{-10}
neat	216	9.7×10^{-11}
EMIM SCN	–	1.8×10^{-9}
EMIM SCN	216	1.1×10^{-8}
EMIM TFSI	–	1.3×10^{-8}
EMIM TFSI	216	4.6×10^{-9}
AMIM TFSI	–	1.3×10^{-8}
AMIM TFSI	216	8.8×10^{-9}

[a] Time – weathering time. [b] σ$_{AC}$ – AC conductivity, 1 kHz, 25 °C.

Surface Analysis

Colorimetric studies in the CIE L*a*b* system provided information on the color characteristics of the composites after weather test (Figure 3). The coefficient ΔE defines to what extent the color of the samples changed during the 216 h exposure time. The obtained data indicated that the color of all the studied samples changed after 24 h of irradiation, especially that of the NBR/SiO$_2$/EMIM SCN composite. The significant change in color of this sample can be explained by the weak light stability of the 1-ethyl-3-methylimidazolium thiocyanate ionic liquid. The EMIM SCN salt is often yellow or orange in color and darkens upon extended exposure to sunlight. The thiocyanate ion is known to dimerize to thiocyanogen $(SCN)_2$ under chemically or electrochemically oxidative conditions in melt and then polymerize to polythiocyanogen $(SCN)_x$. Both thiocyanogen and polythiocyanogen are known to be photoactive.[44–46] Ionic liquids with the TFSI anion seem to not influence significantly on the surface color of the composites during irradiation, as the values of the ΔE coefficients in these samples were similar to those of the neat.

The micro-morphology and microstructures of the composites were investigated by scanning electron microscopy. Figure 4 presents the SEM photos of the NBR/SiO$_2$ and NBR/SiO2/AMIM TFSI composites

before and after 216 h of the weather test. The vulcanizates before aging (4 a, d) are characterized by their smooth surface and uniform structure. A series of cracks of varying size appeared on the surface of the composites after the aging process. This is due to the rupture of the macromolecular network structure on the nitrile rubber surface or molecular chain crosslinking or degradation, thereby forming surface defects. In the case of NBR/SiO$_2$, significant changes in the surface morphology after aging were observed; the cracks are very prominent as a result of the surface oxidation. It is worthwhile to note that the pictures were taken at different areas of the composites. The SEM pictures of NBR/SiO$_2$/AMIM TFSI also showed surface defects, but they were not as serious as those in the NBR/SiO$_2$. In the composites containing ionic liquids, we noticed fewer but deeper cracks and areas that were almost free from damage. To confirm the post-aging chemical changes of the composites, they were analyzed using ATR-FTIR spectroscopy. After a 24 h aging, the changes in the analyzed spectra of the rubber/ionic liquid composites were slightly lower in comparison to those in the spectrum of NBR/SiO$_2$. Nevertheless, further differences between the aged (more than 24 h) composites were found to be marginal.

Conclusion

The weather aging of nitrile rubber composites was investigated and the effect of the presence of hydrophilic and hydrophobic ionic liquid was reported. The mechanical properties NBR/SiO$_2$ and NBR/SiO$_2$/IL at small (DMA) and high deformation (tensile test) were studied. The NBR/SiO$_2$/EMIM SCN composite subjected to the weather test displays the lowest values of elongation at break and tensile strength, as well as the highest stiffness (highest E′ modulus). This result can be explained by the fact that the hydrophilic liquid EMIM SCN not only accelerates the crosslinking
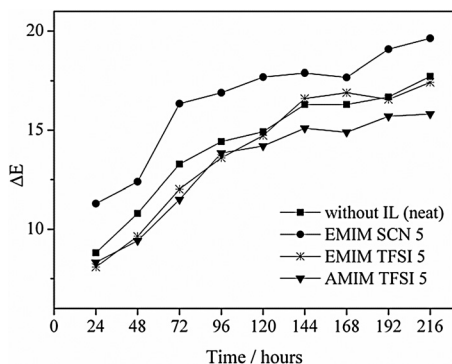
Figure 3.
Color difference (ΔE) of the nitrile composites containing ionic liquids after weather aging.
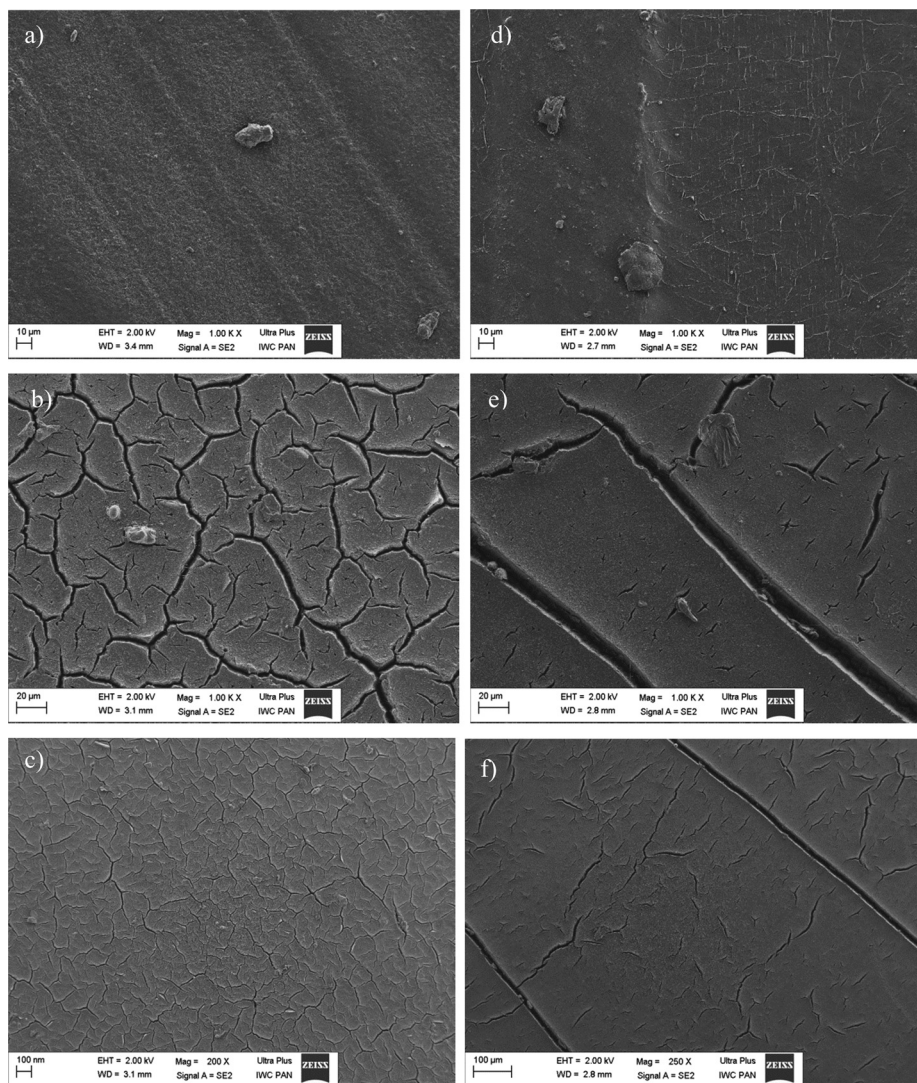
Figure 4.
SEM micrographs of (a) NBR/SiO$_2$ before aging, (b, c) NBR/SiO$_2$ after 216 h aging, (d) NBR/SiO$_2$/AMIM TFSI before aging, (e, f) NBR/SiO$_2$/AMIM TFSI after 216 aging.

during vulcanization but is also activated during aging, contributing to a faster degradation of the polymer. The smallest changes in the mechanical and visco-elastic (tan δ) properties after aging were shown by the rubber/ionic liquids composites with the TFSI anion, especially AMIM TFSI. Moreover, the study on the dependence of the electrical conductivity of the weather aging demonstrated a better stability of the hydrophobic IL (EMIM TFSI, AMIM TFSI) in the polymer matrix compared to the hydrophilic IL (EMIM SCN). The fracture morphology of the composites containing both types of ionic liquids showed less cracks and roughness on the surface than the control composite. Nevertheless, after aging, differences in the spectra of the NBR/SiO$_2$ and NBR/SiO$_2$/IL composites were found to be marginal. It

can be concluded that the studied hydrophobic ionic liquids, 1-ethyl-3-methylimidazolium bis(trifluoromethylsulfonyl)imide (EMIM TFSI) and 1-allyl-3-methylimidazolium bis(trifluoromethylsulfonyl)imide (AMIM TFSI) retarded the aging process of nitrile rubber composites exposed to outdoor conditions.

[1] C. A. Mahieux, D. Lehmann, A. des Ligneris, *Polym. Test* **2002**, *21*, 751.

[2] G. Mertz, F. Hassouna, P. Leclère, A. Dahoun, V. Toniazzo, D. Ruch, *Polym. Degrad. Stab.* **2012**, *97*, 2195.

[3] M. Piton, A. Rivaton, *Polym. Degrad. Stab.* **1996**, *53*, 343.

[4] C. Adam, J. Lacoste, J. Lemaire, *Polym. Degrad. Stab.* **1989**, *24*, 185.

[5] C. Adam, J. Lacoste, J. Lemaire, *Polym. Degrad. Stab.* **1989**, *26*, 269.

[6] P. O. Bussière, J. L. Gardette, J. Lacoste, M. Baba, *Polym. Degrad. Stab.* **2005**, *88*, 182.

[7] G. Y. Li, J. L. Koening, *Rubb. Chem. Technol.* **2005**, *78*, 355.

[8] S. W. Beavan, D. Philips, *Eur Polym. J* **1974**, *10*, 593.

[9] J. Lacoste, C. Adam, N. Siampiringue, J. Lemaire, *Eur. Polym. J.* **1994**, *30*, 443.

[10] M. Piton, A. Rivaton, *Polym. Degrad. Stab.* **1997**, *55*, 147.

[11] K. W. Ho, *J Polym. Sci.* **1986**, *24*, 2467.

[12] R. L. Pecsok, J. R. Shelton, J. L. Koenig, *Rubber Chem. Technol.* **1981**, *49*, 324.

[13] S. Yano, *Rubber Chem. Technol.* **1980**, *54*, 1.

[14] J. Lucki, B. Ranby, J. F. Rabek, *Eur Polym. J* **1979**, *15*, 1089.

[15] F. A. Bottino, A. R. Cinquegrani, G. Di Pasquale, L. Leonardi, A. Pollicino, *Polym. Test* **2004**, *23*, 405.

[16] E. Jubete, C. M. Liauw, K. Jacobson, N. S. Allen, *Polym. Degrad. Stab.* **2007**, *92*, 1611.

[17] T. Gates, The physical and chemical ageing of polymeric composites. In: R. Martin, (Ed., *Ageing of composites*, Woodhead Publishing Limited and CRC Press, LLC **2008**, p. 3–33.

[18] A. R. Azura, S. Ghazali, M. Mariatti, *J. Appl. Polym. Sci.* **2008**, *110*, 747.

[19] S. S. Hamza, *Polym. Test* **1998**, *17*, 131.

[20] A. Choudhury, A. K. Bhowmick, M. Soddemann, *Polym. Degrad. Stab.* **2010**, *95*, 2555.

[21] D. Ruch, J. Exposito, C. Becker, F. Aubriet, *Surf. Interface Anal.* **2008**, *40*, 668.

[22] C. Saron, M. I. Felisberti, F. Zulli, M. Giordano, *J. Braz. Chem. Soc.* **2007**, *18*, 900.

[23] M. P. Scott, C. S. Brazel, M. G. Benton, J. W. Mays, J. D. Holbrey, R. D. Rogers, *Chem. Commun.* **2002**, *7*, 1370.

[24] J. Pernak, A. Czepukowicz, R. Prozniak, *Ind. Eng. Chem. Res.* **2001**, *40*, 2379.

[25] K. Subramaniam, A. Das, G. Heinrich, *Compos. Sci. Technol.* **2011**, *71*, 1441.

[26] A. Das, K. W. Stockelhuber, R. Jurk, J. Fritzsche, M. Kluppel, G. Heinrich, *Carbon* **2009**, *47*, 3313.

[27] K. Subramaniam, A. Das, D. Steinhauser, M. Klüppel, G. Heinrich, *Eur. Polym. J.* **2011**, *47*, 2234.

[28] M. Tunckol, J. Durand, Ph. Serp, *Carbon* **2012**, *50*, 4303.

[29] H. Kreyenschulte, S. Richter, T. Gotze, D. Fischer, D. Steinhauser, M. Kluppel, *Carbon* **2012**, *50*, 3649.

[30] Y. Lei, Z. Tang, L. Zhu, B. Guo, D. Jia, *Polymer* **2011**, *52*, 1337.

[31] Y.D. Lei, Z.H. Tang, B.C. Guo, L.X. Zhu, D.M. Jia, *Express Polym. Lett* **2010**, *4*, 692.

[32] K. Subramaniam, A. Das, L. Häußler Ch. Harnisch, K.W. Stöckelhuber, G. Heinrich, *Polym. Degrad. Stab.* **2012**, *97*, 776.

[33] K. Subramaniam, A. Das, G. Heinrich, *Compos. Sci. Technol.* **2013**, *74*, 14.

[34] A. Laskowska, A. Marzec, G. Boiteux, M. Zaborski, O. Gain, A. Serghei, *Polym. Int.* **2013**, *62*, 1575.

[35] P. J. Flory, J. Rehner, *J. Chem. Phys.* **1943**, *11*, 521.

[36] S. Thiruvarudchelvan, *J. Mater. Process. Technol.* **1993**, *39*, 55.

[37] H. W. Chou, J. S. Huang, *J Appl. Polym. Sci.* **2008**, *110*, 2907.

[38] L. Gonzalez, A. Rodriguez, J. L. Valentin, A. Marcos-Fernandez, P. Posadas, *Kautsch. Gummi Kunstst.* **2005**, *58*, 638.

[39] G. Mertz, F. Hassouna, P. Leclère, A. Dahoun, V. Toniazzo, D. Ruch, *Polym. Degrad. Stab.* **2012**, *97*, 2195.

[40] M. Guzzo, M. A. De Paoli, *Polym. Degrad. Stab.* **1992**, *38*, 41.

[41] M. C. S. Perera, U. S. Ishiaku, Z. A. M. Ishak, *Polym. Degrad. Stab.* **2000**, *68*, 393.

[42] J. Unsworth, Y. Li, *J. Appl. Polym. Sci.* **1992**, *46*, 1375.

[43] E. Marwanta, T. Mizumo, N. Nakamura, H. Ohno, *Polymer* **2005**, *46*, 3795.

[44] J. M. Pringle, J. Golding, C. M. Forsyth, G. B. Deacon, M. Forsyth, D. R. MacFarlane, *J. Mater. Chem.* **2002**, *12*, 3475.

[45] R. E. Panzer, M. J. Schaer, *J. Electrochem. Soc.* **1965**, *11*, 1136.

[46] F. Cataldo, *Polyhedron* **1992**, *1*, 79.

Improving the Ionic Conductivity of Carboxylated Nitrile Rubber/LDH Composites by Adding Imidazolium Bis(trifluoromethylsulfonyl)imide Ionic Liquids

Anna Laskowska,[*1] *Anna Marzec,*[1] *Gisele Boiteux,*[2] *Marian Zaborski,*[1] *Olivier Gain,*[2] *Anatoli Serghei,*[2] *Waldemar Maniukiewicz*[3]

Summary: We investigated the ability of three imidazolium ionic liquids (ILs) (1-ethyl-3-methylimidazolium bis(trifluoromethylsulfonyl)imide (EMIM TFSI), 1-butyl-3-methylimidazolium bis(trifluoromethylsulfonyl)imide (BMIM TFSI), 1-hexyl-methylimidazolium bis(trifluoromethylsulfonyl)imide (HMIM TFSI)) that have the same anion but different alkyl chain lengths of cation in amounts of 2.5, 5, 10 and 15 phr (parts per hundred rubber)to improve the ionic conductivity of carboxylated nitrile butadiene rubber (XNBR)/layered double hydroxide (MgAl-LDH) composites. The presence of these ionic liquids modified the relaxation behavior of the XNBR matrix. Increasing the length of the cation side-chain (from ethyl- to hexyl-) impactsthe glass transition temperature of the rubber matrix, the crosslink density, the mechanical properties and the ionic conductivity of the resulting XNBR/IL-LDH composites. Among this group of ionic liquids, 1-ethyl-3-methylimidazolium bis(trifluoromethylsulfonyl)imide (EMIM TFSI)or alternatively 1-butyl-3-methylimidazolium bis(trifluoromethylsulfonyl)imide (BMIM TFSI)proved most suitable for enhancingthe ionic conductivity of rubber composites without substantial deterioration of their mechanical properties.

Keywords: carboxylated nitrile rubber; composites; dielectric properties; elastomers; ionic liquids

Introduction

Ionic liquids (ILs) are organic salts composed entirely of ions, and most are liquids at room temperature.[1] Many recent publications have demonstrated that ILs play an increasingly important role in the preparation of functional elastomer materi-als. Given their low vapor pressure, non-flammability, high chemical and thermal stability, ILs may serve multiple functions in the preparation of elastomer composites and have been already recognized as processing aids for the melt processing of rubber/filler composites,[2] plasticizers that reduce the glass transition temperature of an elastomer matrix,[3] interfacial modifiers (compatibilizers for improving filler dispersion)[4] and cure accelerators.[5] In addition, ILs can act as ion reservoirsto increase the ionic conductivity of polymer composites.[6] Doping rubbers with ionic liquids is a simple way to change their critical properties including mechanical, thermal and antimicrobial and to prepare composites with high ionic conductivity and good

[1] Institute of Polymer and Dye Technology, Technical University of Lodz, Stefanowskiego 12/16, 90924 Lodz, Poland
Fax: (+48) 426362543;
E-mail: anna.laskowska@hotmail.com
[2] Ingénierie des Matériaux Polymères, Université Claude Bernard Lyon1, UMR CNRS 5223, 15 Bd A.Latarjet, 69622 Villeurbanne, France
[3] Institute of General and Ecological Chemistry, Technical University of Lodz, Zeromskiego 116, 90924 Lodz, Poland

elasticity. High ionic conductivity enables ILs to play an important role in enhancing polymer conductivity.ILs based on the bis(trifluoromethylsulfonyl)imide anion (TFSI⁻) are suitable for a wide range of electrochemical applications (supercapacitors, sensors, biosensors) due to their high conductivity and high electrochemical stability. Generally, ionic liquids have excellent ionic conductivity up to their decomposition temperature. Unlike other highly conductive but much less electrochemically and thermally stable ILs(e.g., those containing dicyanamide ($N(CN)_2$) or thiocyanate (SCN) ions), TFSI-based imidazolium salts are characterized by high chemical and thermal stability up to 380 °C.[7] The thermal stability of ILs is a critical factor in their suitability at the high temperaturesinvolved in the melt-blending process.Hydrophobicity (immiscibility with water)[1] is another advantage of TFSI-based imidazolium ILs making them more compatible with hydrophobic rubber matrices, preventing leakage (migration within the polymer matrix), facilitating rubber processing and improving filler dispersion throughout the elastomer matrix. Additionally, the immiscibility with water increases with increasing length of the cation side chain due to the increased surface activity of longer-chain cations.[8] The use of TFSI-based imidazolium ILs as processing aids, filler-matrix compatibilizers (interfacial modifiers) and conductivity enhancers in elastomers has been already reported for hydrogenated nitrile rubber (HNBR),[9] chloroprene rubber (CR),[10–15] nitrile rubber (NBR)[6,16–19] and solution styrene butadiene rubber (SSBR).[20] Most publications present the ability of IL-modified carbon nanotubes (CNTs) or carbon black (CB)[21] to improve rubber conductivity and filler dispersion. Few studies have investigated the ability of substances containinghigh levels of pure ionic liquids to improve the ionic conductivity of rubber materials[6,16–19] (e.g.,Marwanta et al. prepared a conductive rubber material based on a nitrile elastomer (NBR) and an ionic liquid).[6,17] In addition, no information is

available regarding the effect of the imidazolium salt cation structure on the ionic conductivity and other properties of elastomer composites (e.g., crosslink density, mechanical propertiesand glass transition temperature of the rubber matrix). We report the results of our studies on the cure, mechano-dynamical properties and ionic conductivity of rubber composites based on carboxylated nitrile rubber/layered double hydroxide and hydrophobic ionic liquids with the same anion bis(trifluoromethylsulfonyl)imide with backbone lengths of imidazolium cation ring that vary from ethyl to hexyl. Systems such as XNBR/LDH are based on ionic/polar interactions and yield transparent, ionic elastomer materials when crosslinks form due to the acid-base interactions between the carboxylic groups of the XNBR and the LDH filler.

Experimental Part

Materials

The carboxylated acrylonitrile-butadiene rubber XNBR used in this study was Krynac X 750 (7 wt% carboxyl groups, 27 wt% acrylonitrile, Mooney viscosity (ML1 + 4(100 °C):47)) supplied by Lanxess (Germany). Magnesium aluminum layered double hydroxide MgAl-LDH, designated here as LDH (Sigma Aldrich, Germany), served asboth a filler and a curing agent in the XNBR compounds. The ionic liquids 1-ethyl-3-methylimidazolium bis(trifluoromethylsulfonyl) imide (EMIM TFSI), 1-butyl-3-methylimidazolium bis(trifluoromethylsulfonyl) imide (BMIM TFSI) and 1-hexyl-3-methylimidazolium bis(trifluoromethylsulfonyl) imide (HMIM TFSI) (designated here as the general alkyl-MIM TFSI) were supplied by Sigma Aldrich (Germany).

Preparation of the Composites

The LDH (30 parts per hundred rubber (phr)) was combined with varyingquantities (2.5, 5, 10 and 15 phr) of alkyl-MIM TFSI by grinding it until a homogeneous paste was obtained. The rubber compounds were

processed in an internal Brabender N50 measuring mixer at 40 rpm rotor speed and an initial temperature of 60 °C. After approximately 5 minutes of rubber mastication, the mixture composed of the LDH filler and IL was added and homogenized for around 10 minutes. Then, the compounded rubbers were milled in a laboratory two-roll mill (friction ratio 1:1.2, roll temperature = 40 °C, dimensions: diameter = 200 mm, length = 450 mm). The cure characteristics of the XNBR/IL-LDH composites were determined using a moving die rheometer (M < PREFIX > DR </PREFIX > 3000, MonTech, Germany) at 160 °C for 120 minutes. A sinusoidal strain of 7% and frequency of 1.67 Hz were applied. The optimum cure time (t_{90}), scorch time (t_2), minimum torque (ML), maximum torque (MH) and delta torque (ΔM) were determined from the curing curves. The mixed stocks were cured in a standard hot press at 160 °C, for the $t_{90}$of the respective samples. The rubber sheets obtained from thus had a thickness below 1 mm.

Testing and Characterization

The crosslink density within the vulcanized network was determined via equilibrium swelling. The vulcanizates were subjected to equilibrium swelling in toluene for 48 h at room temperature. The swollen samples were then weighted on a torsion balance, dried to a constant weight in a dryer at 60 °C and reweighed after 48 h. The crosslinking density was determined based on Flory-Rehner's equation.[22] Stress-strain tests were performed on a universal material testing machine (Zwick model 1435) with a crosshead speed of 500 mm/minaccording to the standard PN-ISO 37-2007. To measure the tensile properties, five dumbbell-shaped specimens were punched from each rubber sample and the average value of each formulation was reported. The stress at break, modulus at 100%, 200% and 300% elongation and the elongation at break were measured at room temperature. Differential scanning calorimetry (DSC) measurements (Q 200 DSC, TA Instrument, USA) of the samples were performed

at a heating rate of 10 °C min^{-1} in the temperature range from -80 to 180 °C under a nitrogen atmosphere. The glass transition temperatures (T_g) were determined at the midpoint of the step. Dielectric measurements were conducted via broadband dielectric spectroscopy (BDS) (Novocontrol alpha analyzer, Hundsagen, Germany) in the frequency range from 10^{-1} to 10^7 Hz at room temperature. The samples were placed between two copper electrodes with diameters of 20 mm. Dynamic mechanical analysis (DMA) of composites was performed using a dynamic mechanical analyzer (Q 800 DMA, TA Instruments, USA). The storage modulus (E'), loss modulus (E'') and loss tangent (tan δ) were measured in the tension mode within the temperature range from -90 to 100 °C at a frequency of 10 Hz and a heating rate of 2 °C/min. Thermogravimetric analysis (Q 500 TGA, TA Instruments, USA) was performed in the temperature range from 50 to 600 °C under a helium atmosphere at a heating rate of 10 °C/min. The morphology of the elastomer matrices was observed via SEM with a LEO 1530 SEM microscope. The rubber composites were broken down in liquid nitrogen, and the fractured surfaces of the vulcanizates were examined. Room-temperature powder X-ray diffraction patterns were collected using a PANalyticalX'Pert Pro MPD diffractometer in Bragg-Brentano reflecting geometry with(CuKα) radiation from a sealed tube. Data were collected in the 2θrange of 2–70° with a 0.0167° step and 20-s exposition per step.

Results and Discussion

Cure Characteristics, Crosslink Density and Mechanical Properties

The effects of increasing the alkyl chain length of the imidazolium ring from ethyl to hexyl and the increasing the IL quantity from 2.5 to 15 phr were investigated with regards to the curing behavior, crosslink density and stress-strain behavior of the XNBR/LDH. The rheometric parameters of the rubber mixes are provided in Table 1,

Table 1.
Rheometric characteristics of XNBR/IL-LDH composites crosslinked at 160 °C.

ILtype and content	ML[a]	MH[b]	ΔM[c]	t_2[d]	t_{90}[e]	CRI[f]
phr	dNm	dNm	dNm	min	min	min^{-1}
–	1.4	6.6	5.2	4.1	77	1.37
EMIM TFSI 2.5	1.1	5.3	4.2	2.4	63	1.68
EMIM TFSI 5	1.2	5.0	3.8	2.5	62	1.77
EMIM TFSI 10	1.0	4.6	3.6	3.2	62	1.67
EMIM TFSI 15	1.0	5.2	4.2	3.3	61	1.69
BMIM TFSI 2.5	1.2	5.4	4.2	2.5	65	1.60
BMIM TFSI 5	1.1	5.3	4.2	2.6	63	1.65
BMIM TSFI 10	1.1	4.8	3.7	3.2	64	1.64
BMIM TSFI 15	0.8	4.0	3.2	3.8	63	1.69
HMIM TFSI 2.5	1.1	5.3	4.2	2.0	58	1.78
HMIM TFSI 5	1.1	4.9	3.8	2.5	56	1.90
HMIM TFSI 10	0.8	4.3	3.5	3.4	65	1.62
HMIM TFSI 15	0.7	3.9	3.2	3.9	66	1.61

[a] Min. torque.
[b] Max. torque.
[c] Difference between maximum torque and minimal torque, torque increment.
[d] Scorch time.
[e] Optimal curing time.
[f] Cure rate index.

which indicates that such ILs with TFSI$^-$ anionsslightly accelerate the curing process of XNBR by LDH. The optimal cure time (t_{90}) is reduced when a small quantity (2.5 phr) of IL is added and remained almost unchanged regardless of the alkyl side length and the IL content. From the rheometric data we can also observe changes in the minimum torque (ML), which reflects the viscosity of the rubber mix, and the torque increment (ΔM), which is a good indicator of crosslink formation.

Increasing the alkyl chain length of imidazolium cation from ethyl to hexyl decreases the mix viscosity and hinders network formation,whichare reflected in reduced ML and ΔM values in comparison with the reference sample. Numerous studies have determined that ionic liquids containing TFSI$^-$ ions act as plasticizers in rubber compounds.[6,9,16–19] In the current study, the plasticizing effect of 1-hexyl-3-methylimidazolium was found to be the highest likely due to its bulky structure. The mechanism for crosslinking XNBR with magnesium aluminum layered double hydroxides MgAl-LDHs is based on the neutralization of acidic carboxylic groups -COOH (only 7 wt% carboxyl functionalities) by the basic hydroxyl groups presenton

the LDH surface, additionally MgAl-LDH filler may provide the metal ions for metal-carboxylate curing.[23–26] In such systems, a rubber material is substantially reinforced by the strong chemical interactions (polar/ionic) between the carboxylic rubber and the LDH filler rendering the addition of standard curatives unnecessary. Moreover, the crosslinking of XNBR with MgAl-LDH yields transparent properties in the final composite, even in the presence of 30 phr of mineral. The incorporation of TFSI-based IL at loadings 2.5–10 phr had no significant effect on the XNBR/LDH optical properties, however the presence of IL at higher concentration contributed to obtain a cloudy (milky) color material. The mechanical parameters of the control and samples containing IL are presented in Table 2 and Figure 1.

The incorporation of small quantities (2.5 or 5 phr) of TFSI-based IL with an ethyl side chain attached to the imidazolium ring results in a slight increase in the tensile strength (TS) and elongation at break (EB) of the XNBR/IL-LDH composite, however increasing the quantity of EMIM TFSI to 10 or 15 phr decreases stress at break (TS) and yields a rubbermaterial of higher elasticity. The same trend is observed in
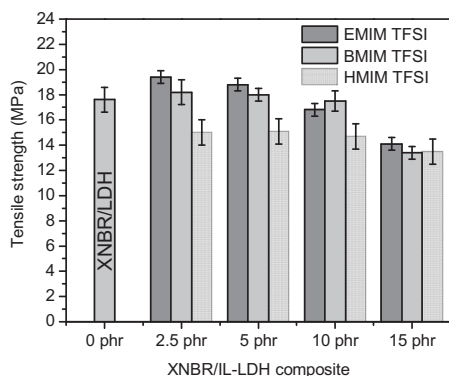
Table 2.
Mechanical properties ofXNBR/IL-LDH composites.

ILtype and content	SE$_{100}$[a)]	SE$_{200}$[b)]	SE$_{300}$[c)]	TS[d)]	EB[e)]	Shore A Hardness
phr	MPa	MPa	MPa	MPa	%	°Sh
–	3.0 ± 0.1	5.3 ± 0.1	6.3 ± 0.1	17.6 ± 2.0	634 ± 20	62
EMIM TFSI 2.5	2.6 ± 0.1	4.4 ± 0.1	5.9 ± 0.1	19.4 ± 0.5	665 ± 20	62
EMIM TFSI 5	2.5 ± 0.1	4.3 ± 0.1	5.9 ± 0.1	18.8 ± 0.5	677 ± 10	62
EMIM TFSI 10	2.2 ± 0.1	3.7 ± 0.1	5.1 ± 0.1	16.8 ± 0.5	678 ± 30	61
EMIM TFSI 15	1.9 ± 0.1	3.3 ± 0.1	4.6 ± 0.1	14.1 ± 0.5	694 ± 20	59
BMIM TFSI 2.5	2.3 ± 0.1	4.0 ± 0.2	5.5 ± 0.2	18.2 ± 1.0	682 ± 10	63
BMIM TFSI 5	2.2 ± 0.1	3.8 ± 0.1	5.2 ± 0.1	18.0 ± 0.5	685 ± 20	62
BMIM TSFI 10	2.2 ± 0.2	3.7 ± 0.3	5.1 ± 0.5	17.5 ± 0.8	690 ± 20	62
BMIM TSFI 15	1.7 ± 0.1	2.8 ± 0.1	3.9 ± 0.1	13.4 ± 0.5	727 ± 20	59
HMIM TFSI 2.5	2.1 ± 0.1	3.5 ± 0.1	4.7 ± 0.1	15.0 ± 1.0	717 ± 20	61
HMIM TFSI 5	2.1 ± 0.1	3.5 ± 0.1	4.8 ± 0.1	15.1 ± 1.0	719 ± 20	60
HMIM TFSI 10	2.0 ± 0.1	3.5 ± 0.1	4.8 ± 0.1	14.7 ± 1.0	725 ± 20	59
HMIM TFSI 15	1.7 ± 0.1	2.8 ± 0.1	3.9 ± 0.1	13.5 ± 1.0	741 ± 20	58

[a)] Stress modulus at 100% elongation.
[b)] Stress modulus at 200% elongation.
[c)] Stress modulus at 300% elongation.
[d)] Tensile strength.
[e)] Elongation at break.

the mechanical parameters when the IL content increasedfor BMIM TFSI and HMIM TFSI. The presence of HMIM TFSI had the greatest impact in increasingthe elongation at break (EB) and decreasingthe tensile strength (TS) of the XNBR/LDH composite. The plasticizing effect from extending the alkyl chain lengthon the imidazolium ring is obvious even at the low concentration of 2.5 phr in the rubber matrix.

The performance characteristics of the rubber materials are maintained despite the

Figure 1.
Effect of ILs type and loading on tensile strength of XNBR/LDH composites.

presence of a high quantity of IL, which in excess acts as a plasticizer in the composite. Additionally, the reduced tensile strength (TS) and increased elongation at break (EB) in the presence of high IL levels in the XNBR/LDH compound result from the lowered crosslink density of the composite. We assume that a thinlayer of IL present onto the filler particle surfacesmay hinderboth the filler-rubber interactions and the formation of ionic crosslinks. The detrimental effect of the TFSI ionic liquids on the rubber network formation in the XNBR/LDH composite was evidenced by equilibrium swelling measurements in toluene. Results from this experiment are presented in Figure 2, which indicates that the decreased crosslink density is a result of the increased IL concentration and the longer alkyl side chain on the imidazolium ring. Compared with BMIM TFSI and HMIM TFSI, the use of EMIM TFSI is more preferable considering mechanical characteristics of the resulting composites.

Effect of ILs on the Glass Transition Temperature (T_g) and Dynamic Mechanical Properties

Dynamic mechanical analysis (DMA) was performed on the reference sample and
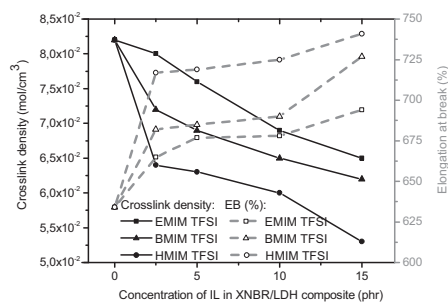
Figure 2.
Effects of ILs type and loading on crosslink density andelongation at break of XNBR/LDH composites.

composites containing 15 phr IL at a vibration frequency of 10 Hz. The loss tangent (tan δ), storage modulus (E') and loss modulus (E'') as functions of temperature are illustrated in Figure 3a–d. The glass transition temperatures (T_g) were measured via DSC and DMA and are reported in Table 3.

Both methods exhibited a single T_g for all composites suggesting no microphase

separation. However, when measuring the T_g of rubber materials, DMA appears more sensitive, providing more precise values than DSC. The incorporation of 15 phr TFSI-based ILs into the XNBR matrix substantially altered the T_g (Table 3) in each case. Increasing the length of the alkyl backbone of the imidazolium ring caused a decrease in T_g (DSC) from -31 °C for the EMIM TFSI sample to -33 °C for the BMIM and HMIM TFSIs. The plasticizing effect of the TFSI-based ILs on various rubber matrices has previously been reported in the literature.[6,9,16–19] Figure 3a demonstrates that the loss tangent (tan δ) of the XNBR/LDH composites presents two relaxations. The low temperature relaxation corresponds to the glass transition temperature (T_g) of the composite. The other relaxation in the temperature range from 20 to 80°C with a maximum at around 50°C is the so-called ionic transition temperature T_i and indicates the existence of ionic crosslinks formed whenthe XNBR is crosslinked by
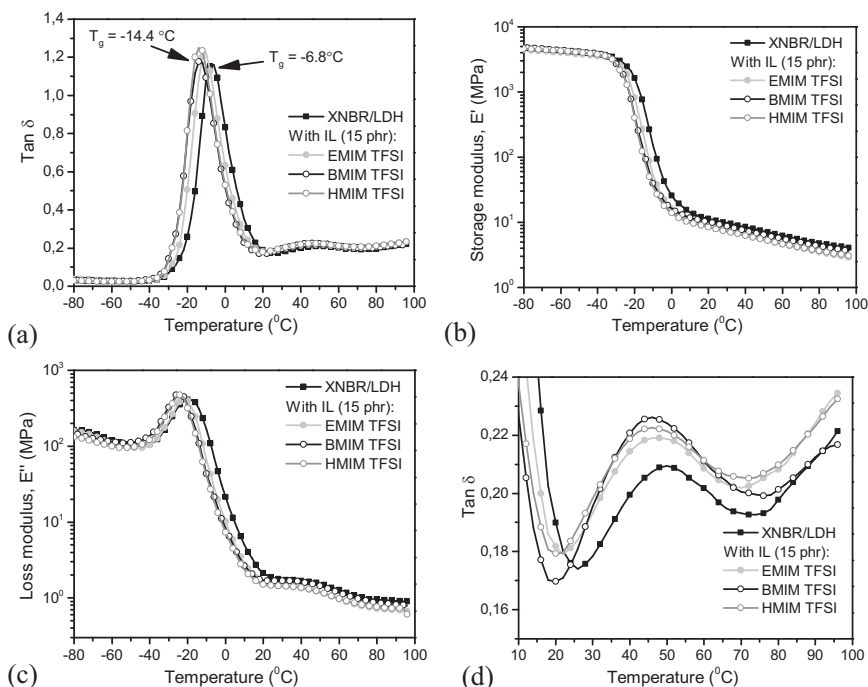
Figure 3.
(a) Plot of tan δ, (b) plot of storage modulusE' (c) plot of loss modulus E''versus temperature (d) ionic transition region of XNBR/LDH composites containing 15 phr of IL.

Table 3.
Glass transition temperature (T_g) derived from DSC and DMA and storage modulus (E') DMA at 10 Hz.

ILtype and content	T_g (DSC)	T_g from E''	T_g from tan δ	Height of tan δ max	E' at 25 °C
phr	°C	°C	°C	–	MPa
–	−23	−17.1	−6.8	1.2	10.4
EMIM TFSI15	−31	−22.0	−10.9	1.2	8.0
BMIM TFSI 15	−33	−24.4	−14.4	1.2	7.9
HMIM TFSI15	−33	−24.9	−14.4	1.3	7.8

the magnesium-aluminum layered double hydroxides LDH.Such clusters melt at higher temperaturescausing an additional tan δ peak during DMA analysis (Figure 3d).

We may observe that the TFSI-based IL at 15 phr of concentration changed the height and position of T_i peak of the XNBR/LDH composite, which is higher
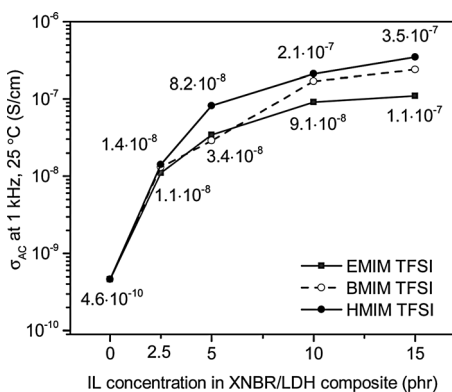
Figure 4.
AC conductivity in function of IL type and amount in XNBR/IL-LDH composites.
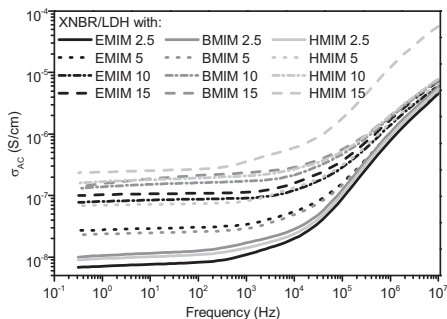
Figure 5.
AC conductivity of XNBR/LDH composites versus frequency, measured at room temperature.

and shifted towards lower temperatures in comparison to the control sample. This transition (ionic transition) takes place in a wide range of temperatures and includes, not only the ionic transition, but also the softening of the material.[27] Analyzing the plots form Figure 3d, we make an assumption that the presence of IL in XNBR/LDH composite softened the hard phase arising from the interactions between XNBR and MgAl-LDH.The tan δ peak maximumis also shifted towards lower temperatures form -6.8 (control) to −10.9 °C (15 phr EMIM TFSI) and approximately −14.4 °C (15 phr BMIM TFSI and 15 phr HMIM TFSI). The changes in T_g in the XNBR/IL-LDH composites depend slightly on the alkyl backbone length in the imidazolium ring of the incorporated IL, however the greatest plasticization was detected in sample containing the HMIM TFSI ionic liquid.

Increased Ionic Conductivity of the XNBR/IL-LDH Composites

The increased level of the ionic liquid in the polymer causes an increase in the ionic conductivity of the composite. However, the improved conductivity of the rubber materials is a function not only of the number of IL ions but also the plasticizing effect of the ILs on the rubber matrix.

The current work (Table 4) confirmed the relationship between the plasticization effect and the increased conductivity of the polymer/IL material. As indicated in Table 4, the decrease in T_g with increasing TFSI-based IL content enhanced the mobility and increased the ionic conductivity. The increased ionic conductivity of the composite can be largely attributed to the

Table 4.
Effects of ILs on glass transition temperature (T_g) and AC conductivity (σ_{AC}) of XNBR/IL-LDH composites (σ_{AC} measured at room temperature).

IL type and content	T_g (DSC)	ΔT_g	σ_{AC}, 1 Hz	σ_{AC}, 1 kHz
phr	°C	°C	$S \cdot cm^{-1}$	$S \cdot cm^{-1}$
–	−23	–	$1.4 \cdot 10^{-10}$	$4.6 \cdot 10^{-10}$
EMIM TFSI 2.5	−24	1	$7.1 \cdot 10^{-9}$	$1.1 \cdot 10^{-8}$
EMIM TFSI 5	−26	3	$2.8 \cdot 10^{-8}$	$3.4 \cdot 10^{-8}$
EMIM TFSI 10	−28	5	$8.0 \cdot 10^{-8}$	$9.1 \cdot 10^{-8}$
EMIM TFSI 15	−31	8	$1.0 \cdot 10^{-7}$	$1.1 \cdot 10^{-7}$
BMIM TFSI 2.5	−24	1	$1.1 \cdot 10^{-8}$	$1.3 \cdot 10^{-8}$
BMIM TFSI 5	−26	3	$2.5 \cdot 10^{-8}$	$2.9 \cdot 10^{-8}$
BMIM TSFI 10	−28	5	$1.2 \cdot 10^{-7}$	$1.7 \cdot 10^{-7}$
BMIM TSFI 15	−33	10	$1.6 \cdot 10^{-7}$	$2.4 \cdot 10^{-7}$
HMIM TFSI 2.5	−24	1	$9.4 \cdot 10^{-9}$	$1.4 \cdot 10^{-8}$
HMIM TFSI 5	−26	3	$7.0 \cdot 10^{-8}$	$8.2 \cdot 10^{-8}$
HMIM TFSI 10	−29	6	$1.3 \cdot 10^{-7}$	$2.1 \cdot 10^{-7}$
HMIM TFSI 15	−33	10	$1.7 \cdot 10^{-7}$	$3.5 \cdot 10^{-7}$

increased motion of the rubber chain segmentsin the XNBR/IL-LDH. In addition, the TFSI-based IL acts a reservoir of effective carrier ions and their increasing concentration in the composite contributes to the higher observed values of σ_{AC}.

Considering the effect of the IL quantity, the sharpest increase in the AC conductivity of a rubber material was observed when 2.5 or 5 phr IL was added, further increases in the IL content resulted in smoother changes in the σ_{AC} for the composites. It seems that theAC conductivity is much more depended on the TFSI-based IL concentration than ontheincrease in the length of the alkyl backbone of the imidazolium ring. The most significant change in $\sigma_{AC}$was reported for the XNBR/LDH sample containing the highest amount of 1-hexyl-3-methylimidazolium TFSI salt. Thedifferences in σ_{AC}values of the samplescontaining EMIM, BMIMand HMIM TFSI at corresponding concentrations are less significant than anticipated.

Effect of ILs on the Thermal Stability
The thermal stability of the XNBR/LDH composites containing 15 phr TFSI-based ILs was analyzed via thermogravimetric analysis (TGA). The TGA curves of the rubber samples with TFSI-based IL exhibited no thermal changes below 252.6°C (Figure 6).

The addition of 15 phr IL increasedthe decomposition temperature at 2% mass loss (T_2) of XNBR/LDH. The ILs used as components in rubber composites should be characterized by sufficient thermal stability to allow them to withstand the high temperatures used during both the melt-blending and curing processes of the composites. The TFSI-based imidazolium ionic liquids satisfy this requirement. The decomposition temperature of the TFSI-based imidazolium ionic liquids is below that of the XNBR/LDH, therefore, the T_5, T_{10} and T_{50} shift toward lower temperatures is observed (Table 5).The observed higher thermal stability of XNBR/LDH/EMIM TFSI composite in
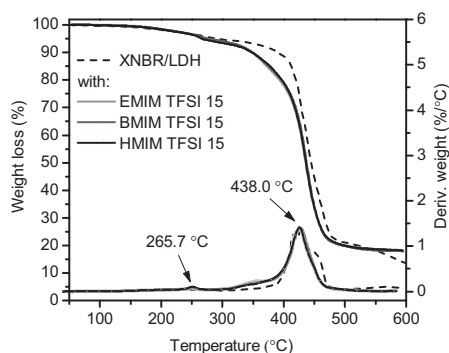
Figure 6.
TGA/DTG curves of XNBR/LDH composites containing 15 phr of TFSI-based IL.

Table 5.
Thermal properties of XNBR/IL-LDH composites containing 15 phr of IL.

| IL type	T_2	T_5	T_{10}	T_{50}	Char residue
	°C	°C	°C	°C	wt%
–	207	291	391	445	13.45
EMIM TFSI	212	274	348	439	18.23
BMIM TFSI	211	265	340	439	18.20
HMIM TFSI	211	264	339	438	18.18

comparison to the others is due to the higher stability of pure EMIM TFSI. The thermal stability decrease with increasing number of carbon atoms in the alkyl chain from methyl to BMIM TFSI, after which no noticeable change in the decomposition temperature (T_d) can be seen.[28]

Effect of the ILs on Morphology
Layered double hydroxide (Figure 7a,b) is characterized by a layered structure and hexagonal shaped particles with lateral dimensions of 50 - 400 nm. We found that the incorporation of a TFSI-based ionic

liquid can improve the filler dispersion throughout the rubber matrix.

The composite containing hydrophobic TFSI-based imidazolium ILs (Figure 7d) exhibited improved filler distribution throughout the elastomer matrix compared with the reference sample (Figure 7c) in which agglomeration within 5 μm was observed. All TFSI-based ionic liquids exhibited good miscibility with the XNBR matrix. The distribution of the TFSI-based ionic liquid in the XNBR/LDH composite was observed via scanning electron microscopy (SEM) combined with energy dispersive
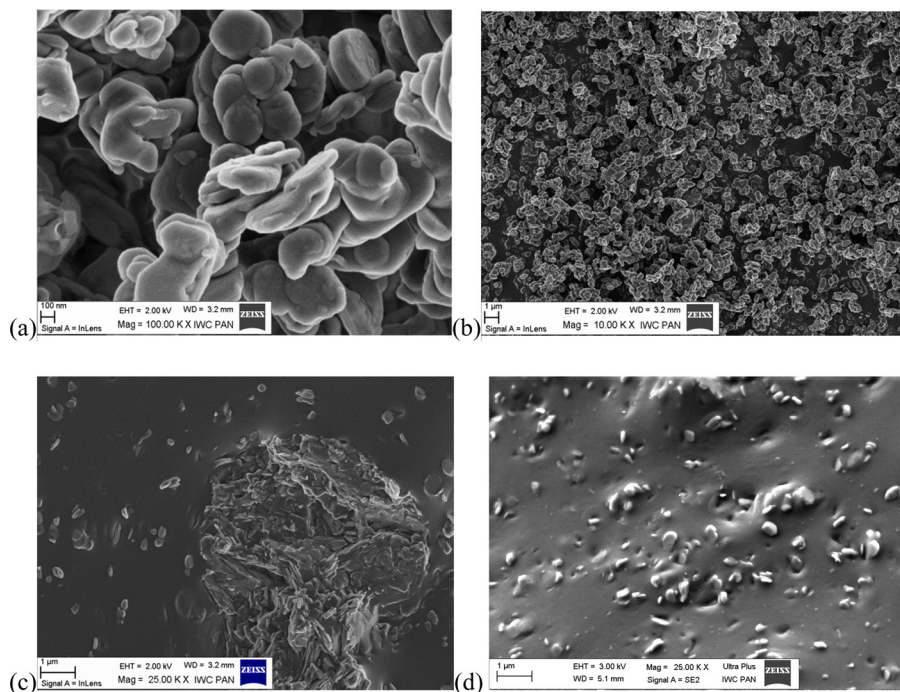
Figure 7.
SEM images of (a, b) LDH particles, (c) XNBR/LDH composite (control sample), (d) XNBR/LDH/BMIM TFSI 15 phr composite.
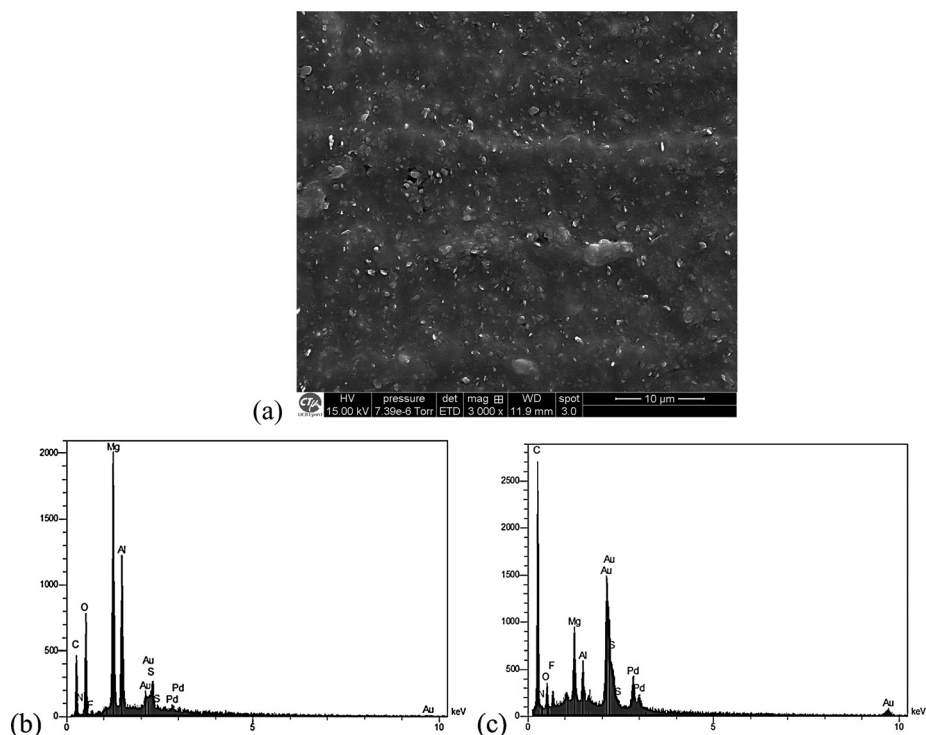
Figure 8.
SEM-EDS mapping of (a) XNBR/LDH/BMIM TFSI 15 phr composite, (b) "filler point", (c) "matrix point".

spectrometry(EDS). The SEM-EDS micrographs of the XNBR/HT containing 15 phr BMIM TFSI are provided in Figure 8(a–c). A higher imidazolium salt concentration (reflected in the intensity of the signal originating from the sulfur and fluorine) was detected in the XNBR matrix (Figure 8c) than at that so-called "filler point" (Figure 8b), which confirms good compatibility between the hydrophobic TFSI IL and the carboxylated rubber.

The effect of 15 phr BMIM TFSI on the XNBR/LDH composite microstructure was also investigated via XRD and the results are presented in Figure 9. The XRD analysis showed the basal reflections (003), (006), (012) and so forth, observed in the crystalline structure of the pure LDH with a 0.76 nm basal spacing (d-value). For the XNBR/LDH and XNBR/LDH/BMIM TFSI composites the positions of the 2θ values remained unchanged from those of the pristine LDH. TheLDH particles used

herein at the substantialconcentration of 30 phr, are rather dispersed as aggregates in rubber matrix,also in the presence of 15 phr BMIM TFSI. The intensities of the reflection peaks for the composite containing IL arebelow those of the control sample, which may be explained through the dilution effect of crystalline phase (30 phr LDH
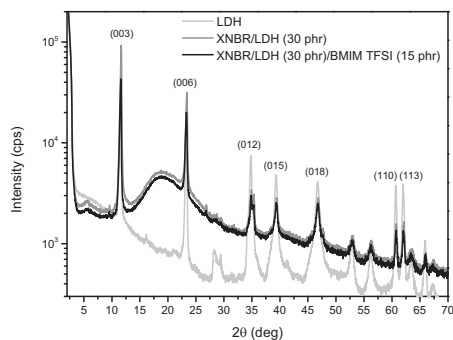
Figure 9.
XRD patterns of pristine LDH and XNBR composites.

and 15 phr BMIM TFSI) or may result from the orientation of the LDH particles in the rubber matrix under the influence of the ionic liquid.

Conclusion

This study examined the relationship between the length of the cation alkyl chain in a TFSI-based IL and the improved ionic conductivity of the XNBR/IL-LDH composite. As indicated, the TFSI-based imidazolium salts act as plasticizers in the rubber matrix and contribute to the reduction in the T_g of the composites. The 1-hexyl-methylimidazolium bis(trifluoro-methylsulfonyl) imide (HMIM TFSI) exhibits the highest plasticizing effect in the XNBR/LDH material and the most efficiently increases the ionic conductivity of the composite. The increased motion in the rubber chain segments and lowered viscosity improve the conductivity. However, the impact of the cation alkyl chain length on this parameter was found to be less significant than it could be anticipated. Therefore, compared with HMIM TFSI, the use of EMIM TFSI (or BMIM TFSI) in rubber composition is more preferable considering both mechanical characteristics and ionic conductivity of the resulting composites.

[1] J. G. Huddleston, A. E. Visser, W. M. Reichert, H. D. Willauer, G. A. Broker, R. D. Rogers, *Green Chem.* **2001**, *3*, 156.

[2] B. Weyershausen, K. Lehmann, *Green. Chem.* **2005**, *7*, 15.

[3] M. D. Bermudez, A. E. Jimenez, J. Sanes, F. J. Carrion, *Macromolecules* **2009**, *14*, 2888.

[4] Y. Lei, Z. Tang, L. Zhu, B. Guo, D. Jia, *Polymer* **2011**, *52*, 1337.

[5] J. Pernak, F. Walkiewicz, M. Maciejewska, M. Zaborski, *Ind. Eng. Chem. Res.* **2010**, *49*, 5012.

[6] E. Marwanta, T. Mizumo, H. Ohno, *Solid State Ionics* **2007**, *178*, 227.

[7] A. A. M. Beigi, M. Abdouss, M. Yousefi, S. M. Pourmortazavi, A. Vahid, *J. Mol. Liq.* **2013**, *177*, 361.

[8] B. D. Fitchett, J. B. Rollins, J. C. Conboy, *J. Electrochem. Soc.* **2005**, *152*, E251.

[9] B. Likozar, *Soft. Matter.* **2011**, *7*, 970.

[10] K. Subramaniam, A. Das, G. Heinrich, *Comp. Sci. Technol.* **2011**, *71*, 1441.

[11] K. Subramaniam, A. das, L. Haussler, C. Harnish, K. W. Stockelhuber, G. Heinrich, *Polym. Degrad. Stab.* **2012**, *97*, 776.

[12] K. Subramaniam, A. Das, D. Steinhauser, M. Kluppel, G. Heinrich, *Eur. Polym. J.* **2011**, *47*, 2234.

[13] D. Steinhauser, K. Subramaniam, A. Das, G. Heinrich, M. Kluppel, *Express Polym. Lett.* **2012**, *11*, 927.

[14] K. Subramaniam, A. Das, G. Heinrich, *Compos. Sci. Technol.* **2013**, *74*, 14.

[15] H. H. Le, X. T. Hoang, A. Das, U. Gohs, K. W. Stoeckelhuber, R. Boldt, G. Heinrich, R. Adhikari, H. J. Radush, *Carbon* **2012**, *50*, 4543.

[16] M. Cho, H. Seo, J. Nam, J. Choi, J. Koo, Y. Lee, *Sens. Actuators, B* **2007**, *128*, 70.

[17] E. Marwanta, T. Mizumo, N. Nakamura, H. Ohno, *Polymer* **2005**, *46*, 3795.

[18] A. Laskowska, A. Marzec, G. Boiteux, M. Zaborski, O. Gain, A. Serghei, *Polym. Int.* **2013**, *62*, 1575.

[19] A. Marzec, A. Laskowska, G. Boiteux, M. Zaborski, O. Gain, A. Serghei, *Eur. Polym. J.* **2014**, *53*, 139.

[20] K. Subramaniam, A. Das, F. Simon, G. Heinrich, *Eur. Polym. J.* **2013**, *49*, 345.

[21] H. Kreyenschulte, S. Richter, T. Gotze, D. Fischer, D. Steinhauser, M. Kluppel, G. Heinrich, *Carbon* **2012**, *50*, 3649.

[22] P. J. Flory, J. Rehner, *J. Chem. Phys.* **1943**, *11*, 521.

[23] A. Laskowska, M. Zaborski, G. Boiteux, O. Gain, A. Marzec, W. Maniukiewicz, *Express Polym. Lett.* **2014**, *8*, 374.

[24] F. R. Costa, S. Pradhan, U. Wagenknecht, A. K. Bhowmick, G. Heinrich, *J. Polym. Sci.* **2010**, *48*, 2302.

[25] D. Basu, A. Das, K. W. Stockelhuber, U. Wagenknecht, G. Heinrich, *Prog. Polym. Sci.* **2014**, *39*, 594.

[26] A. Das, D. Y. Wang, K. W. Stockelhuber, R. Jurk, J. Fritzsche, M. Kluppel, G. Heinrich, *Adv. Polym. Sci.* **2011**, *239*, 85.

[27] L. Ibarra, M. Alzorriz, *J. Appl. Sci.* **2007**, *103*, 1894.

[28] M. Watanabe, H. Tokuda, K. Hayamizu, K. K. Ishii, A. B. H. Susan, *J. Phys. Chem. B* **2005**, *109*, 6103.

Effect of Ionic Liquid Modified Synthetic Layered Silicates on Thermal and Mechanical Properties of High Density Polyethylene Nanocomposites

Sébastien Livi,[1,2,3] *Jannick Duchet-Rumeau,*[*1,2,3] *Jean-François Gérard*[1,2,3]

Abstract: In this work, synthetic layered silicates denoted Somasif ME-100 and Laponite® RD were modified with dialkyl imidazolium and alkyl phosphonium ionic liquids by cationic exchange reaction. In both cases, the phosphonium (P-ME, P-RD) or imidazolium ion (I-ME, I-RD)-treated micas and laponites display an excellent thermal stability compared to commonly used quaternary ammonium salts. To highlight the effect of these ionic liquids, the modified layered silicates were introduced in a high density polyethylene (HDPE). Thus, polyethylene nano-composites filled with a low amount of nanoparticles (2 wt%) were prepared by twin screw extrusion. Then, transmission electronic microscopy (TEM) analysis has been used to investigate the effect of ILs on the different morphologies of these nanocomposites. In addition, the use or not of compatibilizer such as PEgMA (20% by weight) has been also studied on the mechanical behaviour of these polymer nanocomposites. Even though the thermal stability of polyethylene matrix remains unchanged, a good stiffness-thoughness compromise has been observed.

Keywords: cationic exchange; ionic liquid; mechanical properties; nanocomposite; polyethylene; synthetic layered silicates

Introduction

Although the clays are well known for a long time, academic and industrial research were recently focused on the use of organically modified clays as reinforcing agents in polymeric materials.[1–3] In fact, due to their nanometric dimensions, their high specific surface and their high aspect ratios, the addition of layered silicates in polymer matrices can lead to significant effects on the mechanical properties,[4,5] barrier performances[6,7] and flammability resistance.[8] Generally, montmorillonite or synthetic layered silicates (Somasif ME-100) are commonly used.[9,10] However, to obtain a good compatibility between poly-mer and clays during the preparation of nanocomposites, a surface treatment of pristine nanoclays is required.

For years, the alkyl ammonium salts are commonly used[11–13] but nevertheless, their low thermal stability results in a degradation of these salts at 180 °C due to the Hofmann elimination which limits their use in the nanocomposites processing at higher temperatures.[14,15] Thus, to increase the thermal stability of organically modified clays, the use of thermally stable ionic liquids (ILs) such as imidazolium and phosphonium cations can offer a new alternative to ammonium salts.[16–20] According to the literature, imida-zolium and phosphonium ILs are known to have an excellent thermal stability thanks to aromatic ring and phosphore, respectively. However, few studies report the influence of the chemical nature of these surfactant agents on the final properties of the nanocomposites.

In this paper, the use of synthesized ionic liquids as intercalating agents of synthetic

[1] Université de Lyon, F-69003, Lyon, France
[2] INSA Lyon, F-69621, Villeurbanne, France
[3] CNRS, UMR 5223, Ingénierie des matériaux poly-mères, France
Fax: +33 4 72438527;
E-mail: jannik.duchet-rumeau@insa-lyon.fr

clays based on imidazolium and phosphonium cation has been studied in order to obtain thermally stable organically treated clays. Then, a high density polyethylene (HDPE) was selected to be blended with layered silicates treated with thermally stable ionic liquids. Finally, these modified clays with and without the presence of compatibilizing agent denoted PEgMA are incorporated to a HDPE matrix, and the final structure/properties relationships are also studied in detail.

Experimental Part

Materials

A synthetic fluorohectorite, denoted Somasif ME-100 was provided by CO-OP chemical Co., Japan. The Somasif ME-100 has a cation exchange capacity of 70 meq/100g and is described by the following formula $Na_{2x}Mg_{3.0-x}Si_4O_{10}(F_yOH_{1-y})_2$ (x = 0.15-0.5; y = 0.8-1.0). Then, a synthetic hectorite Laponite® RD with intercalated sodium was also selected. The Laponite® RD is a white powder and it's composed of platelets, with a thickness of 1 nm and a diameter of 25-30 nm. The Laponite® RD described by the following formula $Na_{0.65}[Al,Fe]_4$-$Si_8O_{20}(OH)_4$ was purchased from Rockwood additives Ltd. In addition, its cation exchange capacity of 75 meq/100g is similar to Somasif ME-100 one. Triphenylphosphine (Aldrich, 95%), imidazole (Aldrich, 99.5%), iodooctadecyl (Aldrich, 95%), and all the solvents (toluene, sodium methanoate, pentane and acetonitrile) were supplied from Aldrich and used as received.

The polyethylene used in this study, called HDPE, is a high-density polyethylene from Basell, with the trade name Hostalen GF 4750 showing a melt flow index of 0.4. Polybond 3009 was chosen as maleic anhydride grafted HDPE from Chemtura, showing a melt flow index of 5 g/10 min.

Synthesis of Phosphonium and Imidazolium Salts

The synthesis of imidazolium and phosphonium ionic liquids was already reported in previous works.[20,21] The structure of salts

was checked by ^{1}H NMR and ^{13}C NMR spectroscopy collected on a Bruker AC 250 (250 MHz) spectrometer.

Synthesis of Octadecyltriphenylphosphonium Salt
^{13}C NMR (CDCl$_3$): δ 14.00 (**CH**$_3$); 22.67 (**CH**$_2$Me); 23.2; 29.37-29.66; 30.24; 31.85 (P-**CH**$_2$); 118.45; 130.43; 133.70; 135.15 (P-**C**).
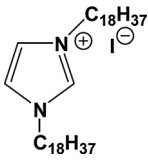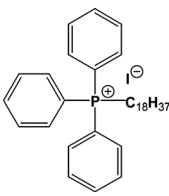
Synthesis of N-octadecyl-N′-Octadecylimidazolium Salt
^{13}C NMR (CDCl$_3$): δ 14.10 (2**CH**$_3$); 22.67 (2**CH**$_2$Me); 26.23; 28.97; 29.35-29.69; 30.24; 31.91 (**CH**$_2$); 50.10; (**CH**$_2$N=); 50.32 (**CH**$_2$N—); 121.69; 122.48 (=**C**N); 136.88 (N—**C**=N).

Organic Modification of Clays

The synthetic layered silicates (2 g, 1.9 meq) were dispersed in 400 mL of deionised water. The amount of surfactant added was about 2 CEC, based on the cation exchanged capacity (CEC = 75 meq/100 g) of the synthetic layered silicates used.[22] This dispersion was mixed and stirred vigorously at 80 °C for 6 h, followed by filtration and continuous washing at 80 °C with deionised water until no iodide ions were detected using an aqueous silver nitrate (AgNO$_3$) solution. The solvent was removed by evaporation *under vacuum*. The modified clays were then dried for 12 hours, at a suitable temperature (not greater than 80 °C). The chemical structure of imidazolium and phosphonium ions used for the exchange reactions are presented in Table 1. The following abbreviations were used to design the different synthetic layered silicates: A phosphonium-treated laponite denoted P-RD, a phosphonium-modified Somasif ME-100 denoted P-ME were obtained when octadecyltriphenylphosphonium iodide was used like surfactant. An imidazolium-modified laponite denoted I-RD, an imidazolium-treated Somasif ME-100 denoted I-ME were obtained when the N-octadecyl-N′-octadecylimidazolium iodide was used like intercalation agent.

Table 1.
Designation of synthesized ionic liquid modified synthetic layered silicates.

Designation	Intercalant
I-ME I-RD	

| P-ME P-RD | |

Processing and Characterization of the HDPE/Clay Nanocomposites

Nanocomposites were obtained by melt intercalation of modified montmorillonite into a high density polyethylene (2% by weight) by using a twin screw DSM micro-compounder. The mixture was sheared for about 3 min with a 100 rpm speed at 190 °C and injected in a 10 mL mould at 30 °C to obtain dumbbell-shaped specimens. Different nanocomposite samples were prepared by varying the surface treatment used to modify the lamellar silicates.

Thermogravimetric Analysis (TGA) of organically modified clay and composites were performed on a Q500 thermogravimetric analyser (TA instruments). The samples were heated from 30 to 800 °C at a rate of 20 K·min^{-1} under nitrogen flow.

Surface Energy of modified clays was determined with the sessile drop method on a GBX goniometer. From contact angles measurements performed with water and diiodomethane as test liquids on pressed modified clay discs, polar and dispersive components of surface energy by using Owens-Wendt theory were determined.[23]

Wide Angle X-ray Diffraction spectra *(WAXD)* were collected on a Bruker D8 Advance X-ray diffractometer at the diffractometry center H. Longchambon. A bent quartz monochromator was used to select the Cu Kα_1 radiation ($\lambda = 0.15406$ nm) and run under operating conditions of 45 mA and 33 kV in Bragg-Brentano geometry. The angle range scanned is 1–10°2θ for the modified clays and 1–30°2θ for the nanocomposite materials.

Uniaxial Tensile measurements were carried out on a MTS 2/M electromechanical testing system at 22 ± 1 °C and 50 ± 5% relative humidity. Tensile tests were performed with a speed of 10 mm·min^{-1}.

The Transmission Electron Microscopy (TEM) was carried out at the Center of Microstructures (Université C. Bernard Lyon) on a Philips CM 120 field emission scanning electron microscope with an accelerating voltage of 80 kV. The samples were cut using an ultramicrotome equipped with a diamond knife, to obtain 60 nm thick ultrathin sections. Then, the sections were set on copper grids.

Results and Discussion

Characterization of Modified Clays

Thermal Stability of Modified Synthetic Layered Silicates

The characterization of imidazolium- and phosphonium-treated synthetic layered silicates was performed by ThermoGravimetric Analysis (TGA) in order to investigate the degradation mechanisms and the influence of the chemical nature of the organic cation on the thermal behaviour of these organically modified clays. Figure 1 represents the TGA and the derivative DTG of P-ME and I-ME while the imidazolium- and the phosphonium-treated laponite RD I-RD and P-RD are reported in Figure 2.

After cationic exchange with the imidazolium and phosphonium salts, the thermal degradation of modified lamellar silicates is similar as one observed for organically treated montmorillonites in a previous study.[24] In fact, two organic species populations have been identified: i) the physically adsorbed species onto the clay surface which are degraded between 300 °C and 400 °C and ii) the interlacted species which are situated in the clay galleries and where the degradation
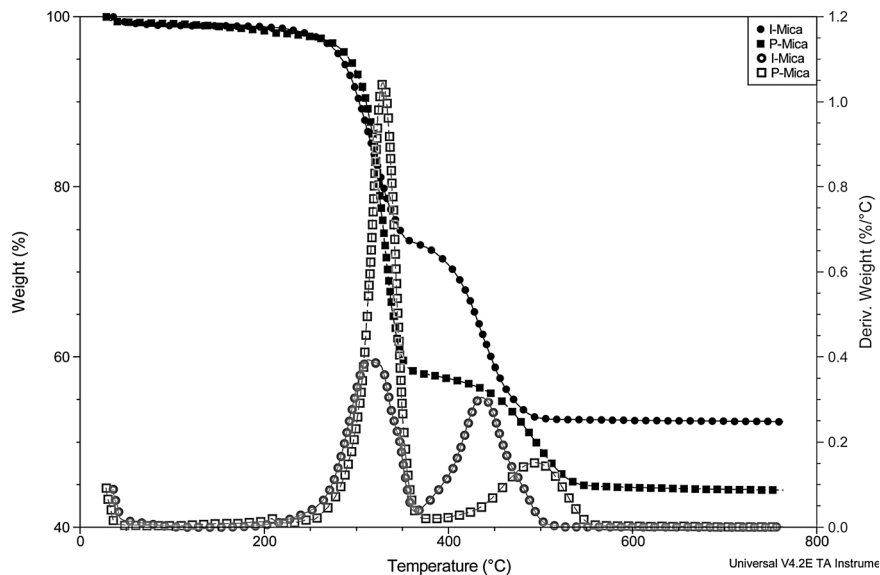
Figure 1.
Weight loss and weight loss derivative as a function of temperature (TGA, DTG) of the imidazolium- and phosphonium-treated mica (I-ME and P-ME) (heating rate: 20 K·min^{-1}, nitrogen atmosphere).

temperatures are between 400 °C and 500 °C. Whatever the chemical nature of surfactant agents (imidazolium or phosphonium), their decomposition temperature clearly exceeds 320°C. These results are in agreement with various studies reported in the literature and highlight the better thermal stability of these ionic liquids compared to commonly used

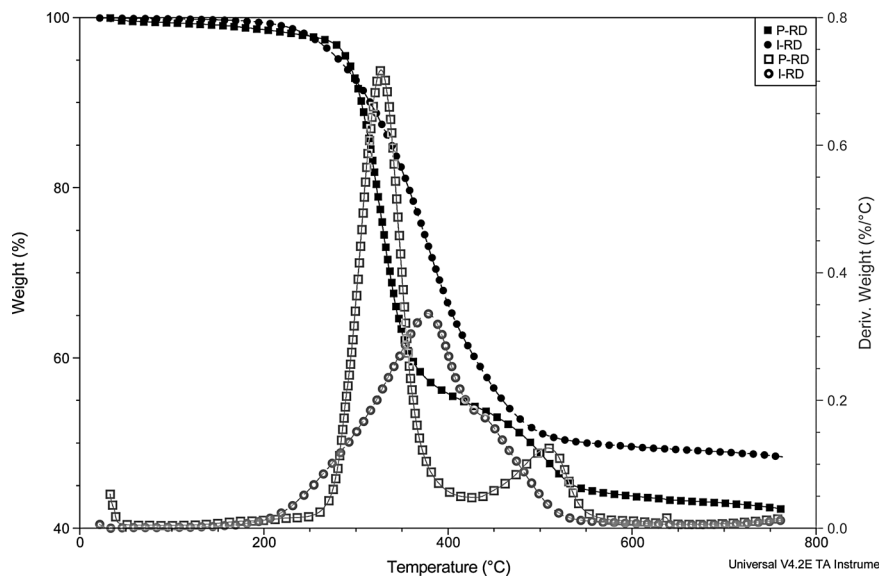

Figure 2.
Weight loss and weight loss derivative as a function of temperature (TGA, DTG) of the imidazolium- and phosphonium-treated laponite (I-RD and P-RD) (heating rate: 20 K·min^{-1}, nitrogen atmosphere).

ammonium salts.[24–25] Nevertheless, the phosphonium IL has a better thermal stability than the imidazolium IL. Indeed, concerning the well intercalated species between clay layers, the use of phosphonium salt causes a shift measured at 60 °C at higher temperatures (500 °C instead of 440 °C) of the degradation peak.

In the case of P-RD, no difference is observed (330 °C for physisorbed species and 510 °C for intercalated ones). Synthetic clays (Mica or Laponite® RD) are modified in the same way by the phosphonium salt. In the opposite, a difference is observed for the imidazolium-treated Laponite® RD. In Figure 2, a main and large peak is observed at 380 °C with the presence of a shoulder at 440 °C. This difference can be explained from the fact that clay has a different geometry and the negative charges are at the surface.

In conclusion, the organic treatment of synthetic clays is successful and is similar to the results obtained for ionic liquid modified montmorillonites in previous study.[20,24] In addition, these new synthesized nanoclays have excellent thermal stability which allows their use in the processing of the nanocomposites at high temperature.[26]

Structural Analysis by WAXD

The cationic exchange is clearly detectable by X-ray diffraction as shown in Figure 3.

Before surface treatment, the basal spacing of the sodic laponite is 1.4 nm, and 1.2 nm for the pristine mica ME-100 which corresponds to the d-spacing of these synthetic clays reported in literature.[27,28] After organic treatment in water by the phosphonium ionic liquid, the P-ME displays a (001) diffraction peak at 2.30°2θ,
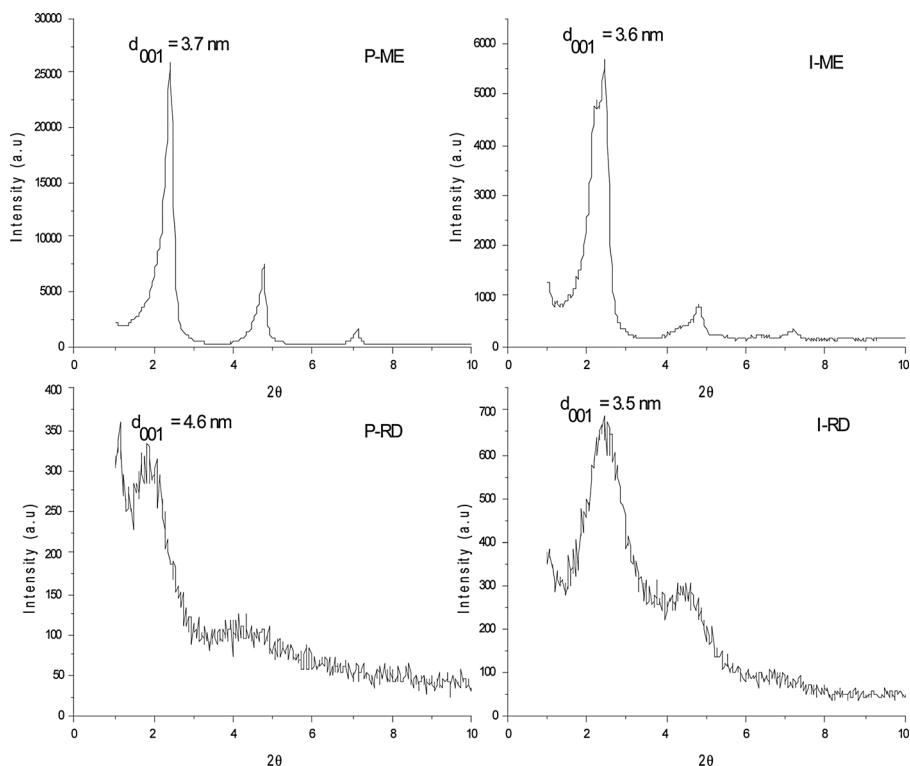
Figure 3.
X-Ray diffraction spectra of ionic liquid modified mica somasif ME-100 and laponite RD: (a) P-ME; (b) I-ME; (c) P-RD; (d) I-RD.

corresponding to an interlayer distance of 3.7 nm while for phosphonium-treated laponite (P-RD), an intercalation distance of 4.6 nm is obtained. These values could be explained by the swelling of layered silicates due to steric volume of the three benzyl rings and the long alkyl chain (C_{18}).

In the case of I-ME and I-RD, the diffraction peaks are situated at 2.35°2θ which corresponds to an interlayer distance of 3.6 nm. These values are characteristics of a paraffinic conformation with trans-trans positions of the alkyl chains. In both cases, the cationic exchange leads to an excellent intercalation of the ionic liquid between basal spacing combined with large interlayer distances (> 3.7 nm) which can allow the intercalation of polymer chains in the clay layers during the preparation of nanocomposites. Compared to ammonium-treated montmorillonites, such as MMT-DMBT (MMT modified with dimethyl benzyl tallow quaternary ammonium) or MMT-DMDT (MMT treated with dimethyl ditallow quaternary ammonium), the interlayer distance values obtained here are higher (3.0 nm for MMT-DMDT and 1.9 nm for MMT-DMBT).[24] Müller et al have also demonstrated that the use of ammonium salts such as hexadecylammonium (HDTA) or octadecylammonium salts in the cation exchange of laponite leads at basal spacings between 2.0 and 2.3 nm which corresponds to a pseudotrimolecular layer of surfactant.[29,30] The authors have also highlighted that high-charged laponite induces an interlayer distance of about 3.0 nm.[31]

Surface Energies of Modified Clays

To evaluate the possible interactions between the organically modified lamellar silicates and polyethylene matrix, the contact angles and surface energy determined by the sessile drop method on pressed powder discs are collected in Table 2.

In both cases, the use of ionic liquids based on phosphonium and imidazolium ions make the synthetic clays (Mica, Laponite) more hydrophobic with a surface energy similar to the surface energy of a polyolefin matrix.[32] In addition, the polar components are very low (0,9–4.6 mN·m^{-1}) which is an evidence that the hydroxyl groups are well covered by the organic chains. In fact, the steric hindrance of imidazolium and phosphonium cations functionalized by benzyl groups and long alkyl chains leads to an efficient screening of the hydrophilic surface of lamellar silicates. However, a slight difference is observed between the Laponite® and mica in terms of surface energy. Indeed, a stronger hydrophobic character is obtained for P-ME and I-ME which can be explained by a larger presence of hydroxyl groups onto the Laponite® surface.

In conclusion, the relevant choice of the surfactant agents i.e its chemical nature plays a key role on the good or poor affinity of modified clays with in the polymer matrix.

Characterization of HDPE/Treated Synthetic Clays Nanocomposites

Morphology of the PE/Clays Nanocomposites

The Figure 4 shows the X-ray spectra performed on the nanocomposites filled

Table 2.
Determination of polar and dispersive components of the surface energy on pristine and on exchanged lamellar silicates from contact angles with water and diiodomethane (determination on pressed clays powders).

Mica/Laponite RD	Θ_{water} (°)	Θ_{CH2I2} (°)	γ polar (mN·m^{-1})	γ dispersive (mN·m^{-1})	γ total (mN·m^{-1})
RD	22.9 ± 0.9	33.6 ± 0.8	30.5	42.7	73.2
I-RD	79.2 ± 0.2	47.5 ± 0.7	4.6	35.7	40.3
P-RD	80.9 ± 0.2	44.1 ± 0.7	3.6	37.6	41.2
I-ME	90.1 ± 0.1	50.2 ± 0.6	3.3	34.1	37.4
P-ME	92.2 ± 0.1	46.2 ± 0.7	0.9	36.4	37.3
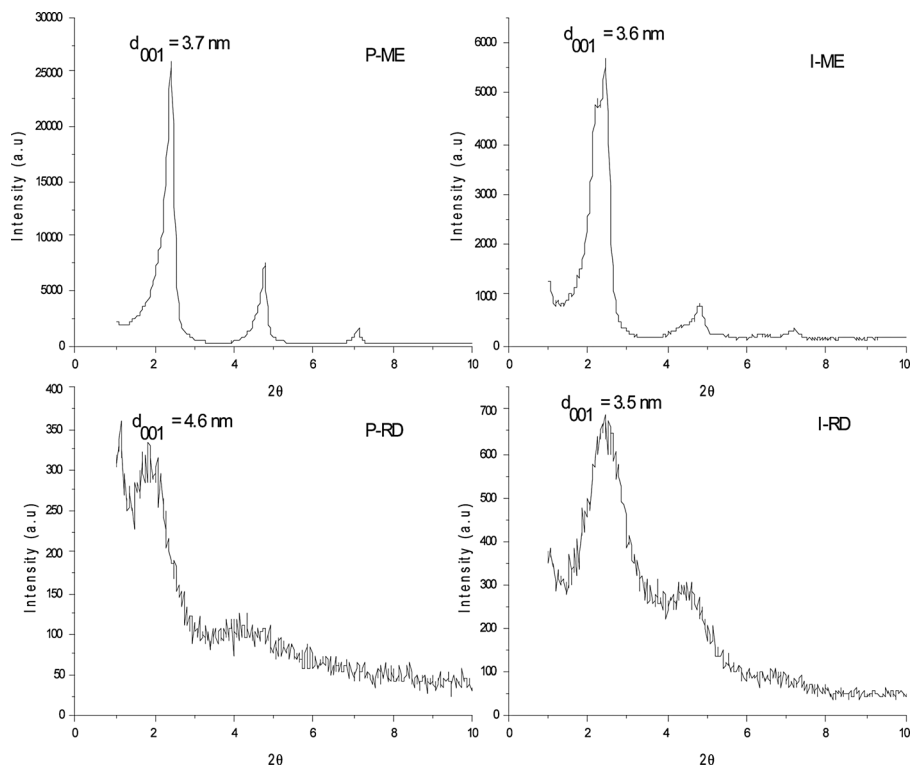
Figure 4.
X-Ray diffraction spectra of nanocomposites based on polyethylene matrix filled with 2 wt% of phosphonium and imidazolium modified mica somasif ME-100 (PE-(P-ME), PE-(I-ME)); phosphonium and imidazolium treated Laponite® RD (PE-(P-RD), PE-(I-RD)).

with the phosphonium and imidazolium modified clays (2 wt%).

The diffraction peaks corresponding to the interlayer distance are located at the same 2θ angle measured for the imidazolium and phosphonium modified synthetic clays (Figure 3). In fact, the nanocomposite based on phosphonium- and imidazolium-modified mica denoted PE-(P-ME) and PE-(I-ME) display a peak at 2.3–2.4°2θ, corresponding to interlayer distances of 3.7–3.8 nm. The same observations were made in the case of PE-(P-RD), PE-(I-RD) nanocomposites. In conclusion, based on the results of the X-Ray diffraction, it seems that the PE chains did not enter in the intergallery spacing when melt intercalation is used to process thermoplastic polymer (TP)-based nanocomposites.

Nevertheless, the distribution and dispersion of synthetic clays in polyethylene

matrix were analyzed by transmission electronic microscopy on the nanocomposites processed with 2 wt% of only P-ME and P-RD. TEM micrographs are reported in Figure 5.

When PE/clays nanocomposites are prepared with phosphonium ionic liquids as intercalating agent of layered silicates (Mica), the morphology is more uniform than the modified laponite one and the TEM micrographs highlight a good level of dispersion of clay layers in the form of isolated layers, despite the presence of small tactoïds. Compared to a previous study,[24] the dispersion of mica in the high density polyethylene matrix is similar to the distribution of the phosphonium- and imidazolium-treated montmorillonites. In the opposite, the surface treatment of the laponite leads to an aggregation of the nanoclays. These results can be explained
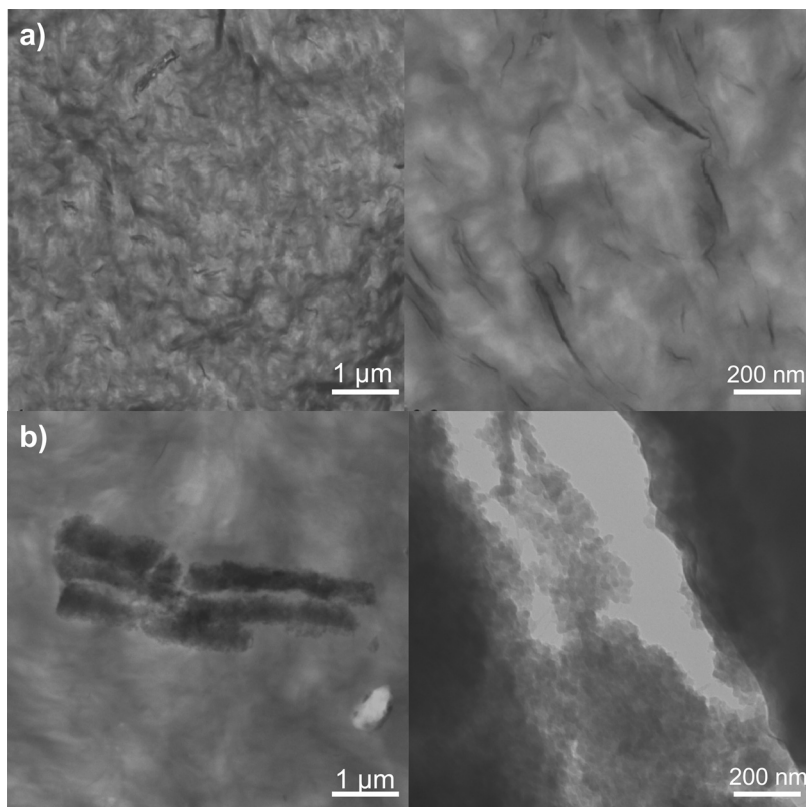
Figure 5.
TEM micrographs performed on 2%wt of (a) phosphonium-treated mica-polyethylene nanocomposites (PE-(P-ME)) and (b) phosphonium-modified Laponite® RD-polyethylene nanocomposites (PE-(P-RD)).

by the small diameter of the laponite (20 nm) and the use of excessive surfactant (2 CEC) which creates a strong attraction of the clay particles. In summary, a very good level of dispersion is obtained for phosphonium- and imidazolium-treated micas without the use of compatibilizing agents such as maleic anhydride-grafted polyethylene (20 wt%), commonly used with ammonium-modified montmorillonites to prepare thermoplastic nanocomposites.[33–35]

Mechanical Properties of the PE/Clays Nanocomposites

The uniaxial tensile properties were performed to highlight the effect of this very small amount of phosphonium- and imidazolium-modified synthetic clays on the mechanical properties of HDPE matrix.

The moduli and fracture properties are summarized in Table 3.

When the polyethylene nanocomposites were processed with imidazolium- and phosphonium-treated micas (PE-(P-ME) and PE-(I-ME)), a significant increase in Young's Modulus is observed without reducing the fracture behaviour. In fact, an improvement of +50% for P-ME and +40% for I-ME are obtained. The effect of phosphonium- and imidazolium-treated micas on the mechanical behavior of these nanocomposites is similar to the influence of ionic liquid modified montmorillonites.[24] In the case of organically modified laponites, their poor dispersion in the polyethylene matrix generates a slight increase in stiffness of 20%. Then, in order to improve the mechanical properties of these nanocomposites, the use of the maleic

Table 3.
Effect of clay on tensile properties of the 2 CEC ionic liquid modified synthetic layered silicates-high density polyethylene nanocomposites (2 wt %) (crosshead speed: 10 mm·min⁻¹).

Sample	Tensile modulus (MPa)	Strain at break (%)	Stress at break (Mpa)
PE	740 ± 10	18 ± 2	84 ± 2
PE-ME	720 ± 25	19 ± 2	71 ± 3
PE-RD	720 ± 25	17 ± 2	62 ± 3
PE-ME-PEgMA	850 ± 15	17 ± 2	75 ± 2
PE-RD-PEgMA	731 ± 20	19 ± 2	78 ± 2
PE-(P-ME)-PEgMA	1033 ± 30	16 ± 2	96 ± 3
PE-(P-RD)-PEgMA	870 ± 10	18 ± 2	76 ± 4
PE-(P-ME)	1100 ± 15	17 ± 2	97 ± 2
PE-(I-ME)	1041 ± 20	17 ± 2	96 ± 4
PE-(P-RD)	887 ± 10	18 ± 2	88 ± 4
PE-(I-RD)	883 ± 15	19 ± 2	87 ± 4

anhydride grafted polyethylene (20 wt%) was investigated.[36] In both cases, when the compatibilizing agent and the ILs-treated synthetic clays are combined, no improvements in mechanical properties are observed. In fact, the addition of PEgMA has no effect on the moduli and on the strain to failure. These results can be explained by the fact that the physisorbed ionic liquids onto the surface of clays act as a compatibilizer and finally, the incorporation of PEgMA is not required. According to the literature, Livi et al have demonstrated that the washing of the excess of salts leads to poor distribution of the fillers in the polymer matrix as well as poor mechanical properties.[24] In conclusion, the ionic liquid has a dual function: it acts as a surfactant agent but also as a compatibilizer.[20,24]

Conclusion

In this work, new surfactants based on imidazolium and phosphonium ionic liquids have been used in order to prepare organically modified synthetic clays with an excellent thermal stability for the processing of nanocomposites at high temperature. In fact, the use of these thermostable ionic liquids as modifier agents leads to a greater increase in the degradation temperature compared to ammonium- and pyridinum-treated

montmorillonites.[11,12] Moreover, large interlayer distance are obtained for P-ME, I-ME, P-RD and I-RD with ionic liquids functionalized by long alkyl chains (C_{18}). In particular, for the phosphonium-treated laponite where an interlayer distances of 4.6 nm is obtained. Compared to the literature, this increase is significantly higher than one induced by the commonly used ammonium-treated laponites.[30,31] Then, the use of ionic liquids-modified mica leads to significant increases in the mechanical properties of polyethylene combined with an excellent dispersion of the clay layers in the polymer matrix without resorting to the use of a compatibilizing agent.

[1] P. C. Le Baron, Z. Wang, T. J. Pinavaia, *Appl. Clay Sci.* **1999**, *15*, 11.

[2] E. P. Giannelis, *Adv. Mater.* **1996**, *8*, 29.

[3] S. M. Auerbach, K. A. Carrado, O. P. K. Dutta, *Handbook of Layered Materials*, Taylor & Francis, New York **2004**.

[4] L. Chui, H. Y. Cho, J. W. Shin, N. H. Tarte, S. I. Woo, *Macromol. Symp.* **2007**, *260*, 49.

[5] S. S. Ray, K. Okamoto, P. Maiti, M. Okamoto, *J. Nanosci. Nanotechnol.* **2002**, *2*, 71.

[6] E. Jacquelot, E. Espuche, J. F. Gerard, J. Duchet, P. Mazabraud, *J. Polym. Sci. Part B: Polym. Phys.* **2006**, *44*, 431.

[7] M. A. Osman, V. Mittal, M. Morbidelli, U. W. Suter, *Macromolecules* **2003**, *36*, 9851.

[8] E. Krishnamoorti, R. A. Vaia, E. P. Giannelis, *Chem. Mater.* **1996**, *8*, 1718.

[9] K. H. Wang, I. J. Chung, M. C. Jang, J. K. Keum, H. H. Song, *Macromolecules* **2002**, *35*, 5529.

[10] S. Sharma, S. Komarneni, *Appl. Clay Sci.* **2009**, *42*, 552.

[11] W. Xie, Z. Gao, K. Liu, W. P. Pan, R. Vaia, D. Hunter, A. Singh, *Thermochim. Acta* **2001**, *339*, 367.

[12] T. D. Fornes, P. J. Yoon, H. Keskkula, D. R. Paul, *Polymer* **2001**, *42*, 9929.

[13] J. W. Gilman, *Appl. Clay Sci.* **1999**, *15*, 31.

[14] A. C. Cope, E. R. Trumbull, *Organic Reactions.* vol. 11, John Wiley and Sons, New York **1960**, pp. 317–487.

[15] S. Y. Lee, W. J. Cho, K. J. Kim, J. H. Ahn, M. Lee, *J. Colloid Interface Sci.* **2005**, *284*, 667.

[16] S. Livi, J. Duchet-Rumeau, J.-F. Gérard, *Eur. Polym. J.* **2011**, *47*, 1361.

[17] V. Mittal, *Eur. Polym. J.* **2007**, *43*, 3727.

[18] W. H. Awad, J. W. Gilman, M. Nyden, R. H. Harris, T. E. Sutto, J. Callahan, P. C. Trulove, H. C. DeLong, D. M. Fox, *Thermochim. Acta* **2004**, *409*, 3.

[19] W. Xie, R. Xie, W. P. Pan, D. Hunter, B. Koene, L. S. Tan, R. Vaia, *Chem. Mater.* **2002**, *14*, 4837.

[20] S. Livi, J. Duchet-Rumeau, T. N. Pham, J.-F. Gérard, *J. Colloid Interface Sci.* **2011**, *354*, 555.

[21] S. Livi, J.-F. Gérard, J. Duchet-Rumeau, *Chem. Commun.* **2011**, *47*, 3589.

[22] S. Y. Lee, W. J. Cho, K. J. Kim, J. H. Ahn, M. Lee, *J. Colloid Interface Sci.* **2005**, *284*, 667.

[23] D. K. Owens, R. C. Wendt, *J. Appl. Polym. Sci.* **1969**, *13*, 1741.

[24] S. Livi, J. Duchet-Rumeau, T.-N. Pham, J.-F. Gérard, *J. Colloid Interface Sci.* **2010**, *349*, 424.

[25] W. Xie, Z. Gao, W. P. Pan, D. Hunter, A. Singh, R. Vaia, *Chem. Mater.* **2001**, *13*, 2979.

[26] K. Stoeffler, P. G. Lafleur, J. Denault, *Polym. Eng. Sci.* **2008**, *48*, 1449.

[27] H. He, J. Duchet, J. Galy, J. F. Gérard, *J. Colloid Interface Sci.* **2006**, *295*, 202.

[28] L. J. Michot, F. Villiéras, *Clay Miner.* **2002**, *37*, 39.

[29] S. Y. Lee, S. J. Kim, *Clays Clay Miner.* **2002**, *50*, 435.

[30] Y. Li, H. Ishida, *Langmuir* **2003**, *19*, 2479.

[31] R. Muller, J. Hrobarikova, C. Calberg, R. Jérôme, J. Grandjean, *Langmuir* **2004**, *20*, 2982.

[32] C. M. Hansen, A. Beerbower, *Kirk-Othmer Encyclopedia of Chemical Technology*. Second ed., vol. 889, Ed. Interscience, New York **1971**.

[33] S. Boucard, J. Duchet, J. F. Gérard, P. Prele, S. Gonzalez, *Macromol. Symp.* **2002**, *194*, 241.

[34] E. Picard, H. Gauthier, J.-F. Gérard, E. Espuche, *J. Colloid Interface Sci.* **2007**, *307*, 364.

[35] M. V. Spencer, L. Cui, Y. Yoo, D. R. Paul, *Polymer* **2010**, *51*, 1056.

[36] S. Boucard, J. Duchet, J. F. Gérard, P. Prele, S. Gonzalez, *Macromol. Symp.* **2002**, *194*, 241.

Influence of Counterion on Thermal, Viscoelastic, and Ion Conductive Properties of Phosphonium Ionenes

Asem I. Abdulahad, Chainika Jangu, Sean T. Hemp, Timothy E. Long*

Summary: Anion metathesis enabled a systematic study focused on the thermal, viscoelastic, and conductivity properties of a 4P,12 phosphonium ionenes with various counterions. Aqueous size exclusion chromatography confirmed the well-defined synthesis of 4P,12-Br from the step-growth polymerization of 1,4-bis(diphenylphosphino) butane and 1,12-dibromododecane at a 1:1 stoichiometric ratio. Subsequent anion-exchange employing a dialysis method exchanged the Br^- counterion to trifluoromethanesulfonate (TfO^-), bis(trifluoromethane) sulfonimide (Tf_2N^-), and tetrafluoroborate (BF_4^-) counterion. ^1H nuclear magnetic resonance spectroscopy of the 4P,12 ionenes showed a distinct upfield chemical shift for methylene protons adjacent to the phosphonium cation after anion-exchange. Thermal characterization using thermogravimetric analysis and differential scanning calorimetry probed the thermal properties of the phosphonium ionenes. Counterion exchange to more bulky and delocalized anions led to improved thermal stabilities and lower glass transition temperatures. Rheological characterization facilitated the generation of time-temperature superposition (TTSp) master curves and pseudo-master curves for each 4P,12 ionene. TTSp revealed two distinct relaxation modes attributed to long-range segmental motion and electrostatic interactions. Anion-exchange resulted in a shift of these two modes of relaxation to higher shear rates. The calculated melt flow activation energy and thermal expansion coefficients were also observed to decrease and increase, respectively. Melt rheological characterization also probed the temperature dependence of the storage and loss moduli and suggested that the counterions have a plasticizing effect on the viscoelasticity of the 4P,12 ionene. Ionic conductivity increased with increasing size of the counterion ($Br^- < BF_4^- < TfO^- < Tf_2N^-$) and demonstrated the viability of these novel materials as potential anion-exchange ionomeric membranes.

Keywords: anion-exchange; conductivity; ionene; phosphonium; structure-property relationship

Introduction

Cationic polyelectrolytes continue to spark intrigue due to their unique physical properties as well as their promise for impacting a variety of emerging technologies. Typical polycations, such as poly(dimethylaminoethyl methacrylate), have positively charged groups within the pendant substituent of the polymer chain, which imparts high charge density and the potential for electrostatic interactions. Due to their inherently high charge density, polycations offer potential in biomedical engineering,[1–4] polymer-based therapeutic formulations,[5–6] battery applications,[7] proton and anion-exchange membranes,[8–9] water and gas purification,[10–12]

Macromolecules and Interfaces Institute, Department of Chemistry, Virginia Tech, Blacksburg, Virginia 24061, USA
Fax: +1 540 231 8517; E-mail: telong@vt.edu

wileyonlinelibrary.com

surface modifiers for chromatographic separations and catalytic applications,[13–14] and electroactive actuation.[15]

Ionenes are a unique class of polycations with cationic charges located within the polymer main chain and are typically prepared according to the Menschutkin reaction of a ditertiary alkylamine with a dihaloalkane.[16] Since Gibbs et al. prepared the first ammonium ionenes from halogenated alkyl dimethylamine A-B monomers,[17] this unique class of polyelectrolytes has expanded to include polycations which incorporate imidazolium,[18] pyridinium,[19] and phosphonium[20] charged groups within the polymer backbone. The breadth of difunctional monomers suitable for step-growth polymerization of ionenes has facilitated the study of charge density and polymer architecture for well-defined polymeric materials with precise spacing between cationic charges in both segmented and non-segmented polymers.

Ionenes are typically designated as x,y-ionene, where x and y respectively correspond to the methylene spacer length of the ditertiary amine and dihaloalkane monomers. The study of structure-property relationships of ionenes has primarily focused on ammonium, pyridinium, and imidazolium containing polymers. Wilkes and co-workers demonstrated the dependence of elastomeric behavior of segmented ammonium ionenes on the poly(tetramethylene oxide) soft segment molecular weight.[19,21] Tamami et al. also showed that the solubility and resulting solution behavior of ammonium-based ionenes is variable as a function of alkyl spacer length and counterion.[22] Hemp and co-workers reported structure-property relationships as a function of alkyl spacer length for novel phosphonium-based ionenes where increasing the alkyl spacer length decreased the charge density of phosphonium ionenes and resulted in dramatic differences in viscoelastic response.[20]

Anion metathesis, with inspiration from ionic liquids, has recently become a popular choice for altering the properties of polyelectrolytes. In several literature reports, dramatic changes in polyelectrolyte solubility, solution behavior, conductivity, and viscoelasticity were observed upon exchanging counterions with varying size and/or basicity.[8,23–32] This manuscript details a fundamental study of the structure-property relationship of counterion size and basicity on the properties of a 4P,12-ionene. Aqueous size exclusion chromatography (SEC) confirmed the preparation of a well-defined 4P,12-Br phosphonium ionene using the Menschutkin reaction. Nuclear magnetic resonance spectroscopy was used to confirmed successful anion metathesis to trifluoromethanesulfonate (TfO^-), bis(trifluoromethane)sulfonimide (Tf_2N^-), and tetrafluoroborate (BF_4^-) counterions. Thermal characterization of each 4P,12-ionene indicated a profound influence from the associated counterion, and rheological characterization was used to elucidate the major relaxations within the bulk material. Rheological characterization as a function of temperature suggests the potential for these polymers in high performance applications, and ionic conductivity measurements demonstrate the viability of these novel materialsas potential anion-exchange membranes.

Materials and Methods

Materials

1,4-bis(diphenylphosphino)butane (98%) was purchased from Sigma-Aldrich and recrystallized from chloroform/methanol. 1,12-Dibromododecane (98%) was acquired from Sigma-Aldrich and was distilled under reduced pressure. Sodium trifluoromethanesulfonic acid (98%), lithium bis-(trifluoromethane)sulfonimide, and sodium tetrafluoroboric acid (48 wt% solution in water) were purchased from Sigma-Aldrich and used without further purification. Tetrahydrofuran, hexanes, methanol, hydrochloric acid, and deionized water were obtained from Spectrum Chemicals and used as received.

Synthesis and Anion Metathesis of 4P,12-Br Phosphonium Ionene

Synthesis of the 4P,12 phosphonium ionene with bromide counterions (4P,12-Br) was accomplished by the Menshutkin reaction as previously reported.[20] Briefly, 1,4-bis-(diphenylphosphino) butane (2.5494 g, 5.98 mmol), 1,12-dibromododecane (1.9612 g, 5.98 mmol), and 14.3 mL dimethylformamide were added to a 25-mL, round-bottomed flask with a magnetic stir bar and purged with argon. The resulting heterogeneous solution was heated to 100 °C to obtain a homogeneous solution, and the polymerization was allowed to proceed for 24 h. The resulting polymer solution was diluted with methanol and dialyzed (SpectraPor dialysis membrane; MWCO = 3500 g/mol) against methanol for 3 d. The methanol was removed using rotary evaporation, and the solid polymer was obtained after drying at 80 °C for 24 h *in vacuo*.

Anion-exchange from bromide counterions to respective counterions of tetrafluoroborate (BF_4^-), trifluoromethanesulfonate (TfO^-), and bis(trifluoromethane) sulfonimide (Tf_2N^-) were each accomplished using a dialysis method. The 4P,12-Br polymer was dissolved in acetone at 5 wt% and 5 molar equivalents of the counterion salt was separately dissolved in acetone. The polymer solution was added to the counterion salt solution dropwise and this mixture was dialyzed against pure acetone. Over a 3 d period, the dialysis solvent was changed and 20 mL of the 5 molar equivalents counterion salt solution was added to the dialysis tubing every 12 h. Subsequently, the anion-exchanged polymer solutions were dialyzed against pure acetone for an additional 3 d (changing the dialysis solvent every 12 h) to remove any excess, non-interacting counterions.

Analytical Methods

Aqueous size exclusion chromatography (SEC) was performed using a mixed mobile phase consisting of 54/23/23 (v/v/v%) water/methanol/acetic acid with 0.1 M sodium acetate, two Waters ultrahydrogel linear columns, and one Waters ultrahydrogel 250 column. The instrumentation used included a Waters 1515 isocratic solvent delivery pump, Waters 717plus autosampler, Waters 2414 refractive index detector, and a Wyatt MiniDawn light scattering detector, which collectively enabled the determination of absolute molecular weight. In order to determine absolute molecular weights, the refractive index dependence on concentration (dn/dc) was obtained using a Wyatt Opti-lab T-rEX refractometer ($\lambda = 658$ nm). Thermogravimetric analysis (TGA) employed a TA Instruments TGA Q50 and the temperature at 5% weight loss was determined by heating from 100 °C to 600 °C at a heating rate of 10 °C/min after an isothermal drying step maintaining a furnace temperature of 100 °C for 60 min. Differential scanning calorimetry (DSC) was accomplished using a TA Instruments DSC Q1000 under nitrogen atmosphere with a heat/cool/heat cycle performed at 10 °C/min. [1]H nuclear magnetic resonance (NMR) spectra were obtained in CD_2Cl_2 at 23 °C using a Varian Unity 400 spectrometer.

Rheological Characterization

Polymer melt rheological characterization was performed under inert atmosphere using a TA Instruments DHR-2 rheometer equipped with an 8 mm parallel plate geometry. Strain-sweep experiments (0.004 - 4.0% oscillatory strain at 1 Hz) were used to first determine the linear viscoelastic region for each anion-exchanged phosphonium ionene. Frequency sweep experiments were performed for each sample at an oscillatory strain of 1.25% using 10 °C temperature steps and an angular frequency range from 0.1 - 100 rad/s. The resulting storage and loss moduli for each polymer were shifted to build master and pseudomaster curves using the TA Instruments provided TRIOS software package. Master curves based on shifting and overlapping of the storage and loss moduli generated horizontal shift factors (a_T). Pseudomaster curves were obtained by fitting only the loss modulus data. According to Arrhenius analysis in the

terminal flow region, the pseudomaster curves provided suitable shift factors for the determination of melt flow activation energies. Figures confirming adherence of master curve shift factors to the Williams-Landel-Ferry equation are displayed in the Supplemental information for Arrhenius analysis to determine values of melt flow activation energy for each ionene. The dependence of storage and loss moduli on temperature was actively assessed with an 8 mm parallel plate geometry using a temperature ramp within the linear viscoelastic region for each phosphonium ionene at 0.5 °C/min, 1.25% oscillatory strain, and an angular frequency of 1.0 rad/s.

Impedance Spectroscopy

Electrochemical impedance spectroscopy (EIS) was performed using an Autloab PGSTAT 302N potentiostat and a four-point electrode sample cell purchased from BekkTeck, Inc. An applied alternating sine-wave potential was applied at 0.2 V with frequencies ranging from 0.1 Hz to 1 MHz. The temperature and relative humidity (RH) was controlled using an ESPEC BTL- 433 environmental chamber, which controlled the temperature to ± 0.1 °C and 10% RH to ± 0.1%. An alternating current was applied to the outer electrodes and the real impedance or resistance, R, was measured between the two inner reference electrodes. The resistance was determined from a high x-intercept of the semicircle regression of the Nyquist plot. The ionic conductivity was determined by $\sigma = L/AR$, where L and A are the distance between the two inner electrodes and the cross-sectional area of the polymer film, respectively. The cross-sectional area is defined as $A = Wl$, where W is the film width and l is the film thickness. Samples were allowed to equilibrate for 1 h at each measurement condition followed by at least five measurements at that condition. The values reported are an average of these steady-state measurements. Polymer films were prepared using a solution cast method. Each anion-exchanged phosphonium ionene was dissolved at 20 wt% in acetone and cast onto

silicon-coated Mylar® film. Each solution casted film was allowed to dry at room temperature for 5 d and subsequently annealed *in vacuo* for an additional 3 d.

Results and Discussion

Polymerization of 4P,12-Br Phosphonium Ionene

Synthesis of phosphonium ionenes was accomplished using the Menschutkin reaction between a ditertiary phosphine and dibromoalkane to yield a cationic phosphonium ionene. Recently published literature from our research group details the preparation of phosphonium ionenes with various alkylene spacer lengths. Similar to ammonium ionenes, phosphonium ionenes were labeled xP,y, where x and y respectively denote the alkyl spacer length in the ditertiary phosphine and dihaloalkane.[20]

Scheme 1A depicts the reaction of 1,4-bis(diphenylphosphino) butane with 1,12-dibromododecane to produce a 4P,12 phosphonium ionene with bromide counterions. The polymerization was accomplished in a one-step synthesis where 1:1 molar equivalents of the ditertiary phosphine and dibromoalkane were added to a 25-mL, round-bottomed flask and reacted in N,N-dimethylformamide for 24 h at 100 °C. Aqueous size exclusion chromatography (SEC) employed a ternary mobile phase mixture of water/methanol/acetic acid (54/23/23 (v/v/v%)) and 0.1 M sodium acetate, which effectively screened electrostatic interactions to enable absolute molecular weight determination using an in-line multi-angle laser light scattering (MALLS) detector. Figure 1 shows the experimentally determined number-average and weight-average molecular weights and the SEC chromatogram for the 4P,12-Br ionene prior to anion metathesis.

Chemical Characterization of Anion-Exchanged 4P,12 Ionenes

Scheme 1B shows a general reaction scheme for the anion metathesis displacing the bromide counterions with tetrafluoroborate (BF_4^-),
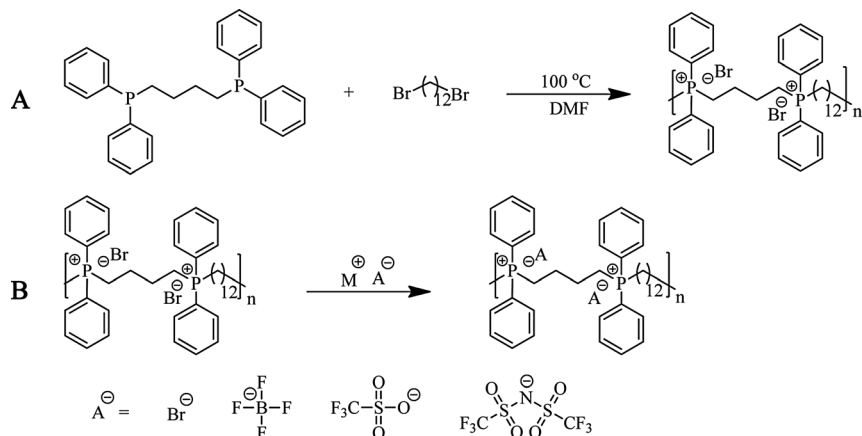
Scheme 1.
Polymerization of 1,4-bis(diphenylphosphino) butane and 1,12-dibromododecae (**A**). Generalized scheme for the anion metathesis of the bromide anion to prepare the 4P,12-BF$_4$, 4P,12-TfO, 4P,12-Tf$_2$N ionenes (**B**).

trifluoromethansulfonate (TfO$^-$), and bis-(trifluoromethane) sulfonimide (Tf$_2$N$^-$). The resulting anion-exchanged phosphonium ionenes were characterized using ^{1}H NMR spectroscopy. The corresponding NMR spectra are displayed in Figure 2, and the spectra interestingly show that anion metathesis from bromide to bulkier fluorinated counterions resulted in an upfield chemical shift for methylene protons adjacent to phosphonium cations. Anion-exchange to Tf$_2$N$^-$ shows the most pronounced upfield shift as compared to the 4P,12-Br precursor. Two distinct chemical shifts exist for the phosphonium ionene precursor at 3.57 and 3.14 ppm, while the 4P,12-Tf$_2$N derivative shows a bimodal

peak near 2.75 ppm. ^{1}H NMR spectroscopy confirmed complete anion metathesis due to the complete shift of the two methylene peaks.

Influence of Thermal Properties on Counterion
Thermogravimetric analysis (TGA) and differential scanning calorimetry (DSC) indicated that the counterion displayed a strong influence on the thermal properties
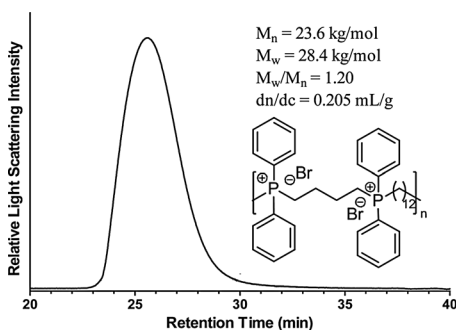
Figure 1.
Aqueous SEC chromatogram of the 4P,12-Br phosphonium ionene.
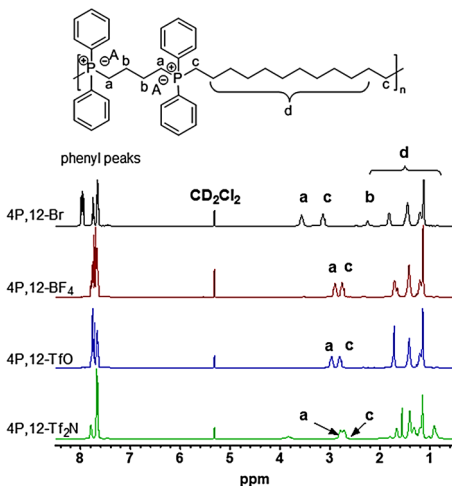
Figure 2.
^{1}H NMR spectra for 4P,12-Br and anion-exchanged analogs: 4P,12-BF4, 4P,12-TfO, and 4P,12-Tf2N.

of 4P,12 ionenes. The DSC curves displayed in Figure 3A show a dramatic dependence on the size of the associated counterion with the glass transition temperature (T_g), decreasing with increasing size of the associated counterion as follows: $Tf_2N^- <$ $TfO^- <$ $BF_4^- <$ Br^-. The glass transition temperatures for Br^-, BF_4^-, TfO^-, and Tf_2N^- containing 4P,12 ionenes as determined by DSC are listed in Table 1. The T_g values indicate that anion metathesis result in an overall change in T_g of approximately $100\,°C$ and suggest that increasing the size of the associated counterion facilitates long range segmental motion. The observed trend in glass transition temperature is in good agreement with previously published literature.[33–37] In one representative study, Hunley et al. also showed that the T_g of protonated poly(dimethylaminoethyl methacrylate) was profoundly influenced by the presence of bulkier fluorinated counterions.[33]

The TGA traces shown in Figure 3B also corroborate previous literature reports on ammonium or imidazolium ionenes, which

Table 1.

Glass transition temperatures and degradation temperatures for 4P,12-ionenes with different counterions as determined by DSC and TGA, respectively.

Ionene	T_g (°C)	$T_{d,5\%}$ (°C)
4P,12-Br	123	320
4P,12-BF₄	90	399
4P,12-TfO	71	415
4P,12-Tf₂N	19	404

indicate that the thermal stability is dependent upon the basicity of the associated counterion.[22,38] Similarly, 4P,12 ionenes showed an improvement in thermal degradation beyond $400\,°C$ for 4P,12-TfO and 4P,12-Tf$_2$N materials. Recent publications from our research group comparing ammonium and phosphonium polymerized ionic liquids present phosphonium-based polymerized ionic liquids as more resistant to degradation through a reverse Menschutkin reaction leading to enhanced thermal stability.[22,39–40] The temperature at 5% weight loss ($T_{d,5\%}$; summarized in Table 1) was enhanced nearly $100\,°C$ upon anion metathesis from bromide to Tf_2N^- counterions, which confirms that counterion exchange heavily influences the thermal properties of ionenes.

Influence of Phosphonium Ionene Counterion on Viscoelasticity

The structure-property relationship dependence of phosphonium ionenes on alkylene spacer length between the ditertiary phosphine and dibromide monomers was recently examined in order to discern the impact of charge density on thermal and viscoelastic properties of these polycations.[20] The unique thermal properties of phosphonium ionenes, including relatively low T_g's and high degradation temperatures, present a unique opportunity to probe the influence of electrostatic interactions on their melt flow dynamics through melt rheological characterization. The influence of counterion on the viscoelasticity of phosphonium ionenes at constant charge density was explored within the linear viscoelastic region by application of the
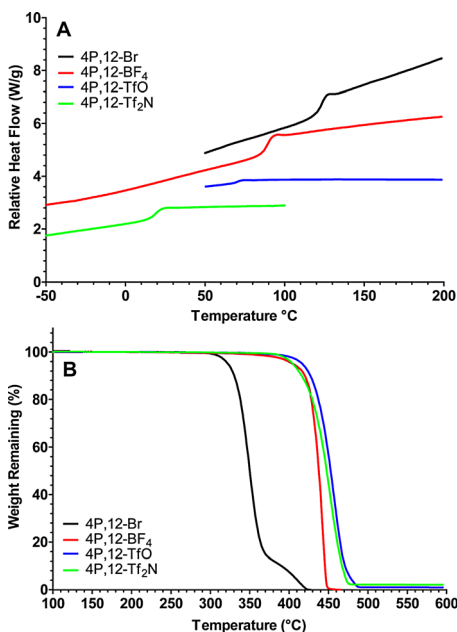
Figure 3.
DSC traces (A) and TGA traces (B) for for 4P,12-ionenes with different counterions.

principles of time-temperature superposition (TTSp). At a constant oscillatory strain of 1.25% within the linear viscoelastic regime, frequency sweep experiments were performed in $10\,^{\circ}C$ temperature steps. Temperature ramp experiments were also performed within the linear viscoelastic region using a constant oscillatory strain of 1.25% and constant oscillation frequency of 1.00 rad/s.

Figure 4A displays master curves for both the storage and loss moduli (respectively denoted as G' and G") for all anion-exchanged phosphonium ionenes. Shift factors for producing TTSp master curves for each anion-exchanged phosphonium ionene were determined using a reference temperature (T_r) of $130\,^{\circ}C$. Superimposition of the experimental data shows acceptable overlap over an angular frequency range spanning 8-10 decades for both G' and G" master curves for all anion-exchanged phosphonium ionenes confirming that TTSp principles are upheld. The

storage and loss moduli master curves also depict two distinct relaxation phenomena. The onset of long range segmental motion of polymer chains is observed at shorter relaxation time-scales (i.e. high oscillation frequency) and is a phenomenon characteristic to viscoelastic materials.[37,41] A second mode of relaxation appears at low oscillation frequencies before the onset of terminal flow. In corroboration with previously published literature from Nakamura and co-workers,[34,36,42] this mode of relaxation is attributed to electrostatic interactions found in polycations. Anion metathesis of the 4P,12 phosphonium ionene had a profound impact on the viscoelastic behavior of the resulting materials with relaxation modes representative of both electrostatic interactions as well as long range segmental motion of polymer chains occurring at longer relaxation time scales, where the size and basicity of the counterion respectively influence the long range segmental motion and the electrostatic interactions of the polymer.

Figure 4B displays pseudo-master curves for the anion-exchanged 4P,12 phosphonium ionenes as a plot of the complex viscosity versus oscillation frequency. The shift factors used to generate these pseudo-master curves were determined from only the loss moduli of the anion-exchanged 4P,12 ionenes. Arrhenius analysis of the shift factors ($T_r = 130\,^{\circ}C$) enabled determination of the melt flow activation energy (summarized in Table 2). The melt flow activation energy also shows a strong dependence upon the size of the counterion. Anion metathesis leads to a wide range of values for melt flow activation energy between 69 and 171 kJ/mol and increases with decreasing counterion size ($Tf_2N^- > TfO^- > BF_4^- > Br^-$).

The dependence of the shift factors on temperature for all anion-exchanged 4P,12 ionenes showed excellent adherence to the Williams-Landel-Ferry (WLF) equation. The WLF equation (equation 1 below) was used to determine the material specific C_1 and C_2 constants, which are dependent upon the reference temperature employed
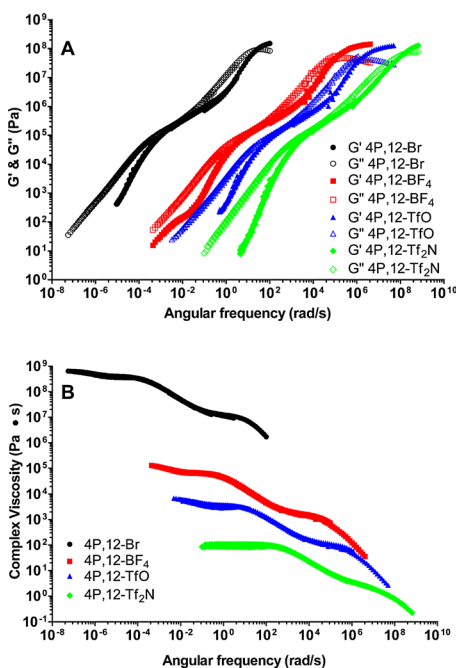
Figure 4.

Master curves of storage and loss moduli (A) and pseudo-master curves of complex viscosity (B) for 4P,12-ionenes with varying counterions ($T_r = 130\,^{\circ}C$).

Table 2.

Williams-Landel-Ferry (WLF) parameters, fractional free volumes, thermal expansion coefficients, and melt flow activation energies for 4P,12-ionenes with various counterions.

Ionene	C_1	C_2 (K)	C_1^g	C_2^g (K)	f_g	α_f (10^{-4} K^{-1})	E_a (kJ/mol)
4P,12-Br	9.79	57.1	11.2	50.1	0.039	7.77	171
4P,12-BF$_4$	6.03	92.0	10.7	52.0	0.041	7.82	120
4P,12-TfO	4.96	112	10.5	53.1	0.041	7.81	97.0
4P,12-Tf$_2$N	2.78	155	9.76	44.2	0.044	10.1	69.0

for generating TTSp master curves. The C_1 and C_2 constants, were normalized by T$_g$ values for the respective anion-exchanged 4P,12 ionenes using the following relationships (equations 2 and 3 below). Comparison of C_1^g and C_2^g values obtained for the anion-exchanged 4P,12 ionenes show good correlation to literature values obtained for charged polymers as well as for neutral polymers.[29,37] C_1^g and C_2^g constants were subsequently employed for the calculation of fractional free volume as well as thermal expansion coefficients for all anion-exchanged 4P,12 ionenes using equations 3 and 4, respectively. Based upon literature precedence, a value of 1 was assumed for B.[40,43] The fractional free volume, thermal expansion coefficients, as well as material specific WLF constants are summarized in Table 2.

$$\log(a_T) = \frac{-C_1(T - T_r)}{C2 + (T - T_r)} \quad (1)$$

$$C_1^g = \frac{C_1 C_2}{C_2 + (T_g - T_r)} \quad (2)$$

$$C_2^g = C_2(T_g - T_r) \quad (3)$$

$$f_g = \frac{B}{2.303 C_1^g} \quad (4)$$

$$a_f = \frac{B}{2.303 C_1^g C_2^g} \quad (5)$$

Melt Flow Rheology of 4P,12 Ionenes

Temperature ramp rheological experiments were performed in order to ascertain the temperature dependence as a function of counterion. To ensure assessment of each phosphonium ionene within the melt state,

rheological measurements were performed within a temperature range that began slightly above T$_g$ and within the viscoelastic regime at low oscillation strain rate and strain % (1.00 rad/s and 1.25% respectively) using an 8mm parallel plate geometry. Figure 5 shows the storage and loss moduli (G' and G" respectively) as a function of temperature. The loss modulus remains greater than the storage modulus for each 4P,12ionene, and the viscosity decreases, as expected, with increasing temperature until the onset of terminal flow. Overall, the counterion has a significant impact on the temperature dependent viscoelasticity. The storage and loss moduli both decrease dramatically with anion-exchange from bromide to the bulkier fluorinated counterions, and the magnitude of the loss and storage moduli show the following trend 4P,12-Br > 4P,12-BF$_4$ > 4P,12-TfO > 4P,12-Tf$_2$N. The impact of counterion size on viscoelasticity suggests that the counterion has a plasticizing effect on the bulk properties of the polymeric materials.
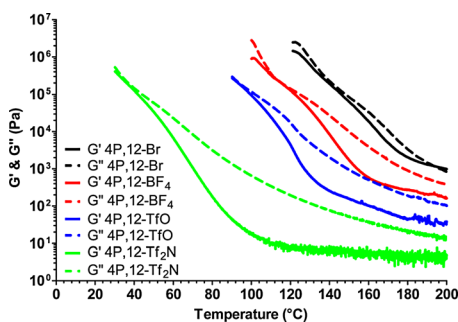
Figure 5.

Temperature ramp rheology showing the dependence of storage and loss moduli (G' and G") on temperature.
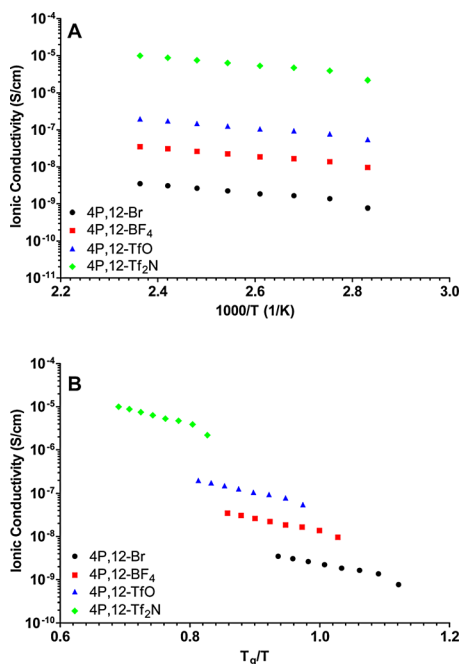
Ionic Conductivity

The temperature-dependent ionic conductivity of 4P,12 ionenes with different counterions are shown in Figure 6. Experimental constraints limited the sample selection to polymers with T_g's below 150 °C, which was the maximum temperature for the environmental chamber. Similar to previous literature reports,[28–29,33,36] the exchange from the more hydrophilic bromide anion to relatively more hydrophobic, bulkier fluorine-containing anions such as BF_4^-, TfO^-, or Tf_2N^-, increased the relative hydrophobicity and resulted in water-insoluble polymers. Anion-exchange from the Br^- counterion to BF_4^-, TfO^- or Tf_2N^- reduced the T_g significantly and increased the thermal stability due to reduced anion basicity as well as the increased size of the counterion. The ionic conductivity increased over an order-of-magnitude when the counterion changed from TfO^- to Tf_2N^-. The 4P,12-Tf_2N polymers have higher ionic conductivities

relative to 4P,12-TfO^- polymers. The higher ionic conductivity was attributed to lower T_g (as observed from DSC and melt rheological characterization displayed in Figure 3A and Figure 5, respectively) of the larger Tf_2N^- anion, which enhances segmental relaxation of the polymer chains and improves ion mobility within the polymer. The ionic conductivity results show that the glass transition temperature (T_g) is a dominant, but not exclusive, parameter in determining ion transport.

Conclusion

4P,12-Br phosphonium ionenes were prepared by step-growth polymerization employing the Menschutkin reaction. Subsequent anion metathesis was used to exchange the bromide counterion to prepare 4P,12-Tf_2N, 4P,12-TfO, and 4P,12-BF_4. A comparison of nuclear magnetic resonance spectroscopy showed characteristic upfield chemical shifts resulting from anion-exchange to the bulkier, fluorinated anions. The size and basicity of the counterion also had a profound impact on the thermal and viscoelastic properties of the resulting materials. Anion metathesis to larger, weaker anions led to dramatically reduced glass transition temperatures while the degradation temperature at 5% weight loss was enhanced from 300 °C to above 400 °C. Time-temperature superposition (TTSp) also showed a profound influence of rheological properties on the associated counterion. Two modes of relaxation corresponding to the onset of long-range segmental motion (T_g) and electrostatic interactions were observed, and anion-exchange led to a shift in these distinct relaxation modes to longer time scales. This observed shift was more pronounced for the bulkier Tf_2N^- and TfO^- counterion containing materials. Melt rheological characterization provided the impact of anion-exchange on the dependence of viscoelastic moduli on temperature. Overall, it was observed that that counterions behave as plasticizers to effectively enhance

Figure 6.
Ionic conductivity for 4P,12 ionenes with various counterions as a function of (a) 1000/T and (b) Tg/T for polymers with various counterions.

polymer chain mobility in the melt; this is also evident from the reduction in glass transition temperature observed from DSC analysis. Ionic conductivity was also greatly influenced by the size and basicity of the associated counterion. The ionic conductivity increased over an order of magnitude when counterion changed from TfO$^-$ to Tf$_2$N$^-$. The 4P,12-Tf$_2$N specimen had higher ionic conductivity relative to 4P,12-TfO polymers. The higher ionic conductivity was attributed to an enhanced plasticization effect of the larger Tf$_2$N$^-$ anion that enhances segmental relaxation of the polymer chains and improves ion mobility within the bulk material.

[1] P. Coimbra, P. Ferreira, H. C. de Sousa, P. Batista, M. A. Rodrigues, I. J. Corriea, M. H. Gil, *Int. J. Biol. Macromol.* **2011**, 48, 112.

[2] D. Raghothaman, M. F. Leong, Z. Yang, K. C. J. Toh, T. C. A. Lim, C. A. A. Wan, H. L. Eng, *J. Tissue Eng. Regener. Med.* **2012**, 6, 69.

[3] B. C. U. Tai, S. Gao, C. Du, A. C. A. Wan, J. Y. Ying, *Tissue Eng., Part A* **2008**, 14, 767.

[4] E. K. F. Yim, I. C. Liao, K. W. Leong, *Tissue Eng.* **2007**, 13, 423.

[5] T. A. Al-Hilal, F. Alam, Y. Byun, *Adv. Drug Deliv. Rev.* **2013**, 65, 845.

[6] J. Panyam, V. Labhasetwar, *Adv. Drug Deliv. Rev.* **2012**, 64, 61.

[7] J. L. Lutkenhaus, P. T. Hammond, *Soft Matter.* **2007**, 3, 804.

[8] K. J. Noonan, K. M. Hugar, H. At. Kostalik, E. B. Lobkovsky, H. D. Abruna, G. W. Coates, *J. Am. Chem. Soc.* **2012**, 134, 18161.

[9] M. Hickner, H. Ghassemi, Y. Kim, B. Einsla, J. McGrath, *Chem. Rev.* **2004**, 104, 4587.

[10] Y. Wan, H. Wu, A. Yu, D. Wen, *Biomacromolecules* **2006**, 7, 1362.

[11] A. Saxena, A. Kumar, V. Shahi, *J. Colloid Interface Sci.* **2006**, 303, 484.

[12] K. C. Trevor, E. B. Jason, L. L. Andrew, L. G. Douglas, D. N. Richard, *J. Membr. Sci.* **2010**, 359.

[13] R. C. Bazito, F. L. Cassio, F. H. Quina, *Macromol. Symp.* **2005**, 229, 197.

[14] M. F. Munhoz, F. H. Quina, *Macromol. Symp.* **2006**, 245, 232.

[15] V. Finkenstadt, *App. Microbiol. Biotechnol.* **2005**, 67, 735.

[16] S. R. Williams, T. E. Long, *Prog. Polym. Sci.* **2009**, 34, 762.

[17] C. F. Gibbs, C. S. Marvel, *J. Am. Chem. Soc.* **1934**, 56, 725.

[18] S. R. Williams, D. Salas-de la Cruz, K. I. Winey, T. E. Long, *Polymer* **2010**, 51, 1252.

[19] D. Feng, G. Wilkes, B. Lee, J. McGrath, *Polymer* **1992**.

[20] S. T. Hemp, M. S. Zhang, M. Tamami, T. E. Long, *Polym. Chem.* **2013**, 4, 3582.

[21] D. Feng, L. N. Venkateshwaran, G. L. Wilkes, M. L. Charles, E. S. John, *J. Appl. Polym. Sci.* **1989**, 38.

[22] M. Tamami, D. Salas-de la Cruz, K. I. Winey, T. E. Long, *Macromol. Chem. Phys.* **2012**, 213, 965.

[23] P. M. Carrasco, A. R. de Luzuriaga, M. Constantinou, P. Georgopanos, S. Rangou, A. Avgeropoulos, N. E. Zafeiropoulos, H. J. Grande, G. Cabanero, D. Mecerreyes, I. Garcia, *Macromolecules* **2011**, 44, 4936.

[24] T. Sata, S. I. Emori, K. Matsusaki, *J. Polym. Sci., Part B: Polym. Phys.* **1999**, 37, 793.

[25] T. Sata, K. Matsusaki, *J. Polym. Sci. Pol. Chem.* **1996**, 34, 2123.

[26] T. Sata, S. Nojima, K. Matsusaki, *Polymer* **1999**, 40, 7243.

[27] T. Sata, M. Tsujimoto, T. Yamaguchi, K. Matsusaki, *J. Membr. Sci.* **1996**, 112, 161.

[28] T. Sata, Y. Yamane, K. Matsusaki, *J. Polym. Sci. Pol. Chem.* **1998**, 36, 49.

[29] Y. S. Ye, Y. A. Elabd, *Polymer* **2011**, 52, 1309.

[30] R. Marcilla, J. A. Blazquez, R. Fernandez, H. Grande, J. A. Pomposo, D. Mecerreyes, *Macromol. Chem. Phys.* **2005**, 206, 299.

[31] R. Marcilla, J. A. Blazquez, J. Rodriguez, J. A. Pomposo, D. Mecerreyes, *J. Polym. Sci. Pol. Chem.* **2004**, 42, 208.

[32] R. Marcilla, M. Sanchez-Paniagua, B. Lopez-Ruiz, E. Lopez-Cabarcos, E. Ochoteco, H. Grande, D. Mecerreyes, *J. Polym. Sci. Pol. Chem.* **2006**, 44, 3958.

[33] M. T. Hunley, J. P. England, T. E. Long, *Macromolecules* **2010**, 43, 9998.

[34] K. Nakamura, K. Fukao, T. Inoue, *Macromolecules* **2012**, 45, 3850.

[35] G. Godeau, L. Navailles, F. Nallet, X. R. Lin, T. J. McIntosh, M. W. Grinstaff, *Macromolecules* **2012**, 45, 2509.

[36] K. Nakamura, T. Saiwaki, K. Fukao, T. Inoue, *Macromolecules* **2011**, 44, 7719.

[37] Q. Wu, R. A. Weiss, *Polymer* **2007**, *48*, 7558.

[38] M. D. Green, D. Salas-de la Cruz, Y. S. Ye, J. M. Layman, Y. A. Elabd, K. I. Winey, T. E. Long, *Macromol. Chem. Phys.* **2011**, *212*, 2522.

[39] S. T. Hemp, M. Zhang, M. H. Allen, S. Cheng, R. B. Moore, T. E. Long, *Macromol. Chem. Phys.* **2013**, *214*, 2099.

[40] N. K. Tierney, R. A. Register, *Macromolecules* **2003**, *36*, 1170.

[41] V. Jovanovski, R. Marcilla, D. Mecerreyes, *Macromol. Rapid Commun.* **2010**, *31*, 1646.

[42] K. Nakamura, K. Fukao, *Macromolecules* **2011**, *44*, 3053.

[43] Y. Ikeda, H. Masui, Y. Matoba, *J. Appl. Polym. Sci.* **2005**, *95*, 178.

Thiazolium-Containing Poly(ionic liquid)s and Ionic Polymers

Konrad Grygiel, Laurent Chabanne, Yongjun Men, Jiayin Yuan*

Summary: This paper reports on the synthesis of a new type of ionic polymers, including poly(ionic liquid)s, which contain 4-methylthiazolium-based ionic liquid pending groups along the polymer chain. The monomers were prepared via simple quaternization reaction of 4-methyl thiazole with 4-vinylbenzyl chloride and the subsequentanion exchange with various anions. Free radical polymerization and anion exchange reactions were employed to prepare several 4-methylthiazolium-based ionic polymers. These polymers show anion-dependent tuneable solubility in water and organic solvents. In addition, the new polycations' ability to stabilize single-walled as well as multi-walled carbon nanotubes in water and acetone is presented.

Keywords: ionic liquid; ionic polymers; stabilization; thiazolium ionic liquid

Introduction

One century history of ionic liquids (ILs) has brought abundant types of organic and some inorganic ions for salts which melt below 100 °C.[1] It is believed that the asymmetric chemical structure, low intermolecular interactions as well as weak tendencyto coordinate with oppositely charged ions are the most noticeable factors to lower down the melting point of ionic substance. The reason why ILshavedrawn widespread attention among scientists from various fields are their extraordinary properties, such as superior thermal stability, high ionic conductivity, non-flammability, high heat capacity, negligible vapour pressure, strong polarizability and solubilizing effect.[2–6] This property profile opens a wide applicationspectrum for ILs. Scientists have investigated ILsas solvents in different reactions, catalysts, stabilizers for various particles, and polymer additives.[7–11] Moreover, certain ILs appear to be very good solvents of biopolymers that are usually insoluble in common organic solvents, for instance cellulose.[12]

In order to implement some of the above-mentioned unique properties into solid state materials, researchers are nowadays studying the possible covalent incorporation of ILs into polymers. It allows one to enhance mechanical stability, and improveprocessability, durability and spatial control of ILs.[13–15] These polymers can be conveniently synthesized from a monomeric IL (m.p. below 100 °C) or an organic saltcontaining IL moiety. The most common approach involves free radical polymerization,[16–18] but modern polymerization techniques, such as atom transfer radical polymerization,[19,20] cobalt-mediated radical polymerization,[21] reversible addition-fragmentation transfer polymerization,[22,23] ring opening metathesis polymerization[24] and "click chemistry"[25–27] have been also employed for that purpose. It is worth noting that a high density of ILs in the polymer chains allows one tointroduce IL chemistry into the polymer research. For example, compared to common polyelectrolytes, the IL-rich polymers are usually soluble in organic solvents and show tuneable solubility depending on counter ion.[28,29] Among polycation, polyanion

Department of Colloid Chemistry, Max Planck Institute of Colloids and Interfaces, Am Mühlenberg 1, OT Golm, D-14476 Potsdam, Germany
E-mail: jiayin.yuan@mpikg.mpg.de

as well as polyzwitterion polymers, polycations are the most popular.[30–40] Typically employed polymerizable cationic species are imidazolium,[16,41–52] tetraalkyl ammonium or phosphonium,[52–54] pyridinium,[55,56] piperidinium,[57] pyrrolidinium,[58] pyrrolium[57] and triazolium.[25,30] Substances bearing thiazolium cations are widely known in the field of ILs. However, thiazoliumcation-based ionic polymers have been rarely reported so far.[5,59] Thiazolium ILs have been reported as precursors of carbenes.[60] Moreover, thiazolium-type ILscan be employed as catalysts for benzoin condensation[61] and Stetter reactions[62,63] as well as for gas separation.[64] They also offer some ionic conductivity and show strong binding to Au.Thiazolium salts have been also used for the preparation of nitrogen – sulphur co-doped carbons showing tuneable degree of doping as well as catalytic monolayers on a gold substrate.[65,66] Considering the interesting features of thiazoliumcations, this paper is devoted to the introduction of 4-methylthiazolium-based IL species into the ionic polymer family. Some of these polymers can be classified as poly(ionic liquid)s or polymerized ionic liquids.

On the other hand, carbon nanotubes (CNTs) show extraordinary mechanical, electrical, chemical, optical and thermal properties. Due to the multitude of possible applications of CNTs in such meaningful areas as drug delivery,[67] nanoelectronics[68] or optical sensors,[69] they have attracted tremendous interest. One of the main drawbacks of CNTs, which has to be overcome, is their tendency to agglomerate due to hydrophobic interactions. It may effectively disenable their functions in some applications. Therefore CNTs in liquids, usually in water, need to be stabilized. It could be achieved by using a deagglomeration agent, which is able to stabilize CNTs after their exfoliation into individual tubes from bundles. Typical approaches applied for this purpose might be divided into two groups – described as "covalent" or "physical" methods. The first one assumes creating covalent bonds between surface of CNTs and the stabilization agent.[70] Unfortunately this method shows a major drawback, because it may disrupt π-networks on CNTs, negatively affecting both mechanical and electronic properties. The second method bases on employing a stabilizing agent, which shows strong non-covalent interactions with CNTs surface.[71,72] The advantage of this approach is that after treatment, CNTs retain their physical properties. It has been reported that several organic compounds or polymers are capable to act as efficient physical stabilizers for CNTs.[73–76] Among them, ability of both ILs as well as PILs to stabilize CNTs has been investigated. Imidazolium-based ILs could support the exfoliation of CNT bundles in the process leading tostable gel-like products.[77,78] The same approach has been employedfor IL monomers in order to synthesize solid composites or polymeric gels. Moreover, CNT dispersions stabilized by PILs could be reversibly transferred from water to organic solvents. It opens the new possibilities of using straightforward methods to processCNTs in order to obtain certain composite materials.[2] As an application example, the newly synthesized thiazolium-based ionic polymers have been tested as dispersant for CNTs in both aqueous solution as well as organic solvents.

Experimental Part

Materials

4-Methylthiazole (99%), potassium hexafluorophosphate (99%) and sodium trifluoromethanesulfonate (98%) were purchased from Alfa Aesar and used without further purification. Lithium bis(trifluoromethylsulfonyl) imide (99%, Io-li-tec), 4-vinylbenzyl chloride (90%, Acros), 2,6-ditertbutyl-4-methyl phenol (99.0%; Aldrich), sodium tetrafluoroborate (98%, Sigma Aldrich), 2,2'-azobis[2-methyl-N-(2-hydroxyethyl)propionamide] (Wake Chemicals),NMR solvents (DMSO-d_6, 99.9%;DMF-d_7, 99.5%; D_2O, 99.9% from Aldrich), single-walled carbon nanotubes (Sigma-Aldrich) and multi-walled

carbon nanotubes (Baytubes® C150P) were used as received. All used solvents were of analytic grade.

Monomer Synthesis

4-methyl-3-(4-vinylbenzyl)thiazol-3-ium chloride (MVBT$^+$Cl$^-$): 4-methylthiazole (20.0 g; 0.20 mol), 2,6-ditertbutylo4-methyl phenol (0.300 g, 1.36 mmol) and ethyl acetate (100 mL) were charged into a 250 mL round bottom flask. Under vigorous stirring 4-chloromethyl styrene (102.6 g; 0.61 mol) was added and stirred at 70 °C for 20 days. Every 5 days, the precipitate was collected by filtration, washed several times with ethyl acetate and dried under high vacuum at 40°C for 24 h (21.45 g, yield 42%).^{1}H NMR (400.1 MHz, D$_2$O): 7.87 (s, 1H, CH), 7.6 (d, 2H; ArH), 7.3 (d, 2H; ArH), 6.8 (q,1H; CH), 5.9 (d, 1H; CH$_2$), 5.64 (s, 2H; CH$_2$), 5.4 (d, 1H; CH$_2$), 2.50 (s, 3H; CH$_3$); due to a fast proton exchange of the acidic proton bonded to thiazole ring in D$_2$O, the peak is absent, however the existence of thisproton was proved in DMSO-d$_6$in Figure 3.

4-methyl-3-(4-vinylbenzyl)thiazol-3-ium bis (trifluoromethylsulfonyl) imide (MVBT$^+$TF$_2$N$^-$): MVBT$^+$Cl$^-$ (1.50 g, 5.96 mmol) was dissolved in 10 mL of water. LiTF$_2$N (1.82 g, 6.34 mmol) was dissolved in 40 mL of water and added dropwise under vigorous stirring.Phase separation was observed. After 24 h the upper phase was removed. The bottom part was washed with water 3 times, dissolved in 50 mL of methanol, and re-precipitated out in water. The product was collected and dried under high vacuumat 40 °C for 48 h (2.10 g, yield 71%). ^{1}H NMR (400 MHz, DMSO-d_6): 10.14 (s, 1H, CH), 8.05 (s, 1H, CH), 7.5 (d, 2H; ArH), 7.3 (d, 2H; ArH), 6.8 (q,1H; CH), 5.9 (d, 1H; CH$_2$), 5.7 (s, 2H; CH$_2$), 5.3 (d, 1H; CH$_2$), 2.4 (s, 3H; CH$_3$)

4-methyl-3-(4-vinylbenzyl)thiazol-3-ium hexafluorophosphate (MVBT$^+$PF$_6^-$): it was obtained in the similar manner to MVBT$^+$TF$_2$N$^-$ except that acetone was used instead of methanol for to dissolvethe crude product. (2.15 g, yield 76%).^{1}H NMR (400 MHz, DMSO-d_6): 10.14 (s, 1H, CH), 8.05 (s, 1H, CH), 7.6 (d, 2H; ArH), 7.3 (d,

2H; ArH), 6.8 (q,1H; CH), 5.9 (d, 1H; CH$_2$),), 5.7 (s, 2H; CH$_2$), 5.3 (d, 1H; CH$_2$), 2.4 (s, 3H; CH$_3$).

4-methyl-3-(4-vinylbenzyl)thiazol-3-ium trifluoromethanesulfonate (MVBT$^+$TFO$^-$): MVBT$^+$Cl$^-$(1.50 g, 5.96 mmol), sodium trifluoromethanesulfonate (NaTFO; 1.15 g, 6.55 mmol) and 100 mL of acetonitrile were charged into a round bottom flask and stirred at room temperature for 72 h. Then, the solid particles were centrifuged out. The supernatant was collected, followed by the removal of acetonitrile under reduced pressure. The product was dried under high vacuum at 40 °C for 48 h. ^{1}H NMR (400 MHz, DMSO-d$_6$): 10.14 (s, 1H, CH), 8.05 (s, 1H, CH), 7.6 (d, 2H; ArH), 7.3 (d, 2H; ArH), 6.8 (q, 1H; CH), 5.9 (d, 1H; CH$_2$),), 5.74 (s, 2H; CH$_2$), 5.3 (d, 1H; CH$_2$), 2.44 (s, 3H; CH$_3$).

Polymer Synthesis

Two methods were used in this manuscript to prepare ionic polymers, either by direct solution polymerization of MVBT$^+$Cl$^-$ or by anion exchange with chloride-containing ionic polymerP (MVBT$^+$Cl$^-$).

P(MVBT$^+$Cl$^-$): MVBT$^+$Cl$^-$(7.6 g, 30.1 mmol), 2,2′-azobis[2-methyl-N-(2-hydroxyethyl)propionamide] (0.23 g, 0.79 mmol) and 40 mL of MiliQ water were loaded into a 100 mL Schlenk flask and stirred. The mixture was degassed by 3 cycles of freeze-pump-thaw procedure. The reaction was carried out under argon at 90 °C for 24 h. The crude product was purified by dialysis against deionized water, and freeze-dried. (6.35 g, yield 84%).

P(MVBT$^+$TF$_2$N$^-$): P(MVBT$^+$Cl$^-$) (1.00 g, 3.97 mmol of repeating units) was charged into a 100 mL round bottom flask and dissolved in 30 mL of water. ALiTF$_2$N (1.25 g, 4.35 mmol) solution in 20 mL of MiliQ water was added dropwise under vigorous stirring at room temperature. A white precipitate was observed. After 24 h, the precipitate was filtered off on a Büchner funnel, washed several times with water and dried at 40 °C for 48 h (1.63 g, yield 89%).

P(MVBT$^+$PF$_6^-$): it was obtained in the similar fashion to P(MVBT$^+$TF$_2$N$^-$),

but potassium hexafluorophosphate(0.81 g, 4.36 mmol) was used as exchanged salt. Crude product was purified by centrifugation and 5 times of washing with water (1.03 g, yield 72%).

P(MVBT$^+$TFO$^-$): P(MVBT$^+$Cl$^-$) (100 mg, 0.40 mmol of repeating units), NaTFO (77.0 mg, 0.448 mmol) and 20.0 mL of acetonitrile were charged into a 25 mL round bottom and stirred at room temperature for 24 h. Then, solid particles were centrifuged out. Supernatant was collected followed by removal of acetonitrile under reduced pressure. Crude product was washed with water, dried under high vacuum at 40 °C for 48 h (109.1 mg, yield 75%).

Stabilization of CNTs

In the case of stabilization of MWCNTs and SWCNTs, 1.0 mg of CNTs, 100 mg of P(MVBT$^+$Cl$^-$) and 25 mL of water were charged into a beaker. The mixture was then sonicated using a Branson Digital Sonifier model W450D (60% of amplitude, 10 min, 5 s on/15 s off). During the sonication the beaker was placed in an ice bath. A black dispersion formed that was stable for weeks. For anion exchange, 15 mL of the stable MWCNTs/P(MVBT$^+$Cl$^-$) dispersion was transferred to a 25 mL vial and KPF$_6$ (80 mg, 0.43 mmol) solution in 10 mL of water was added dropwise. After 24 hours, the black precipitate was centrifuged out, washed 5 times with water, and re-dispersed in acetone.

Characterization

Proton nuclear magnetic resonance (^{1}H-NMR) spectra were recorded at room temperature using a Bruker DPX-400 spectrometer operating at 400.1 MHz. The carbon nuclear magnetic resonance (^{13}C-NMR) and the heteronuclear multiple bond correlation (^{1}H-^{13}C HMBC) NMR spectra were recorded at room temperature on a VARIAN 400-MR (400 MHz) spectrometer. DMSO-d$_6$ was used as a solvent for all measurements except MVBT$^+$Cl$^-$, for which D$_2$O was also used to avoid peaks overlap.

Differential scanning calorimetry (DSC) measurements were done under a nitrogen flow at a heating rate of 10 K min^{-1} using a Perkin-Elmer DSC-1 instrument.

Thermogravimetric analysis (TGA) experiments were performed under a nitrogen flow at a heating rate of 10 K min^{-1} using a Netzsch TG209-F1 apparatus.

Elemental analysis was accomplished as a combustion analysis using a Vario Micro device.

Gel permeation chromatography (GPC) was performed using NOVEMA-column with mixture of 80% of acetatebuffer and 20% of methanol (flow rate 1.00 mL min^{-1}, PEO standards using RI detector - Optilab-DSP-InterferometricRefractometer (Wyatt-Technology).

Transmission electron microscopy (TEM) measurementswere performed on a Zeiss EM 912 Omega microscope operating at 120 kV. TEM samples were prepared by dropping 5 μL of a diluted stabilized CNT dispersion on a 200 mesh carbon-coated copper TEM grid.

Solubility tests were performed by mixing 10 mg of ionic polymer samples with different solvents (1 weight percent) in 5 mL vials. After 24 h of shaking, the presence of solid inside the vials was checked.

Results

The synthetic route to monomers and ionic polymers is shown in Figure 1. The monomer with chloride as anion was synthesized via the quaternization reaction of 4-methyl thiazole and 4-vinylbenzyl chloride in ethyl acetate at 70 °C in the presence of 2,6-ditertbutylo 4-methyl phenol as an inhibitor to avoid the polymerization of the styrenic unit. This reaction leads to the formation of a thiazolium monomer 4-methyl-3-(4-vinylbenzyl)thiazol-3-ium chloride (MVBT$^+$Cl$^-$). The polymer P-(MVBT$^+$Cl$^-$) was prepared directly via free radical polymerization of MVBT$^+$Cl$^-$ at 90 °C in water for 24 h using a non-ionic thermal initiator 2,2′-azobis[2-methyl-N-(2-hydroxyethyl) propionamide] (VA86). Anion exchange reactions are frequently used in IL chemistry to modify the physical/
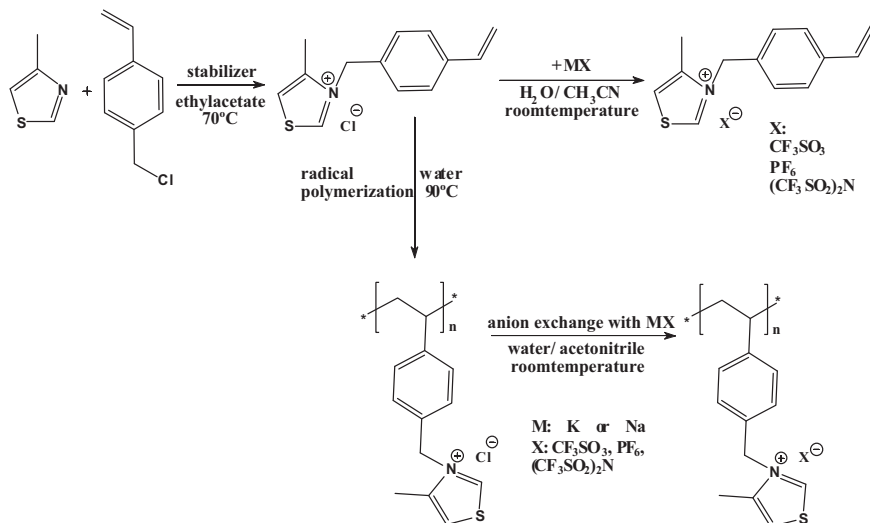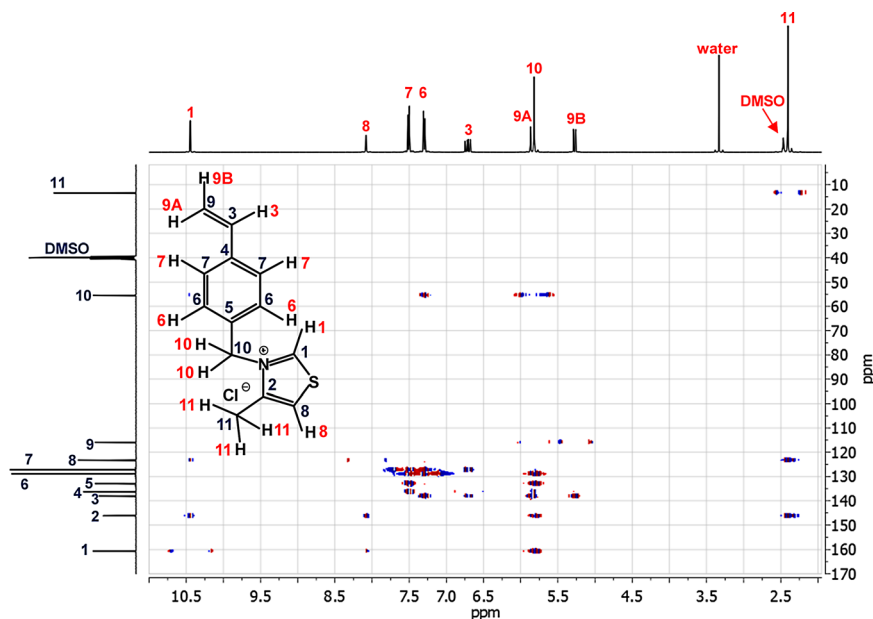
Figure 1.
Synthetic route and chemical structures of the obtained thiazolium-type ILmonomersand ionic polymers.

chemical properties of the ILs. Here, anion exchange was performed to both $MVBT^+Cl^-$ and $P(MVBT^+Cl^-)$ to replace the chloride with hexafluorophosphate, triflurosulfonate and bis(trifluoromethane-sulfonate)imide anions. It should be mentioned that direct solution polymerization of non-halide thiazolium IL monomers in DMF has been tried in this study as well. However, as opposed to the polymerization of monomer $MVBT^+Cl^-$, these runs failed to provide the non-halide ionic polymers. These polymers were then prepared via the anion exchange with $P(MVBT^+Cl^-)$.

The chemical structure of monomer $MVBT^+Cl^-$ was confirmed by proton nuclear magnetic resonance spectroscopy (^{1}H-NMR) and carbon nuclear magnetic resonance spectroscopy(^{13}C-NMR). In the thiazole monomers, both the nitrogen and the sulphur can potentially undergo quaternization. In order to assess whether the product was indeed obtained by creating a bond between 4-vinylbenzyl groups and the nitrogen instead of the sulphur atom of the thiazole ring, a proton-carbon heteronuclear multiple bond correlation (^{1}H-^{13}CHMBC) measurement was performed. The spectrum data agreed well with the proposed structure. In Figure 2, the

HMBC correlation is shown. As can be clearly seen, the spectrum showedthe direct coupling between proton 10 and carbon 2, but no coupling between proton 10 and carbon 8 was observed. It allows us also to detect that carbon 10 is coupled to proton 1, but not to proton 8. The ^{1}H/^{13}C couplings thus indicate that the obtained pure product was synthesized via bonding of 4-vinyl-benzyl group to the nitrogen atom, i.e. the quaternization reaction took place only onthe nitrogen rather than the sulphur in the thiazole ring.

The anion exchange reactions with $MVBT^+Cl^-$ and $P(MVBT^+Cl^-)$ were performed using two different methods. In the case of TF_2N^- and PF_6^- counter anions, the anion exchange proceeded by dropping an aqueous solution of the corresponding salt into the monomer or polymer solution. Following the addition of the salt solution, flocculation occurred immediately. This is indicative of the replacement of the hydrophilic chloride anion by the hydro-phobic PF_6^- or Tf_2N^- anions, which turn the monomer $MVBT^+Cl^-$ orpolymer $P(MVBT^+Cl^-)$ insoluble in aqueous solution. In the case of TFO^- anion, the anion exchange with chloride proceeded by simply mixing 1.1 mol equivalent of NaTFO
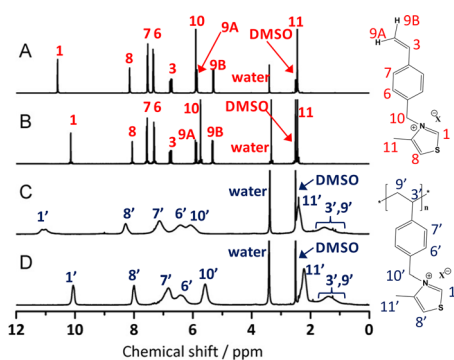
Figure 2.
^{1}H-^{13}C HMBC spectrum of monomer MVBT$^+$Cl$^-$.

with MVBT$^+$Cl$^-$ or P(MVBT$^+$Cl$^-$) in dry acetonitrile. Following the slow dissolution of these two salts, NaCl precipitated out of the solution due to its rather low solubility in acetonitrile. After filtration to remove NaCl, the monomers with TFO$^-$ anions were obtained by evaporating acetonitrile under high vacuum at room temperature.

Figure 3 shows the ^{1}H-NMR spectraof MVBT$^+$Cl$^-$, MVBT$^+$TF$_2$N$^-$ and their corresponding polymers in DMSO-d_6. In case of MVBT$^+$TF$_2$N$^-$ synthesized from MVBT$^+$Cl$^-$, it shows very similar spectrum pattern. Only a noticeable shift of the two thiazoliumcation ring was observed, for instance, from 10.59 (proton 1) and 8.14 ppm (proton 8) to 10.14 and 8.05 ppm, respectively. We observed analogous peak shifts in theproducts of other monomers with PF$_6$$^-$ and TFO$^-$ anions. The melting points of these monomer samples were determined by DSC. MVBT$^+$TF$_2$N$^-$ and MVBT$^+$TFO$^-$ showed melting points at 60 and 69 °C, respectively (Figure 4). According to the definition, they are classified as classic ionic liquids and their

corresponding polymers are poly(ionic liquid)s. For other obtained monomers no melting endotherms were observed in the DSC traces up to 100 °C, thus they belong to organic salts, and therefore their corresponding polymers are in the general scope of ionic polymers.

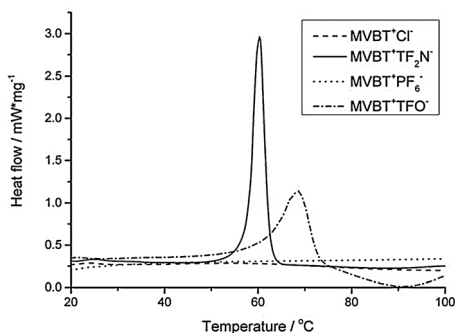Figure 3C shows the ^{1}H-NMR spectrum of P(MVBT$^+$Cl$^-$). Compared with its monomer spectrum in Figure 3A, we can

Figure 3.
^{1}H-NMR spectra of: A) monomer MVBT$^+$Cl$^-$; B) monomer MVBT$^+$TF$_2$N$^-$; C) polymer P(MVBT$^+$Cl$^-$); D) polymer P(MVBT$^+$TF$_2$N$^-$).
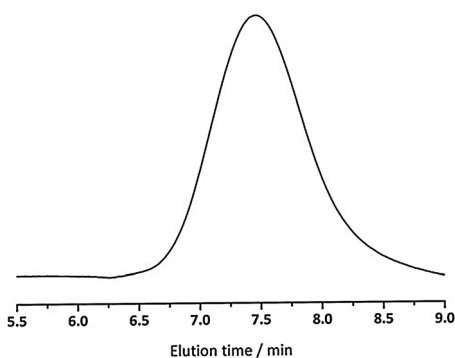
Figure 4.
DSC curves recorded for ionic monomers.

observe broadening of some particular peaks as well as the disappearance of the vinyl group signals at 6.73, 5.84, and 5.29 ppm after the reaction. Moreover, the appearance of a broad signal in the high field range (between 1 and 2 ppm), which can be attributed to protons connected to polymer backbone, is clearly seen. Figure 3D shows the ^{1}H-NMR spectrum of P(MVBT+TF2N−) prepared via anion exchange reaction from P(MVBT+Cl−). After the reaction, both resonance signals of protons of the thiazolium ring at 11.0, 8.3 ppm as well as a peak of the CH2 group at 6.1 ppm shift to 10.1, 8.0 and 5.6 ppm, respectively. The ^{1}H-NMR spectra of the other anion-exchanged polymers resemble that of P(MVBT+TF2N−).

The molecular weight of these polymers was determined by gel permeation chromatography. Figure 5 shows the elugram of

P(MVBT+Cl−). It displayed a monomodal distribution of P(MVBT+Cl−). The number-average molecular weight of the polymer (measured in water, calculated using PEO standard) was 15,000 g/mol with a polydispersity index of 3.0, which is expected from a free radical polymerization. Since the other non-halide ionic polymers were prepared via anion exchange with P(MVBT+Cl−), the degree of polymerization and the molecular weight distribution are similar to P(MVBT+Cl−).

Thermal behavior of the obtained thiazolium polymers was evaluated by TGA. As expected, polymerization of monomer MVBT+Cl− results in the elevation of the decomposition temperature (defined as 10 wt%) from 170 °C for MVBT+Cl− to 200 °C in the case of P(MVBT+Cl−) (Figure 6). The initial weight loss in the MVBT+Cl− monomer from 100–150 °C is due to the evaporation of trace amount of water due to a limited drying temperature, which is necessarily low to avoid thermal polymerizations. According to previous study, thermal stability of ionic liquid-containing polymers can be tuned by anion exchange reactions.[82] Altering anions from chloride to less basic, fluorinated anions allows to further elevate T_d of polymers, for instance even 280 °C in the case of PMVBT+TF2N−. Thermal stability of P(MVBT+PF6−) and P(MVBT+TFO−) was enhanced as well when compared to
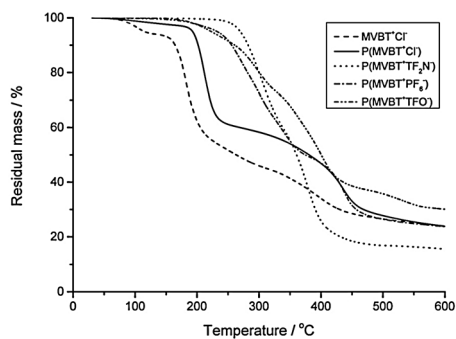
Figure 6.
TGA curves of the IL monomer MVBT+Cl− and the synthesized ionic polymers under nitrogen atmosphere.

Figure 5.
GPC trace measured for P(MVBT+Cl−).

P(MVBT$^+$Cl$^-$). So the thermal stability of the thiazolium-based ionic polymers follows the sequence of Cl$^- <$ PF$_6^-$, TFO$^- <$ Tf$_2$N$^-$. The obtained data indicate a strong correlation between the type of counteranion and the thermal properties of the synthesized ionic polymers. As expected, introducing bigger anions, whosecharge is more effectively delocalized to decrease the chain-chain interaction, can significantly lower down the T$_g$ of polymers.[82,83]
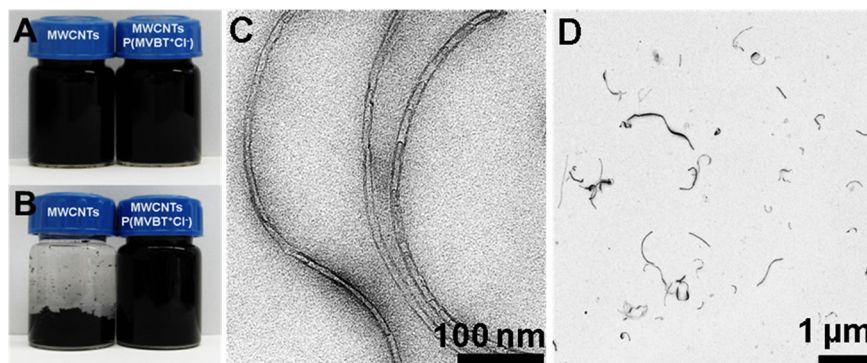
Another effect of the anion exchange is the solubility property of the polymers.The results of the solubility tests are summarized in Table 1. P(MVBT$^+$Cl$^-$) bearing hydrophilic Cl$^-$ counteranion was soluble in water as well as in polar organic solvents of high polarity (e.g. in methanol). Hydrophobic solvents as well as organic solvents with medium polarity (THF, chloroform and acetone) cannot dissolve this polymer. Unexpectedly, this polymer was found to be insoluble in DMF despite of several tries. Exchanging counteranions to more hydro-

phobic ones enables them to be soluble in DMF. Moreover the polymers with PF$_6^-$ and TF$_2$N$^-$ anionsbecame soluble in acetone, whilethose bearingPF$_6^-$ were not soluble in methanol anymore. It should be mentioned that all obtained polymer products show fairly good solubility in dimethyl sulfoxide.

The capability of these thiazolium-based ionic polymers to stabilize multi walled carbon nanotubes (MWCNTs) as well as single walled carbon nanotubes (SWCNTs) in water was also discussed. Stabilization was performed in asimilar manner to the literature procedure employed for poly(-ionic liquid)s bearing imidazoliumcations.[84] By sonication of MWCNTs and P(MVBT$^+$Cl$^-$) in aqueous media a homogenous, dark and stable dispersion was obtained (Figure 7A and 7B). As depicted in Figure 7C and 7D, very good quality of the CNT dispersion was confirmed using transmission electron microscopy (TEM). The observed MWCNTs were well separated, without the presence of large

Table 1.
Solubility tests of P(MVBT$^+$X$^-$)in different solvents.

P(MVBT$^+$X)	H$_2$O	MeOH	acetone	DMF	DMSO	THF, EtAc, toluene, CHCl$_3$
Cl$^-$	+	+	−	−	+	−
TFO$^-$	−	+	−	+	+	−
PF$_6^-$	−	−	+	+	+	−
Tf$_2$N$^-$	−	+	+	+	+	−

Figure 7.
A) Photographs of MWCTs dispersionin waterand P(MVBT$^+$Cl$^-$) stabilized MWCNs dispersionin water-immediately after sonication; B) Photographs of MWCT dispersionin waterand P(MVBT$^+$Cl$^-$) stabilized MWCN dispersionin water24 h after sonication; C and D) TEM images of P(MVBT$^+$Cl$^-$) stabilized MWCNT dispersion.

agglomerates. A control experiment was also performed, where MWCNTs were dispersed in water using ultrasonic horn, but precipitation was observed shortly after the sonication. The same results were obtained for SWCNTs as well. It is widely known, that imidazolium cation can support the stabilization of CNT dispersions via the cation-π interaction.[85,86] According to our results, thiazoliumcations in ionic polymer offer similar solubilizing effect. Moreover, MWCNTs stabilized with the thiazolium polymer can be easily transferred to organic solvents, such as acetone. This was performed by precipitating P(MVBT$^+$Cl$^-$)-stabilized MWCNTs from their aqueous dispersion by adding KPF$_6$ solution. This leads to theanion exchange between Cl$^-$ and PF$_6^-$on the polymer and turns the MWCNT surface hydrophobic. The precipitated MWCNTs become then soluble in acetone.

Conclusion

In summary, a series of thiazolium-based monomers and ionic polymers have been studied in detail. The MVBT$^+$Cl$^-$ monomer was first prepared by simple quaternization of 4-methyl thiazole with 4-vinylbenzyl chloride. The quaternization reaction occurred selectively at the nitrogen atom rather than the sulfur atom in the thiazolemolecule, as confirmed using ^{1}H-^{13}CHMBC NMR spectroscopy. The ionic polymer P(MVBT$^+$Cl$^-$) was obtained via free radical polymerization of MVBT$^+$Cl$^-$. Thiazolium-based monomers bearing fluorinated anions were prepared by anion exchange to afford non-halide monomers. Their polymers were obtained via anion exchange reaction of the P(MVBT$^+$Cl$^-$)polymer. The Tf$_2$N$^-$ and TFO$^-$-based monomers and polymers can be classified as classic ILs and poly-(ionic liquid)s. These new ionic polymers were fully characterized and exhibited excellent ability to stabilize CNTs in water and organic solvents.

[1] J. S. Wilkes, *Green Chem.* **2002**, *4*, 73.

[2] J. Yuan, M. Antonietti, *Polymer* **2011**, *52*, 1469.

[3] N. V. Tsarevsky, K. Matyjaszewski, *Chem. Rev.* **2007**, *107*, 2270.

[4] M. Isik, R. Gracia, L. C. Kollnus, L. C. Tomé, I. M. Marrucho, D. Mecerreyes, *ACS Macro Lett.* **2013**, 975.

[5] Y. Yoshida, O. Baba, G. Saito, *J. Phys. Chem. B* **2007**, *111*, 4742.

[6] M. Yoshio, T. Mukai, H. Ohno, T. Kato, *J. Am. Chem. Soc.* **2004**, *126*, 994.

[7] F. Liu, L. Wang, Q. Sun, L. Zhu, X. Meng, F.-S. Xiao, *J. Am. Chem. Soc.* **2012**, *134*, 16948.

[8] J. Pinaud, J. Vignolle, Y. Gnanou, D. Taton, *Macromolecules* **2011**, *44*, 1900.

[9] Y. Kohno, H. Ohno, *Chem. Commun.* **2012**, *48*, 7119.

[10] Z. Chen, F. Yan, L. Qiu, J. Lu, Y. Zhou, J. Chen, Y. Tang, J. Texter, *Langmuir* **2010**, *26*, 3803.

[11] Y. Zhou, L. Qiu, Z. Deng, J. Texter, F. Yan, *Macromolecules* **2011**, *44*, 7948.

[12] R. P. Swatloski, S. K. Spear, J. D. Holbrey, R. D. Rogers, *J. Am. Chem. Soc.* **2002**, *124*, 4974.

[13] O. Green, S. Grubjesic, S. Lee, M. A. Firestone, *Polym. Rev. (Philadelphia, PA, U.S.)* **2009**, *49*, 339.

[14] Q. Zhao, T.-P. Fellinger, M. Antonietti, J. Yuan, *Macromol. Rapid Commun.* **2012**, *33*, 1149.

[15] Q. Zhao, P. Zhang, M. Antonietti, J. Yuan, *J. Am. Chem. Soc.* **2012**, *134*, 11852.

[16] M. Hirao, K. Ito, H. Ohno, *Electrochimica Acta* **2000**, *45*, 1291.

[17] D. Batra, S. Seifert, L. M. Varela, A. C. Y. Liu, M. A. Firestone, *Adv. Funct. Mater.* **2007**, *17*, 1279.

[18] J. Yuan, S. Wunder, F. Warmuth, Y. Lu, *Polymer* **2012**, *53*, 43.

[19] X. He, W. Yang, X. Pei, *Macromolecules* **2008**, *41*, 4615.

[20] J. Texter, V. A. Vasantha, R. Crombez, R. Maniglia, L. Slater, T. Mourey, *Macromol. Rapid Commun.* **2012**, *33*, 69.

[21] C. Detrembleur, A. Debuigne, M. Hurtgen, C. Jérôme, J. Pinaud, M. v. Fèvre, P. Coupillaud, J. Vignolle, D. Taton, *Macromolecules* **2011**, *44*, 6397.

[22] K. Vijayakrishna, S. K. Jewrajka, A. Ruiz, R. Marcilla, J. A. Pomposo, D. Mecerreyes, D. Taton, Y. Gnanou, *Macromolecules* **2008**, *41*, 6299.

[23] J. Yuan, H. Schlaad, C. Giordano, M. Antonietti, *Eur. Polym. J.* **2011**, *47*, 772.

[24] Y. S. Vygodskii, A. S. Shaplov, E. I. Lozinskaya, K. A. Lyssenko, D. G. Golovanov, I. A. Malyshkina, N. D. Gavrilova, M. R. Buchmeiser, *Macromol. Chem. Phys.* **2008**, 209, 40.

[25] P. Dimitrov-Raytchev, S. Beghdadi, A. Serghei, E. Drockenmuller, *J. Polym. Sci., Part A: Polym. Chem.* **2013**, 51, 34.

[26] J. Yuan, D. Mecerreyes, M. Antonietti, *Prog. Polym. Sci.* **2013**, 38, 1009.

[27] A. S. Shaplov, P. S. Vlasov, E. I. Lozinskaya, O. A. Shishkan, D. O. Ponkratov, I. A. Malyshkina, F. Vidal, C. Wandrey, I. A. Godovikov, Y. S. Vygodskii, *Macromol. Chem. Phys.* **2012**, 213, 1359.

[28] R. Marcilla, J. Alberto Blazquez, J. Rodriguez, J. A. Pomposo, D. Mecerreyes, *J. Polym. Sci., Part A: Polym. Chem.* **2004**, 42, 208.

[29] O. Mel'nik, A. Shaplov, E. Lozinskaya, N. Popova, M. Makarov, I. Odinets, K. Lysenko, G. Timofeeva, I. Malyshkina, Y. Vygodskii, *Polym. Sci. Ser. B* **2010**, 52, 316.

[30] D. Mecerreyes, *Prog. Polym. Sci.* **2011**, 36, 1629.

[31] S. Cheng, M. Zhang, T. Wu, S. T. Hemp, B. D. Mather, R. B. Moore, T. E. Long, *J. Polym. Sci. Part A: Polym. Chem.* **2012**, 50, 166.

[32] W. Ogihara, S. Washiro, H. Nakajima, H. Ohno, *Electrochimica Acta* **2006**, 51, 2614.

[33] M. D. Green, T. E. Long, *Polym Rev* **2009**, 49, 291.

[34] J. Texter, *Macromol. Rapid Commun.* **2012**, 33, 1996.

[35] H. Ohno, *Macromol. Symp.* **2007**, 249–250, 551.

[36] A. S. Shaplov, P. S. Vlasov, M. Armand, E. I. Lozinskaya, D. O. Ponkratov, I. A. Malyshkina, F. Vidal, O. V. Okatova, G. M. Pavlov, C. Wandrey, I. A. Godovikov, Y. S. Vygodskii, *Polymer Chemistry* **2011**, 2, 2609.

[37] M. Koebe, M. Drechsler, J. Weber, J. Yuan, *Macromol. Rapid Commun.* **2012**, 33, 646–651.

[38] Y. Men, X.-H. Li, M. Antonietti, J. Yuan, *Polym. Chem.* **2013**, 3, 871.

[39] Q. Zhao, M. Yin, A. P. Zhang, S. Prescher, M. Antonietti, J. Yuan, *J. Am. Chem. Soc.* **2013**, 135, 5549.

[40] P. Zhang, J. Yuan, T.-P. Fellinger, M. Antonietti, H. Li, Y. Wang, *Angew. Chem., Int. Ed.* **2013**, 52, 6028.

[41] M. D. Green, D. Wang, S. T. Hemp, J.-H. Choi, K. I. Winey, J. R. Heflin, T. E. Long, *Polymer* **2012**, 53, 3677.

[42] J. Yuan, S. Soll, M. Drechsler, A. H. E. Müller, M. Antonietti, *J. Am. Chem. Soc.* **2011**, 133, 17556.

[43] R. Marcilla, E. Ochoteco, C. Pozo-Gonzalo, H. Grande, J. A. Pomposo, D. Mecerreyes, *Macromol. Rapid Commun.* **2005**, 26, 1122.

[44] Y. Ye, Y. A. Elabd, *Macromolecules* **2011**, 44, 8494.

[45] R. L. Weber, Y. Ye, A. L. Schmitt, S. M. Banik, Y. A. Elabd, M. K. Mahanthappa, *Macromolecules* **2011**, 44, 5727.

[46] D. England, N. Tambe, J. Texter, *ACS Macro Lett.* **2012**, 1, 310.

[47] Q. Zhao, S. Soll, M. Antonietti, J. Yuan, *Polymer Chemistry* **2013**, 4, 2432.

[48] A. Wilke, J. Yuan, M. Antonietti, J. Weber, *ACS Macro Lett.* **2012**, 1028.

[49] L. Zhao, R. Crombez, F. P. Caballero, M. Antonietti, J. Texter, M.-M. Titirici, *Polymer* **2010**, 51, 4540.

[50] F. Yan, J. Texter, *Adv. Colloid Interface Sci.* **2006**, 128–130, 27.

[51] K. Tauer, N. Weber, J. Texter, *Chem. Commun.* **2009**, 6065.

[52] Y. Men, H. Schlaad, J. Yuan, *ACS Macro Lett.* **2013**, 2, 456.

[53] S. Supasitmongkol, P. Styring, *Energy Environ. Sci.* **2010**, 3, 1961.

[54] P. G. Mineo, L. Livoti, M. Giannetto, A. Gulino, S. Lo Schiavo, P. Cardiano, *J. Mater. Chem.* **2009**, 19, 8861.

[55] M. Watanabe, S-i. Yamada, N. Ogata, *Electrochim. Acta* **1995**, 40, 2285.

[56] J. Yuan, A. G. Marquez, J. Reinacher, C. Giordano, J. Janek, M. Antonietti, *Polym. Chem.* **2011**, 2, 1654.

[57] W. S. Ogihara, H. Nakajima, H. Ohno, *Electrochimica Acta* **2006**, 51, 6.

[58] A.-L. Pont, R. Marcilla, I. De Meatza, H. Grande, D. Mecerreyes, *J. Power Sources* **2009**, 188, 558.

[59] J. H. Davis, Jr, K. J. Forrester, *Tetrahedron Lett.* **1999**, 40, 1621.

[60] A. J. Arduengo, J. R. Goerlich, W. J. Marshall, *Liebigs Annalen* **1997**, 1997, 365.

[61] J. Castelk, F. Lopez-Calahorra, L. Domingo, *J. Org. Chem.* **1988**, 53, 4.

[62] A. G. M. Barrett, A. C. Love, L. Tedeschi, *Org. Lett.* **2004**, 6, 3377.

[63] Z.-Z. Zhou, F.-Q. Ji, M. Cao, G.-F. Yang, *Adv. Synth. Catal.* **2006**, 348, 1826.

[64] P. C. Hillesheim, S. M. Mahurin, P. F. Fulvio, J. S. Yeary, Y. Oyola, D-e. Jiang, S. Dai, *Ind. Eng. Chem. Res.* **2012**, 51, 11530.

[65] J. P. Paraknowitsch, B. Wienert, Y. Zhang, A. Thomas, *Chem.-Eur. J.* **2012**, 18, 15416.

[66] K. Motesharei, D. C. Myles, *J. Am. Chem. Soc.* **1997**, 119, 6674.

[67] A. Bianco, K. Kostarelos, M. Prato, *Curr. Opin. Chem. Biol.* **2005**, 9, 674.

[68] Q. Cao, J. A. Rogers, *Adv. Mater.* **2009**, 21, 29.

[69] P. W. Barone, S. Baik, D. A. Heller, M. S. Strano, *Nat. Mater.* **2005**, 4, 86.

[70] S. Qin, D. Qin, W. T. Ford, D. E. Resasco, J. E. Herrera, *J. Am. Chem. Soc.* **2003**, 126, 170.

[71] W. Peng, C. Xing, H. Nancy, T. Un Chong, B. Ola, Z. Alex, R. B. Carolyn. *Angew. Chem.* **2008**, 120, 5100.

[72] V. C. Tung, J. Kim, L. J. Cote, J. Huang, *J. Am. Chem. Soc.* **2011**, 133, 9262.

[73] S. Meuer, L. Braun, R. Zentel, *Macromol. Chem. Phys.* **2009**, 210, 1528.

[74] M. Zheng, A. Jagota, E. D. Semke, B. A. Diner, R. S. McLean, S. R. Lustig, R. E. Richardson, N. G. Tassi, *Nat. Mater.* **2003**, 2, 338.

[75] D. Wang, W.-X. Ji, Z.-C. Li, L. Chen, *J. Am. Chem. Soc.* **2006**, *128*, 6556.

[76] M. Antonietti, Y. Shen, T. Nakanishi, M. Manuelian, R. Campbell, L. Gwee, Y. A. Elabd, N. Tambe, R. Crombez, J. Texter, *ACS Appl. Mater. Interfaces* **2010**, *2*, 649.

[77] T. Fukushima, T. Aida, *Chem.-Eur. J.* **2007**, *13*, 5048.

[78] T. Fukushima, A. Kosaka, Y. Ishimura, T. Yamamoto, T. Takigawa, N. Ishii, T. Aida, *Science* **2003**, *300*, 2072.

[79] J. P. Paraknowitsch, A. Thomas, *Energy Environ. Sci.* **2013**, *6*, 2839.

[80] J. P. Paraknowitsch, A. Thomas, J. Schmidt, *Chem. Commun. (Cambridge, U. K.)* **2011**, *47*, 8283.

[81] S.-A. Wohlgemuth, R. J. White, M.-G. Willinger, M.-M. Titirici, M. Antonietti, *Green Chem.* **2012**, *14*, 1515.

[82] C. P. Fredlake, J. M. Crosthwaite, D. G. Hert, S. N. V. K. Aki, J. F. Brennecke, *J. Chem. Eng. Data* **2004**, *49*, 954.

[83] R. S. Bhavsar, S. C. Kumbharkar, U. K. Kharul, *J. Membr. Sci.* **2012**, *389*, 305.

[84] S. Soll, M. Antonietti, J. Yuan, *ACS Macro Lett.* **2011**, *1*, 84.

[85] R. Marcilla, M. L. Curri, P. D. Cozzoli, M. T. Martínez, I. Loinaz, H. Grande, J. A. Pomposo, D. Mecerreyes, *Small* **2006**, *2*, 507.

[86] S. Bellayer, J. W. Gilman, N. Eidelman, S. Bourbigot, X. Flambard, D. M. Fox, H. C. De Long, P. C. Trulove, *Adv. Funct. Mater.* **2005**, *15*, 910.

Ionic Liquids as Advantageous Reaction Media for Free Radical Polymerization

Veronika Strehmel,[*1] *Hendrik Wetzel,*[2] *André Laschewsky*[2,3]

Summary: Ionic liquids are attractive solvents for polymer synthesis because their properties can be easily and broadly tuned by varying the structure of both the cation and the anion. Application of ionic liquids as reaction medium for free radical polymerization of vinyl monomers, such as methacrylates or styrene, results in high yields and high molecular weights of the polymers. Reasons for these effects are only partially due to the high viscosity of ionic liquids, which may reduce bimolecular termination of the propagating chains, but are also due to solvent cage effects that differ from those in traditional organic solvents because of strong ionic interactions between the individual ions of the ionic liquids. Furthermore, the high dissolving power of ionic liquids for both weakly polar as well as highly polar monomers makes ionic liquids interesting as solvents for statistical copolymerization. Interestingly, variation of the alkyl chain length of substituents at the cation of the ionic liquid allows altering of copolymer composition.

Introduction

Free radical polymerization is the mostly applied mechanism to manufacture polymers because of high polymerization rate and tolerance to many functional groups bound at monomers.[1] Often, a solvent is used to avoid the Trommsdorff-Norrish effect.[2,3] Solvents do not only reduce the polymerization rate and improve heat transfer during polymerization, they also may strongly influence both the polymerization process and the polymer structure.[4,5]

Ionic liquids have received increased interest among modern solvents virtue of their negligible vapor pressure, and of the possibility to tailor their dissolution capability by variation of the structures of either one or both ions constituting the ionic liquids.[6–8] The structure of ionic liquids can be varied in a huge range covering various anions, such as small anions, e.g., tetrafluoroborate, hexafluorophosphate, and dicyanamide, or anions with apolar alkyl or aryl substituent, e.g., octyl sulfate or tosylate, or anions with delocalized charge, e.g., bis(trifluoromethylsulfonyl)imide. The structure of the ionic liquid cation can be varied analogously. This includes for example imidazolium, pyridinium and ammonium ions that are substituted with alkyl groups of different lengths at the nitrogen, or with additional substituents at the carbon atoms of the aromatic rings. Structure variation results in changes of viscosity and polarity of ionic liquids.[9–11] This opens a high application potential of ionic liquids on the one hand, but renders the selection of appropriate ion pairs intricate for a given application, if the structure property relations are not well known.

[1] Niederrhein University of Applied Sciences, Department of Chemistry and Institute of Coatings and Surface Chemistry, Adlerstrasse 32, D-47798 Krefeld, Germany
Fax: (+49)2151 822 4195;
E-mail: veronika.strehmel@hsnr.de
[2] Fraunhofer Institute for Applied Polymer Research, Geiselbergstr. 69, D-14476 Potsdam-Golm, Germany
[3] University of Potsdam, Institute of Chemistry, Karl-Liebknecht-Str. 24-25, D-14476 Potsdam-Golm, Germany

wileyonlinelibrary.com

Ionic liquids have been investigated in radical polymerization since several years[12–55] as summarized and discussed in several reviews.[56–59] Compared to the use of traditional solvents, rates of polymerization are mostly higher in ionic liquids, and molecular weights are often increased.[29,33,34] In certain cases, the achieved molecular weights are even higher when polymerized in ionic liquids than when prepared in bulk.[34,45] Furthermore, molecular weights and molecular weight distributions were found to be sensibly affected by variation of the cation or the anion of the ionic liquid employed.[34] For instance, the increase of the length of alkyl substituents at the nitrogen of imidazolium cations typically increases viscosity and decreases polarity and micropolarity, respectively.[9,10] Furthermore, an additional methyl substituent at the 2-position of the imidazolium ring increases viscosity as well. Nonetheless, hydrogen bonding between the acidic hydrogen atom at the 2-position at the imidazolium ring and any hydrogen acceptor is thus reduced in comparison to simple 1-alkyl-3-methylimidazolium based ionic liquids.[60] The variation of the behavior of ionic liquids is more difficult to predict when the nature of the anion is varied, as cation-anion interactions affect the properties much more than a simple change of the substituent size at the cation.[60,61] Electrostatic interactions, hydrogen bonding, and van der Waals interactions in ionic liquids contribute to the solubilization behavior of monomers, which is important for copolymerization of monomers of strongly differing polarity, e. g. of hydrophilic and hydrophobic monomers.[29,33,41] Moreover, solvent cage effects may be important regarding the efficient formation of initiating radicals in free radical polymerization. Investigation of photogenerated model radicals and their recombination in the dark as function of both ionic liquid structure and temperature gives information about the influence of radical diffusion and solvent cage on radical recombination in ionic liquids.[62,63] The understanding of these effects may help to select the most suitable ionic liquids for radical polymerization processes.

In this context, the results presented shall contribute to a better understanding of the role of ionic liquids in free radical polymerization. Methacrylates of both low and high polarity, as well as styrene were selected as model monomers for polymerization in ionic liquids. The ionic liquids employed comprise imidazolium based ionic liquids with tetrafluoroborate, hexafluorophosphate, triflate, octylsulfate, dicyanamide, tosylate and bis(trifluoromethyl)sulfonylimide anions as well as pyrrolidinium and tetraalkylammonium bis(trifluoromethylsulfonyl)imides. Additionally, one alkyl substituent of the imidazolium, pyrrolidinium or tetraalkylammonium cations was varied. These structural variations modulate both viscosity and polarity of the ionic liquids. This paper focuses on the influence of the ionic liquid structure on molecular weight and polydispersity of the model homopolymers, and on the influence on the composition of the statistical methacrylate copolymers combining both hydrophilic and hydrophobic comonomers, i.e., of copolymers of marked amphiphilic character.

Polymethacrylate Synthesis in Ionic Liquids

Ionic liquids bearing bis(trifluoromethylsulfonyl)imide or dicyanamide as anion (Figure 1) belong to room temperature ionic liquids exhibiting rather low viscosity.[63,64] Therefore, such ionic liquids seemed particularly suitable for free radical polymerization of methacrylates, and thus were primarily engaged. Indeed, such ionic liquids proved to be useful reaction media, and give rise to high molar mass polymers, as exemplified in Figure 2 for polybenzylmethacrylate. As common feature, samples made in the ionic liquids **1–4** show rather broad molecular weight distributions. Apart from that, significant differences in the molecular weight distributions of polybenzylmethacrylate are observed between
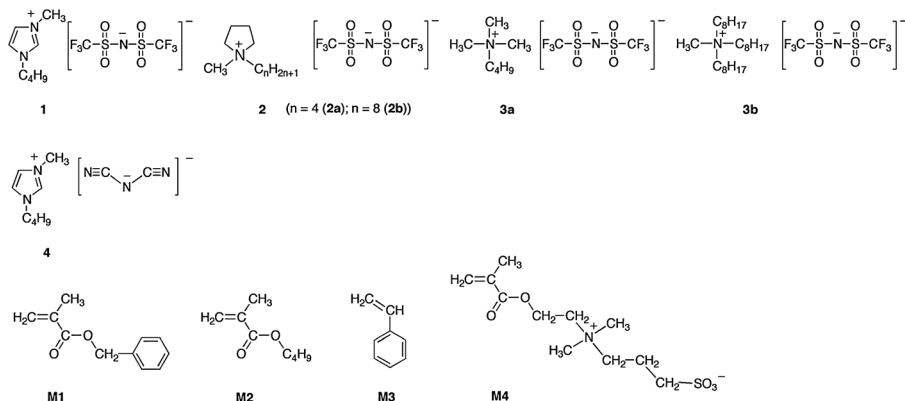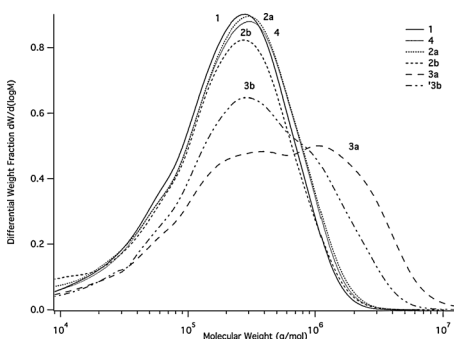
Figure 1.
Chemical structure of ionic liquids and of the monomers used in the free radical polymerization studies: (1-butyl-3-methylimidazolium (**1**), 1-alkyl-1-methylpyrrolidinium (**2a** (n = 4); **2b** (n = 8)), tetraalkylammonium based ionic liquids **3a** and **3b** bearing bis(trifluoromethylsulfonyl)imide as anion, and 1-butyl-3-methylimidazolium dicyanamide (**4**); monomers: (benzylmethacrylate (**M1**), n-butylmethacrylate (**M2**), styrene (**M3**), and zwitterionic methacrylate bearing a sulfobetaine moiety (**M4**)).

polymerizations conducted in the imidazolium (**1**, **4**) or pyrrolidinium (**2a**, **2b**) based ionic liquids, and those based on tetraalkylammonium cations (**3a**, **3b**) although comparable reactions conditions (1 mole-% azobis(isobutyronitrile) (AIBN); 70 °C; 24 h polymerization time) were used for all polymerization experiments. The tetraalkylammonium bis(trifluoromethylsulfonyl)-imides **3a** and **3b** result in pronounced bimodal distributions with more or less separated higher molecular weight fractions, which are absent in the case of

Figure 2.
GPC elugrams of polymer samples obtained by free radical polymerization of **M1** in selected ionic liquids (**1**; **2a**; **2b**; **3a**; **3b**; **4**) using AIBN (1 mole-% relative to the monomer) as initiatior at 70 °C for 24 h.

imidazolium (**1** and **4**) and pyrrolidinium (**2**) based ionic liquids. According to the values listed in Table 1, viscosity cannot explain the occurence of higher molecular weight fractions when using the aliphatic ammonium based ionic liquids. In fact, the viscosity of **3a** is relatively low while the viscosity of **3b** is at the upper end of the viscosity range covered by the various ionic liquids investigated. Nevertheless, the average degree of polymerization obtained by free radical polymerization in ionic liquids tends to correlate more or less with their viscosity (Figure 3).[36] We note also that polymer yields differ substantially under otherwise identical conditions when using ionic liquids **1–4**, as summarized in Table 1. Yields were particularly high if butyl substituted imidazolium or pyrrolidinium bis(trifluoromethylsulfonyl)imides (**1** and **2a**) were used for polymerization, while the use of the other ionic liquids gave considerably lower yields although reaction conditions were identical. Despite the differing yields, weight average molecular weights (M_w) are surprisingly similar when using **1**, **2**, and **4** as reaction media (Table 1).

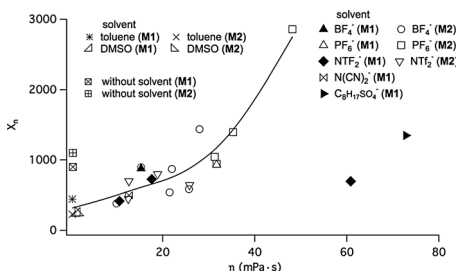Although differences in viscosity alone cannot explain the differences in the molecular weight of the polymers obtained,

Table 1.

Yield number average molecular weight (M_n), weight average molecular weight (M_w), and polydispersity (PDI) of polybenzylmethacrylate synthesized in the ionic liquids depicted in Figure 1 (1 mole-% AIBN relative to the monomer; 70 °C; 24 h polymerization time) including viscosity of the ionic liquids at a shear rate of 10 s^{-1} at 70 °C

Ionic liquid	η_{10} (mPa·s) at 70 °C	yield (%)	Mn (g/mol)	Mw (g/mol)	PDI
1	13	92	73000	311000	4.3
2a	18	89	106000	351000	3.3
2b	26	57	87000	290000	3.3
3a	18	34	127000	1024000	8.1
3b	61	39	122000	596000	4.9
4	13	43	87000	344000	3.9

a general trend exists between ionic liquid viscosity and the degree of polymerization (X_n) made by free radical polymerization in ionic liquids (Figure 3). In any case, X_n is higher when ionic liquids are used as media for polymerization in comparison with using organic solvents, such as toluene or dimethylsulfoxide (Figure 3). As expected from theory, X_n is significantly lower in the case that organic solvents were used in radical polymerization than for polymerizations conducted in bulk. Still, polymerization in certain ionic liquids, in particular in such with increasing viscosity causes a general increase in the degree of polymeri-
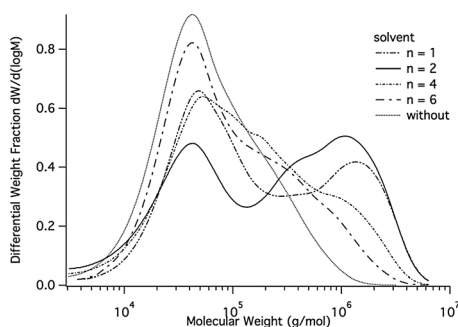

Figure 3.

Degree of polymerization of polybutylmethacrylate and polybenzylmethacrylate obtained by free radical polymerization of **M1** or **M2** in ionic liquids (imidazolium based ionic liquids bearing a variation of the alkyl group bound at the nitrogen atom of the cation and tetrafluoroborate (BF$_4^-$), hexafluorophosphate (PF$_6^-$), octylsulfate (C$_8$H$_{17}$SO$_4^-$), bis(trifluoromethylsulfonyl)-imide (NTf$_2^-$) or dicyanamide (N(CN)$_2^-$) as anion; pyrrolidinium and ammonium bis(trifluoromethylsulfonyl)imides (NTf$_2^-$)) and organic solvents (toluene, dimethylsulfoxide (DMSO)) as function of the reaction medium viscosity. Furthermore, results obtained by bulk polymerization are included as well.

zation of the polymethacrylates. The two notable exceptions of ionic liquids from this general trend exist that have viscosities higher than 50 mPa.s and longer alkyl substituents either at the cation (*N,N,N,N*-trioctylmethylammonium bis(trifluoromethylsulfonyl)imide) or at the anion (1-butyl-3-methylimidazolium octylsulfate). All other ionic liquids investigated within this row show a rough increase of the degree of polymerization of the polymer synthesized in the ionic liquids with increasing ionic liquid viscosity. Increasing viscosity of ionic liquids seems to reduce the bimolecular termination reaction of growing polymer chains, thus increasing the degree of polymerization.[65] Additionally, the propagation seems to be accelerated in many ionic liquids.[42,47] Yet, ionic liquids with extremely high viscosity may considerably reduce diffusion of the monomer as well. This may limit the degree of polymerization. Interestingly, similar results were obtained for polybutylmethacrylate and polybenzylmethacrylate made in ionic liquids regarding molecular weight and molecular weight distribution. This suggests that the interaction of the methacrylate moiety with various ionic components of the ionic liquids plays an important role.

Polystyrene Synthesis in Ionic Liquids

Hypothesizing that methacrylate moieties can interact with the ionic liquid via

hydrogen bonding, we explored the polymerization of styrene in selected ionic liquids as hydrogen bonding is inherently absent in the case of styrene. Results are exemplified in Figure 4. We found that polystyrene samples synthesized in 1-alkyl-3-methylimidazolium tosylates show a high molecular weight fraction, which exceeds the molecular weight obtained in bulk polymerization (Figure 4). This result supports the hypothesis of protected radicals discussed in literature.[44] This hypothesis may be applied either on all radicals occuring during polymerization or just on the primary radicals that initiate the polymerization. Investigation on model radicals resulted in discussion of an increase in radical recombination within the solvent cage in ionic liquids to significantly higher extent compared to traditional organic solvents.[62,63,66] This effect may reduce the concentration of active radicals that can start polymer growth, thus increasing the molecular weight. These results may support the hypothesis that increasing radical recombination within the solvent cage results in reduced concentration of active radicals that are able to start polymer growth. Extended recombination reaction of primary radicals within the solvent cage results in reduction of primary radical concentration, and therefore, in an increase in the molecular weight of the

polymer obtained. Interestingly, the content on the higher molecular weight fraction becomes smaller when the alkyl substituent at the imidazolium ion is slightly longer. The longer alkyl substituent reduces micropolarity of the ionic liquids, and enhances the compatibility of the solvent with the nonpolar monomer styrene (**M3**). Therefore, the lower compatibility of **M3** with imidazolium tosylates bearing only small alkyl substituents is a further reason for the broad molecular weight distribution. The higher the compatibility of **M3** is with the imidazolium tosylate bearing one longer alkyl substituent at the cation that smaller is the molecular weight distribution.

Noteworthy, the use of a mixture of 1-ethyl-3-methylimidazolium tosylate and 1-dodecyl-3-methylimidazolium tosylate (ratio wt:wt = 1:2) as polymerization medium narrows the extremely broad molecular weight distribution, although the molecular weight of the polystyrene sample remains higher than when made by bulk polymerization (Figure 5). Obviously, the less polar ionic liquid 1-dodecyl-3-methylimidazolium tosylate is a more suitable solvent for styrene than the ethyl substituted imidazolium tosylate. Yet, as dodecyl substituted
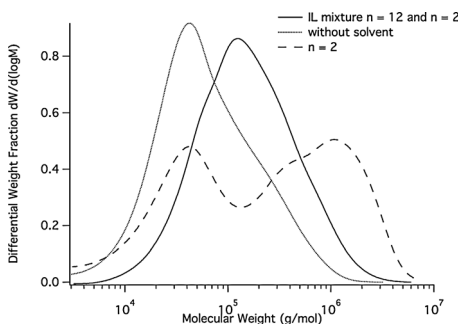

Figure 4.
GPC elugrams of polystyrene obtained by free radical polymerization of styrene (**M3**) using AIBN (1 mole-% relative to the monomer) as initiator at 70 °C in various reaction media for 24 h: 1-alkyl-3-methylimidazolium tosylates: n = 1 (methyl); n = 2 (ethyl); n = 4 (butyl); n = 6 (hexyl), and in bulk.

Figure 5.
GPC elugrams of polystyrene obtained by free radical polymerization of styrene (**M3**) at 70 °C using AIBN (1 mole-% relative to the monomer) in various reaction media for 24 h: 1-ethyl-3-methylimidazolium tosylate (n = 2), mixture of 1-ethyl-3-methylimidazolium tosylate (n = 2) and 1-dodecyl-3-methylimidazolium tosylate (n = 12) using weight ratio of wt: wt = 1: 2, and in bulk.

imidazolium tosylate is not useful alone for polymerization at 70 °C because its melting point is higher compared to the polymerization temperature, and crystallization occurs at the polymerization temperature even in the presence of monomer, free radical polymerization of **M3** is best conducted in the mixture of the two imidazolium tosylates. Clearly, further studies are needed to clarify this aspect.

Polarity effects of ionic liquids as discussed for polymerization of **M3** using imidazolium tosylates as matrices do not only influence the homopolymerization of this non-polar monomer they also strongly affect copolymerization of different polar monomers bearing similar polymerizable functional groups.

Copolymer Synthesis in Ionic Liquids

High solubilization power of ionic liquids for both less polar and highly polar monomers makes these solvents interesting for copolymerization of markedly differing polar monomers. This is instructively illustrated by the free radical copolymerization of the hydrophobic **M2** and the zwitterionic monomer **M4**. Both methacrylate monomers are immiscible with each other. In fact, it is even difficult to find common solvents that dissolve both monomers. The use of acetonitrile as reaction medium results in polymers that contain mainly the zwitterionic moiety **M4**.[29,33,36,41] Noteworthy, the composition of the polymers obtained is independent on the feed ratio of the monomers **M2** and **M4** if the copolymerization is conducted in acetonitrile. In contrast to this, many ionic liquids do well dissolve both monomers, and copolymers are obtained that contain both monomer units. Interestingly, the precise ionic liquid structure, especially the length of alkyl substituents at the imidazolium ion, can influence copolymer composition beyond the comonomer ratio. For example, the mole fraction of **M2** in the copolymer increases from about 0.46 when using 1-butyl-3-methylimidazolium tetrafluoroborate as solvent for copolymerization to 0.7 when the analogous ionic liquid bearing a decyl substituent served as reaction medium, though the monomer feeds contained stoichiometric amounts of **M2**: **M4** in both experiments. This clearly demonstrates that the polarity of ionic liquids is a crucial parameter for their use as reaction medium, and may be advantageously exploited to tune, e.g., the composition of copolymers of a given comonomer pair.

Conclusion

The results presented demonstrate that a number of factors such as viscosity, polarity, and solvent cage effects strongly influence the structure of polymers made in ionic liquids. Accordingly, the broad variability of the structure of ionic liquids opens huge possibilities in the field of polymer synthesis. However, the rational and successful application of ionic liquids as reaction media for synthesizing new homopolymers and copolymers requires thorough knowledge of structure-property relations of ionic liquids and of their interaction with the monomers. While certain relationships have been elucidated now, it is evident that the current state of knowledge is yet far from complete.

[1] K. Matyjaszewski, T. P. Davis, *Handbook of Radical Polymerization*, J. Wiley & sons, Inc., Hoboken **2002**.

[2] R. G. W. Norrish, R. R. Smith, *Nature* **1942**, *150*, 336.

[3] E. Trommsdorff, H. Köhle, P. Lagally, *Makromol. Chem.* **1948**, *1*, 169.

[4] J. M. G. Cowie, I. J. McEwen, D. J. Yule, *Eur. Polym. J.* **2000**, *36*, 1795.

[5] M. L. Coote, T. P. Davis, *Prog. Polym. Sci.* **1999**, *24*, 1217.

[6] V. N. Emel'yanenko, S. P. Vervkin, A. Heintz, C. Schick, *J. Phys. Chem. B* **2008**, *112*, 8095.

[7] J. M. S. S. Esperanca, J. N. C. Lopes, M. Tariq, L. M. N. F. Santos, J. W. Magee, L. P. N. Rebelo, *J. Chem. Eng. Data* **2009**, *55*, 3.

[8] D. H. Zaitsau, A. V. Yemalayeu, V. N. Emel'yanenko, A. Heintz, S. P. Verevkin, C. Schick, S. Berdzinski, V. Strehmel, *J. Mol. Liq.*, in press.

[9] V. Strehmel, H. Rexhausen, P. Strauch, *Phys. Chem. Chem. Phys.* **2010**, *12*, 1933.

[10] V. Strehmel, R. Lungwitz, H. Rexhausen, S. Spange, *New. J. Chem.* **2010**, *34*, 2125.

[11] G. Yu, D. Zhao, L. Wu, S. Yang, X. Chen, *AIChE* **2012**, *58*, 2885.

[12] T. Sabu, K. Matyjaszewski, *Macromol. Chem. Phys.* **2001**, *202*, 3379.

[13] T. Biedron, P. Kubisa, *Macromol. Rap. Commun.* **2001**, *22*, 1237.

[14] H. Zhang, K. Hong, J. W. Mays, *Macromolecules* **2002**, *35*, 5738.

[15] S. Harrison, S. R. Mackenzie, D. M. Haddleton, *Chem. Commun.* **2002**, 2850.

[16] H. Zhang, L. Bu, M. Li, K. Hong, A. E. Visser, R. D. Rogers, J. W. Mays, *ACS Symp. Ser. 818*. In: R. D., Rogers, K. R. Seddon, Eds., American Chemical Society, Washington, DC **2002**, 114.

[17] M. G. Benton, C. S. Brazel, *ACS Symp. Ser. 818*. In: R. D., Rogers, K. R. Seddon, Eds., American Chemical Society, Washington, DC **2002**, 125.

[18] K. Hong, H. Zhang, J. W. Mays, A. E. Visser, C. S. Brazel, J. D. Holbrey, W. M. Reichert, R. D. Rogers, *Chem. Commun.* **2002**, 1368.

[19] H. Zhang, K. Hong, J. W. Mays, *Macromolecules* **2002**, *35*, 5738.

[20] S. Perrier, T. P. Davis, A. J. Carmichael, D. M. Haddleton, *Chem. Commun.* **2002**, 2226.

[21] T. Biedron, P. Kubisa, *J. Polym. Sci. Part A: Polym. Chem.* **2002**, *40*, 2799.

[22] S. Harrisson, S. R. Mackenzie, D. M. Haddleton, *Macromolecules* **2003**, *36*, 5072.

[23] T. Biedron, P. Kubisa, *Polym. Int.* **2003**, *52*, 1584.

[24] H. Ma, X. Wan, X. Chen, Q.-F. Zhou, *J. Polym. Sci. Part A: Polym. Chem.* **2003**, *41*, 143.

[25] H. Ma, X. Wan, X. Chen, Q.-F. Zhou, *Polymer* **2003**, *36*, 5072.

[26] S. Perrier, T. P. Davis, A. J. Carmichael, D. M. Haddleton, *Eur. Poly. J.* **2003**, *39*, 417.

[27] L. Cheng, Y. Zhang, T. Zhao, H. Wang, *Macromol. Symp.* **2004**, *216*, 9.

[28] M. G. Benton, C. S. Brazel, *Polym. Int.* **2004**, *53*, 1113.

[29] V. Strehmel, A. Laschewsky, H. Kraudelt, H. Wetzel, E. Görnitz, in "*Ionic Liquids in Polymer Systems*" *ACS Symp. Ser*, **2005**, *913*, 17.

[30] S. Ding, M. Radosz, Y. Shen, *Macromolecules* **2005**, *38*, 5921.

[31] D. Li, Y. Zhang, H. Wang, J. Tang, B. Wang, *J. Appl. Polym. Sci.* **2006**, *102*, 2199.

[32] D. Li, Y. Zhang, H. Wang, J. Tang, B. Wang, *J. Appl. Polym. Sci.* **2006**, *102*, 4254.

[33] V. Strehmel, A. Laschewsky, H. Wetzel, *e-polymers* **2006**, 011.

[34] V. Strehmel, A. Laschewsky, H. Wetzel, E. Görnitz, *Macromolecules* **2006**, *39*, 923.

[35] J. Li, J. Zhang, Z. Liu, *J. Polym. Sci. Part A: Polym. Chem.* **2006**, *44*, 4420.

[36] V. Strehmel, *Macromol. Symp.* **2007**, *254*, 25.

[37] J. Ueda, H. Yamaguchi, T. Yamauchi, N. Tsubokawa, *J. Polym. Sci. Part A: Polym. Chem.* **2007**, *45*, 1143.

[38] G. Schmidt-Naake, I. Woecht, A. Schmalfuss, *Macromol. Symp.* **2007**, *259*, 226.

[39] Y. S. Vygodskii, O. A. Mel'nik, E. I. Lozinskaya, A. S. Shaplov, I. A. Malyshkina, N. D. Gavrilova, K. A. Lyssenko, M. Y. Antipin, D. G. Golovanov, A. A. Korlyukov, N. Ignat'ev, U. Welz-Biermann, *Polym. Adv. Technol.* **2007**, *18*, 50.

[40] I. Woecht, G. Schmidt-Naake, *e-Polymers* **2007**, no. 100.

[41] V. Strehmel, H. Wetzel, A. Laschewsky, E. Moldenhauer, T. Klein, *Polym. Adv. Technol.* **2008**, *19*, 1383.

[42] I. Woecht, G. Schmidt-Naake, S. Beuermann, M. Buback, N. Garcia, *J. Polym. Sci. Part A: Polym. Chem.* **2008**, *46*, 1460, (Propagation kinetics).

[43] H. Minami, K. Yoshida, M. Okubo, *Macromol. Rapid Commun.* **2008**, *29*, 567.

[44] K. J. Thurecht, P. N. Gooden, S. Goel, C. Tuck, P. Licence, D. J. Irvine, *Macromolecules* **2008**, *41*, 2814.

[45] V. Strehmel, E. Reynaud, H. Wetzel, E. Görnitz, A. Laschewsky, *Macromol. Symp.* **2009**, *275–276*, 242.

[46] I. Woecht, G. Schmidt-Naake, *Macromol. Symp.* **2009**, *275–276*, 219.

[47] A. Jelicic, N. Garcia, H.-G. Löhmannsröben, S. Beuermann, *Macromolecules* **2009**, *42*, 8801.

[48] Z. Chen, F. Yan, L. Qiu, J. Lu, Y. Zhou, J. Chen, Y. Tang, J. Texter, *Langmuir* **2010**, *26*, 3803.

[49] V. H. Nguyen, Y. Haldorai, Q. L. Pham, S. K. Noh, W. S. Lyoo, J.-J. Shim, *Eur. Polym. J.* **2010**, *46*, 2190.

[50] P. D. Haller, R. J. Frank-Finney, M. Gupta, *Macromolecules* **2011**, *44*, 2653.

[51] D. S. Sundar, R. Vijayaraghavan, J. Subramaniam, M. Surianarayanan, A. B. Mandal, *J. Appl. Polym. Sci.* **2011**, *120*, 3733.

[52] Y. S. Vygodskii, D. A. Sapozhnikov, A. S. Shaplov, E. I. Lozinskaya, N. V. Ignat'Ev, M. Schulte, P. S. Vlasov, I. A. Malyshkina, *Polym. J. (Tokyo, Jpn.)* **2011**, *43*, 126.

[53] S. Brusseau, O. Boyron, C. Schikaneder, C. C. Santini, B. Charleux, *Macromolecules* **2011**, *44*, 215.

[54] Y. Terayama, M. Kikuchi, M. Kobayashi, A. Takahara, *Macromolecules* **2011**, *44*, 104.

[55] K. Matsumoto, B. Talukdar, T. Endo, *Polym. Bull.* **2011**, *66*, 199.

[56] P. Kubisa, *Prog. Polym. Sci.* **2004**, *29*, 3.

[57] T. Biedron, P. Kubisa, *J. Polym. Sci. Part A: Polym. Chem.* **2005**, *43*, 3454.

[58] P. Kubisa, *J. Polym. Sci. Part A: Polym. Chem.* **2005**, *43*, 4675.

[59] V. Strehmel, *Chem. Ing. Tech.* **2011**, *83*, 1443.

[60] A. Wulf, F. Fumino, R. Ludwig, *Angew. Chem. Int. Ed.* **2010**, *49*, 449.

[61] F. Fumino, A. Wulf, R. Ludwig, *Angew. Chem. Int. Ed.* **2008**, *47*, 3830.

[62] V. Strehmel, J. F. Wishart, D. E. Polyansky, B. Strehmel, *ChemPhysChem* **2009**, *10*, 3112.

[63] S. Berdzinski, J. Horst, P. Straßburg, V. Strehmel, *ChemPhysChem* **2013**, *14*, 1899.

[64] K. Ueno, H. Tokuda, M. Watanabe, *PhysChemChemPhys* **2010**, *12*, 1649.

[65] G. Schmidt-Naake, A. Schmalfuß, I. Woecht, T. Glück, *Chem. Ing. Tech.* **2009**, *81*, 459.

[66] V. Strehmel, *ChemPhysChem* **2012**, *13*, 1649.